UNIVERSIDAD DE CHILE
FACULTAD DE CIENCIAS FÍSICAS Y MATEMÁTICAS
DEPARTAMENTO DE FÍSICA

RELATIVISTIC EFFECTS IN LARGE SCALE STRUCTURE

TESIS PARA OPTAR AL GRADO DE
MAGÍSTER EN CIENCIAS, MENCIÓN FÍSICA

CRISTIAN GUZMARO BARRERA HINOJOSA

PROFESOR GUÍA:
DOMENICO SAPONE

MIEMBROS DE LA COMISIÓN:
GUILLERMO BLANC MENDIBERRI
GONZALO PALMA QUILODRÁN
NELSON ZAMORANO HOLE

SANTIAGO DE CHILE
2018

RESUMEN DE LA MEMORIA PARA OPTAR
AL GRADO DE MAGÍSTER EN CIENCIAS, MENCIÓN FÍSICA
POR: CRISTIAN GUZMARO BARRERA HINOJOSA
FECHA: 2018
PROF. GUÍA: DOMENICO SAPONE

RELATIVISTIC EFFECTS IN LARGE SCALE STRUCTURE

En esta tesis estudiamos efectos relativistas en la estructura a gran escala del universo en ΛCDM y modelos de energía oscura. El término observado de sobredensidad de materia es derivado en el regimen lineal, donde se muestra de forma natural que este se encuentra relacionado no solo a la distribución de materia oscura subyacente, sino que también es sensible a otros efectos tales como el Redshift-space Distortion, el efecto Doppler y a lentes gravitacionales. De la misma forma, se muestra que existen contribuciones provenientes de un conjunto de efectos denominados 'relativistas', el cual consiste en el efecto Shapiro, el efecto Sachs-Wolfe Integrado y términos de potenciales gravitacionales locales. Con lo anterior se calcula una expresión general para el espectro angular de potencias de materia válida para una amplia clases de modelos de energía oscura y teorías de gravedad modificada ya que se basa en una descripción fenomenológica que introduce dos parametros, Q y η, los que capturan de una forma efectiva el clustering modificado (o constante gravitacional efectiva) y el stress anisotrópico que puede aparecer en algunos modelos cosmológicos alternativos.

Como caso particular, en este trabajo consideramos un modelo de fluido efectivo para la energía oscura tipo quintaesencia, el cual es caracterizado por un parámetro de ecuación de estado $w \neq -1$ y una velocidad del sonido $0 \leq c_s^2 \leq 1$. Ambos grados de libertad contribuyen explícitamente a los parametros efectivos Q y η así como también a la tasa de crecimiento de estructuras en el universo. Exploramos el espectro angular de potencias en este modelo para cinco valores de c_s^2 y comparamos los resultados con respecto a una cosmología ΛCDM de referencia hasta multipolos $\ell = 100$ y redshift $z = 2$. En general, las desviaciones de ΛCDM son mayores a bajo redshift ya que el fluido de energía oscura puede diferenciarse mejor de la constante cosmológica durante el universo tardío. Encontramos que en este modelo las sobredensidades de materia varían hasta un $\sim 15\%$ a bajo redshift, mientras que el redshift-space distortion y efecto Doppler pueden desviarse hasta $\sim 115\%$ respecto a ΛCDM para el caso $c_s^2 = 0$, donde las perturbaciones en el fluido efectivo pueden crecer a cualquier escala. A redshift mayores las diferencias en estos términos permanecen acotadas, aunque para el caso de lentes gravitacionales se obtienen diferencias de hasta 20% en $z = 2$ debido a que se trata de un efecto integrado.

Para los efectos relativistas encontramos que el retraso Shapiro y los potenciales gravitacionales locales se comportan de manera cualitativamente similar, mostrando diferencias de hasta un $\sim 20\%$ a redshift bajo. Finalmente, el efecto Sachs-Wolfe integrado muestra la mayor influencia del modelo de energía oscura mostrando hasta $\sim 90\%$ de diferencia relativa con respecto a ΛCDM debido a su capacidad de probar la tasa de crecimiento de estructuras pero también su variación temporal. Además, este efecto se ve potenciado por la tasa de clustering del fluido oscuro y es el único sensible a la posible presencia de viscosidad en el mismo, por lo cual representa una herramienta importante para probar modelos alternativos a ΛCDM usando surveys de galaxias.

Abstract

We study relativistic effects in the large scale structure of the universe in ΛCDM and alternative cosmological models. The observed galaxy overdensity is derived in the linear regime, showing that it is related to the underlying dark matter density fluctuations, to standard contributions such as Redshift-space distortion, Doppler effect and gravitational lensing, as well as to the set of so-called relativistic effects consisting in the Shapiro time-delay effect, the Integrated Sachs-Wolfe effect and local potential terms.

A general expression for the observed angular power spectrum of galaxies in the relativistic regime is presented, which is valid for a wide class of dark energy/modified gravity models as it is based on a phenomenological approach that introduces two parameters, Q and η, quantifying the modified clustering (or effective gravitational constant) and the anisotropic stress that may arise in some models.

In this work we consider a quintessence-like effective dark energy fluid that is characterized by an equation of state parameter $w \neq 1$ and a sound speed $0 \leq c_s^2 \leq 1$, which directly contribute to the clustering parameter Q and also to the growth rate of structures in the universe. We study the angular power spectra for this model considering five different sound speed cases and we compare the predictions against a fiducial ΛCDM cosmology up to multipoles $\ell \sim 100$ and redshift $z = 2$.

We find that, in general, deviations from ΛCDM are stronger at lower redshift, since the dark energy fluid starts to cluster more effectively during the late time universe. We find that matter density fluctuations deviates up to $\sim 15\%$ at $z = 0.1$, while redshift-space distortion and Doppler effect are enhanced up to $\sim 115\%$ with respect to ΛCDM for $c_s^2 = 0$, where the perturbations in the dark energy fluid are able to grow at all scales. At higher redshifts, deviations in these terms decrease and remain bounded, except for gravitational lensing which shows deviations of up to 20% at $z = 2$ as it is an integrated effect from source to observer.

For the relativistic effects we find that the Shapiro time-delay and the local potential terms behave in a qualitatively similar way, deviating up to $\sim 20\%$ at low redshift. Finally, the integrated Sachs-Wolfe effect shows the most impact from the dark energy fluid, as its deviations may reach up to $\sim 90\%$ of relative difference with respect to ΛCDM around $z = 2$ due to its capacity to probe cumulatively not only the evolution of the growth rate of structures but also the clustering rate of the dark energy fluid, which is consistent with previous studies. Furthermore, we find that this effect is the only one able to detect the presence of viscosity in the dark fluid, and then represents a valuable tool for testing and constraining alternative models using galaxy surveys.

A mi familia.

Agradecimientos

Primero que todo, me gustaría agradecer a Domenico por su apoyo y paciencia a lo largo de este proyecto, y por animarme incluso en los momentos mas difíciles. Gracias por la visión, experiencia y herramientas que pudiste compartirme durante este tiempo. También quiero agradecer a Susana Garay por su ingente (y a veces invisible) labor articulando diaramente el DFI, a Rodrigo Soto por su impecable gestión como coordinador de Postgrado, y a Nelson Zamorano por su especial empatía y cercanía.

Agradezco también a cada uno de los miembros de la Comisión, Guillermo Blanc, Gonzalo Palma y Nelson Zamorano, tanto por aceptar este proyecto como también por sus valiosos comentarios que ayudaron a dar forma final a esta tesis.

Finalmente, no puedo dejar de agradecer a mis padres, amigos, y especialmente a Yanira, por apoyarme, quererme y aguantarme de forma incondicional durante esta etapa (y muchas otras). A todos ustedes, muchas gracias por estar ahí!

Contents

List of Tables

List of Figures

Chapter 1

Introduction

Modern cosmology was born as one of the first applications of General Relativity for studying the properties of the cosmos on large scales, and from there on it has become one of the main topics in modern science. The advent of sophisticated instrumentation during the last decades has made it possible to observe deeper in the sky and at larger distances, which has allowed to reveal not only new features of the cosmos at different stages of its history but also key insights about the ultimate nature of our Universe.

1.1 The Large Scale Structure of the Universe

In the last decades, large surveys have revealed that galaxies are coherently distributed in the universe, forming structures up to very large scales. This large scale structure takes the form of a complex network called the Cosmic Web, which consists mainly of galaxy clusters, filaments, sheets and voids. Historically, these components were first characterized by Zel'dovich [1] in 1970 under the assumption of a hot dark matter universe in which large structures form first, and smaller structures form later by fragmentation. Even if this formation process is the opposite to today's hierarchical (bottom-up) understanding, this set of structures is still valid to describe the large scale structure in our universe with cold dark matter. Voids are vast and mostly empty regions which are surrounded by two-dimensional structures, i.e. sheets, where matter is concentrated. One-dimensional structures, filaments, are even denser than sheets, bridging galaxy clusters that reside at the nodes of filaments, the densest regions. These structures are also related to the flow of matter, which moves from voids to sheets, then to filaments, and finally into clusters. Examples of the observed [2] galaxy and simulated [3] dark matter distributions are shown in Fig 1.1.

The large scale structure of the universe contains valuable information about its fundamental properties. Since the formation of structures is based on the growth of tiny primordial perturbations (seeds) due to gravitational instabilities, they carry information about the initial conditions, the nature of gravity itself and the matter-energy content in our Universe.

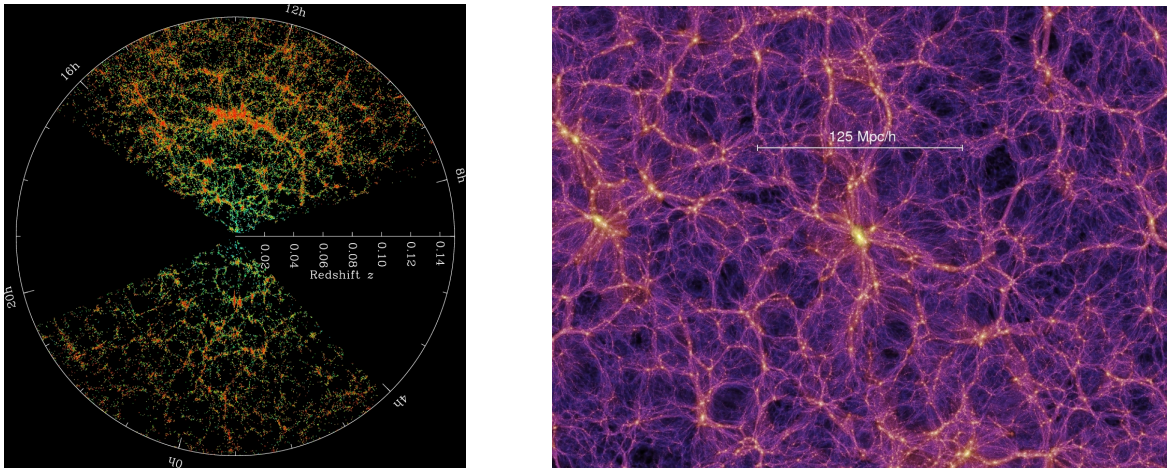

Figure 1.1: Left: the SDSS galaxy map. Right: a portion of the $z = 0$ slice of the Millenium Simulation. The 'cosmic web' is evident in both matter and dark matter distributions.

Over the past decade, rapid progress in observations has been made in this field, following the advent of large galaxy redshift surveys such as the Sloan Digital Sky Survey [2] (SDSS) and the Two Degree Field Galaxy Redshift Survey [4] (2dFGRS), and much higher precision measurements with larger survey volumes such as Euclid [5] and LSST [6] will open new horizons for constraining cosmological parameters and testing cosmological theories through galaxy distribution. In order to adequately interpret data coming from such increasingly precise observations, an accurate description of the large scale structure of the universe is required.

1.2 The Accelerated Cosmic Expansion and Dark Energy

In 1998, almost seven decades after the discovery of the cosmic expansion by Hubble in 1929 [7], the observation and analysis of type Ia supernovae (SNIa) brought to light a completely striking picture as astronomers pointed out that their apparent luminosities were lower than expected in a matter dominated universe due to extra redshifting. Then, it was concluded that the Universe was not only in phase of expansion, but for some reason this expansion is currently accelerating [8]. The origin and nature of this accelerated cosmic expansion is one of the most challenging puzzles in modern cosmology and physics, as this phenomenon is not predicted in a matter dominated universe, assuming that gravity is well described by Einstein's General Relativity. In such case the expansion will at some point slow down due to gravitational interaction (and maybe even recollapse the Universe). Regardless of the fact that the accelerated cosmic expansion is well supported by a host of cosmological data besides type Ia supernovae, such as the cosmic microwave background radiation [9] and the large scale structure [10], we are still far from a consensus on what is the physical mechanism responsible for such phenomenon, which is then dubbed generically as Dark Energy.

The current standard cosmological model, ΛCDM, explains the cosmic expansion within the framework of Friedmann-Lemaître-Robertson-Walker cosmology in a straightforward manner with the inclusion of a cosmological constant Λ. Although this model is consistent with nearly all the observational data collected over the past two decades, this explanation gives rise to a coincidence problem, and the fine-tuning required for the extremely small value of the cosmological constant makes it difficult to support it theoretically [11]. The elusive nature of dark energy and the lack of a consistent fundamental description underlying this model has encouraged to study alternative paradigms for explaining the observed late-time accelerated expansion of our Universe, such as modified gravity and dark energy models [12]. The former approach aim at revising the geometrical description of gravity rather than introducing 'dark' components in the stress-energy tensor, and include theories like $f(R)$ gravity [13], non-local gravity [14], Dvali-Gabadadze-Porrati (DGP) model [15] and Horndeski theories [16]. Dark energy models build on the latter idea and comprise quintessence [17] and k-essence [18], among others.

1.3 Relativistic effects in the Large Scale Structure

A key realization for understanding the data collected in galaxy surveys is that for measuring the distribution of galaxies in the universe we do not observe their actual positions, but rather redshifted photons coming from a particular direction in the sky. Then, one can obtain the fluctuations in the number of galaxies across the sky by pixelising galaxy maps in bins of redshift and solid angle. The volume elements constructed using the observed redshift and observed angle might differ from the real physical volume that the galaxies actually occupy, and the observed flux and redshift of the source galaxies also differ from their intrinsic properties since photons are perturbed when travelling across the universe toward our detectors. Then, the observed galaxy number density contains additional contributions arising from the distortion in the observable quantities, in contrast to the standard description where galaxies simply trace the underlying matter distribution with a bias factor, an issue that is naturally resolved if we construct theoretical predictions in terms of observable quantities. The fact that observations are made in redshift-space rather than in position-space was realized in the late 80's by Kaiser [19] who introduced the phenomenon known as redshift-space distortion (RSD), showing that the clustering in real space and redshift space were not equivalent due to peculiar motions. The fact that the observed galaxy distribution is not only sensitive to the underlying dark matter but also to the peculiar velocities also introduces a Doppler effect in the observed clustering [20]. In addition, during the 90's it was shown that gravitational lensing also affects the observed distribution of galaxies via the magnification bias [21, 22]. This effect relies on the fact that surveys are limited in magnitude and that gravitational lensing changes the observed luminosity of galaxies.

During the last decade, this set of extra (and denominated *standard*) contributions that appears intrinsically in the observed clustering of matter has been naturally extended by developing a fully relativistic description of the large scale structure of the universe [23, 24, 25, 26], leading to the inclusion of a set of *relativistic effects* accounting for the impact of General Relativity onto the photons' propagation. These effects comprise gravitational redshift, Sachs-Wolfe effect, Shapiro time delay and Integrated Sachs-Wolfe effect, and share

the common feature of being suppressed at sub-horizon scales with respect to the standard contributions. Nevertheless they allow to consistently interpret observables like the power spectra of galaxies, the Cosmic Microwave Background (CMB) and gravitational waves [27], specially at large scales, where the signature of galaxy clustering in General Relativity is significantly different from its Newtonian description [28, 29]. As such, it has been suggested that relativistic effects might provide a new horizon-scale test of cosmological models [30]. Compared to ΛCDM, in alternative theories the metric potentials and the velocity respond different to the same matter distribution. It has been argued that these differences may be prominent on very large scales, which may provide an interesting tool to probe gravity and dark energy [31].

1.4 Outline of this thesis

In the present work we aim at extending the analysis of relativistic effects in the large scale structure to cosmological models beyond ΛCDM. In particular, we consider dark energy and modified gravity models which can be described by a convenient phenomenological parametrization [32, 33, 34]. Using such framework, we can calculate the observed matter angular power spectrum for a wide class of models, which are effectively described by two new parameters which enter directly at the level of the Einstein Equations. As a particular realization we consider a quintessence-like dark energy fluid (instead of a cosmological constant Λ) which is not completely homogeneous in space but may have non-vanishing dark energy perturbations, namely it behaves as a fluid that might cluster at scales above a certain sound horizon.

The rest of this thesis is organized as follows:

In Chapter 2 we review the basics of the Friedmann-Lemaître-Robertson-Walker (FLRW) universe, which describes the background expansion history of the ΛCDM model as well as in some alternative models. We present the Friedmann equations considering a universe filled with matter, radiation, curvature and dark energy, and we discuss the solutions in some simple but characteristic scenarios.

In Chapter 3 we discuss the inhomogeneous universe as a closer approximation to our observable Universe, which settles the foundations of most modern cosmological models. We introduce the general relativistic formalism of linear cosmological perturbation theory which allows us to derive the governing equations for scalar perturbations, which are key for studying the clustering of matter in the universe and therefore structure formation. We introduce the concept of transfer functions and growth rate that characterize the evolution of matter overdensities in the universe.

Chapter 4 is devoted to discuss the so-called relativistic effects in the context of the large scale structure by carefully building the observed matter density fluctuations in terms of the coordinate system in which we perform the measurements. For this we analyze the propagation of photons travelling from galaxies towards our detectors in presence of inhomogeneities in the matter distribution, and we arrive at a general expression for the observed matter

overdensity. The result is independent of the underlying cosmological model as it only relies on the spacetime geometry of our universe but not on field equations. We then identify the different contributions appearing in this result and classifying them in terms of their relative scaling and redshift dependence.

In Chapter 5 we review the ΛCDM model, which represents the current cosmological standard model, summarizing its virtues and issues. In particular, we discuss the so-called cosmological constant problem and how it opens the door for alternative models that might explain the accelerated cosmic expansion, i.e. modified gravity and dark energy models, and we give a brief review of some of the most notable alternatives.

Having in mind cosmological models beyond ΛCDM, in Chapter 6 we present the phenomenological parametrization used to represent them in a fairly generic way. We introduce the effective parameter Q and the anisotropic stress parameter η at the level of Einstein Equations, and we show that the former can be regarded either as an effective 'clustering parameter' or an effective Newton's Constant G_{eff} [33, 35], thus allowing to treat dark energy models in terms of an effective fluid description as well as modified gravity models. In particular, we discuss a quintessence-like dark energy model under this parametrization.

In Chapter 7 we use the result for the observed matter overdensity derived in Chapter 4 and the (Q, η) parametrization discussed in Chapter 6 to calculate the angular power spectrum of galaxies in the relativistic regime for a generic class of cosmological models. We emphasize that the parameters Q and η characterize the relations between the various transfer functions of the perturbation variables as we discussed at the end of Chapter 3. We then present the expressions for the autocorrelations of each effect as well as their cross-correlation with the intrinsic matter density contrast, which is the contribution dominating the total angular power spectrum.

In Chapter 8 we consider a particular application of the general result derived in the previous chapter to study the angular power spectrum of the effective dark energy fluid model discussed at the end of Chapter 6, which is characterized by an equation of state parameter w and a sound speed c_s^2. We consider five different sound speed cases and we compare the predictions against a fiducial ΛCDM cosmology up to multipoles $\ell \sim 100$ and redshift $z = 2$. We analyze each contribution appearing in the power spectrum, i.e. standard and relativistic effects.

Finally, we wrap up this thesis by presenting our conclusions, highlights and outlooks.

Chapter 2

The Homogeneous Universe

The cornerstone of modern cosmological models is the so-called Cosmological Principle, which states that, at large scales, our Universe can be regarded as homogeneous and isotropic up to a high precision. Of course, locally this assertion is not quite accurate as we can clearly observe planets, stars, galaxies, clusters, etc., but at cosmological scales these represent only small inhomogeneities in the distribution of matter. Then, as a first approximation we can regard the Universe as filled by some homogeneous and isotropic fluid made up of different kind of constituents. In this chapter we will discuss this homogeneous universe which will fix the background dynamics of the 'real' universe in the perturbative approach used in the next chapters.

2.1 Einstein's General Relativity and the Cosmological Constant

In Einstein's General Relativity (herein after GR), the equations relating geometric properties of the spacetime to the matter-energy present are ($c = 1$)

$$G_{\mu\nu} = 8\pi G_N T_{\mu\nu} \,, \tag{2.1}$$

where the Einstein tensor $G_{\mu\nu}$ is defined as

$$G_{\mu\nu} \equiv R_{\mu\nu} - \frac{1}{2} R g_{\mu\nu} \,. \tag{2.2}$$

Here, $R_{\mu\nu}$ is the Ricci tensor, R the Ricci scalar, and $g_{\mu\nu}$ the spacetime metric. The right hand side of (2.1) features the energy-momentum tensor $T_{\mu\nu}$ which describes the matter-energy content of the theory, and G_N is Newton's constant. In practice, the Einstein equations are a complex set of non-linear equations which is almost impossible to solve analytically except for a few cases involving strong assumptions such as vacuum, homogeneity and/or isotropy.

In order to use GR for cosmological settings one needs to introduce the (in)famous cosmological constant Λ, which has a critical influence on the large scale dynamics of the universe.

The Einstein equations (2.1) in such case transform into

$$R_{\mu\nu} - \frac{1}{2}Rg_{\mu\nu} + \Lambda g_{\mu\nu} = 8\pi G_N T_{\mu\nu}\,. \tag{2.3}$$

Notice that, in practice, the cosmological constant term can be absorbed into a redefinition of the energy-momentum tensor as $\tilde{T}_{\mu\nu} = T_{\mu\nu} - (\Lambda/8\pi G_N)g_{\mu\nu}$. Then, after dropping the tilde, we formally rewrite (2.3) as (2.1) where we implicitly assume the presence of Λ in $T_{\mu\nu}$. In fact, from the point of view of particle physics the cosmological constant is regarded as the energy density of the vacuum. This identification, however, gives rise to the so-called cosmological constant problem [11] which we will comment in Chapter 5. In our next discussion we will assume that Einstein's General Relativity featuring the cosmological constant Λ is the correct theory for describing our Universe. Later, we will discuss possible alternatives to this scheme.

2.2 The Friedmann-Lemaître-Robertson-Walker Metric

As a first approximation for describing our Universe, let us start by discussing a completely homogeneous and isotropic. In the language of GR, this assumptions implies that the metric describing the spacetime $\mathcal{M}$ must satisfy such symmetries, i.e. $g_{\mu\nu}$ must be invariant under spatial translations and rotations. The most general metric satisfying these assumptions is the so-called Friedmann-Lemaître-Robertson-Walker (FLRW) metric. Adopting the $(-,+,+,+)$ convention for the metric, the line element in this spacetime is

$$\begin{aligned} ds^2 = g_{\mu\nu}dx^\mu dx^\nu &= -dt^2 + a^2(t)\gamma_{ij}dx^i dx^j \\ &= a^2(\tau)[-d\tau^2 + \gamma_{ij}dx^i dx^j]\,. \end{aligned} \tag{2.4}$$

Here, t is the cosmic (physical) time, τ is the conformal time, $a(t)$ is known as conformal factor, and γ_{ij} is the metric describing a 3-dimensional space with constant curvature K which classifies the geometry of the FLRW universe as Euclidean ($K = 0$), spherical ($K > 0$) or hyperbolic ($K < 0$). The spatial metric in the general case is given by

$$\gamma_{ij}dx^i dx^j = dr^2 + \chi^2(r)d\Omega^2\,, \tag{2.5}$$

where the coordinate χ is given in each case by

$$\chi(r) = \begin{cases} r & \text{Euclidean case,} \quad K = 0\,, \\ \frac{1}{\sqrt{K}}\sin(\sqrt{K}r) & \text{spherical case,} \quad K > 0\,, \\ \frac{1}{\sqrt{|K|}}\sinh(\sqrt{|K|}r) & \text{hyperbolic case,} \quad K < 0\,. \end{cases} \tag{2.6}$$

The scale factor $a(t)$ gives the relative size of the spacelike hypersurfaces at different times, so that the metric (2.4) may describe an expanding (or contracting) spacetime satisfying the principles of homogeneity and isotropy at each instant in time. It is then useful to define a quantity for comparing the size of the universe at two different instants in time. If we consider the propagation of a light signal of any given wavelength emitted by some source at a particular time t_1, which is then received by us at the present time $t_0 > t_1$, then the

observed wavelength of the photons will become stretched (contracted) as the signal travels across the universe due to its expansion (contraction). We define the redshift z of the light signal between the emission and observation time as

$$1 + z \equiv \frac{a(t_0)}{a(t_1)} \,. \tag{2.7}$$

Then, if the scale factor increases with time it causes the wavelength to move towards infrared (i.e. it gets redshifted) by a factor $a(t_0)/a(t_1)$, and then $z > 0$. It is usual to normalize the scale factor such that today $a(t_0) = 1$, and we will adopt this convention throughout this work.

Furthermore, since we are interested in the expansion rate of the universe itself, this is quantified by means of the Hubble parameter

$$H(t) \equiv \frac{1}{a}\frac{da}{dt} \equiv \frac{a'}{a} \,, \tag{2.8}$$

which is positive for an expanding universe and negative for a contracting one. Current observations show that our universe is expanding, and the Hubble constant $H_0 > 0$ is defined in terms of the present value of (2.8), $H_0 \equiv H(t_0)$. It is useful to also define the conformal Hubble parameter as

$$\mathcal{H}(\tau) \equiv \frac{\dot{a}}{a} = aH \,, \tag{2.9}$$

where the over-dot indicates a derivative with respect to the conformal time τ, i.e. $\dot{(\,)} \equiv d/d\tau$. We will stick to these conventions to denote time derivatives throughout this thesis.

In order to study the dynamics of the homogeneous universe we need to build the geometric quantities $R_{\mu\nu}$ and R appearing in the Einstein equations (2.3) considering the FLRW metric defined in (2.4). Let us begin by computing the Christoffel symbols (connection coefficients) associated to this metric, which are also necessary to define covariant derivatives on the manifold. A straightforward calculation shows that, in terms of the conformal time, the FLRW metric in the second line of (2.4) has the following non-vanishing Christoffel symbols,

$$\begin{aligned} &\Gamma^0_{00} = \mathcal{H}, && \Gamma^i_{00} = 0, && \Gamma^0_{i0} = 0 \,, \\ &\Gamma^i_{j0} = \mathcal{H}\delta^i_j, && \Gamma^0_{ij} = \mathcal{H}\gamma_{ij}, && \Gamma^k_{ij} = {}^{(3)}\Gamma^k_{ij} \,, \end{aligned} \tag{2.10}$$

where ${}^{(3)}\Gamma^k_{ij}$ denotes the three-dimensional Christoffel symbols associated to the spatial metric γ_{ij}. Using the previous expressions we find that the non-vanishing components of the Ricci tensor are then

$$R_{00} = -3\dot{\mathcal{H}}, \qquad R_{ij} = [\dot{\mathcal{H}} + 2(\mathcal{H}^2 + K^2)]\gamma_{ij} \,, \tag{2.11}$$

so that the Ricci scalar is given by $R = 6a^{-2}(\dot{\mathcal{H}}+\mathcal{H}^2+K)$. Then, working out the components of the Einstein tensor (2.2) with these expressions we find that

$$G_{00} = 3(\mathcal{H}^2 + K) \,, \tag{2.12}$$

$$G_{ij} = -(2\dot{\mathcal{H}} + \mathcal{H}^2 + K)\gamma_{ij} \,. \tag{2.13}$$

We then have all the ingredients for writing down the left hand side of the Einstein equation, which is related to the geometry of spacetime. Let us next discuss the right hand side of (2.3), related to the matter-energy content of the universe.

2.3 The energy-momentum tensor

In order to obtain the dynamical equations for the universe we now need to specify the matter-energy content through T^μ_ν. Due to our assumption of homogeneity and isotropy, the energy-momentum tensor is constrained to be of the form $T^\mu_\nu = \mathrm{diag}(-\rho, P, P, P)$ or, explicitly

$$T^\mu_\nu = (\rho + P)u^\mu u_\nu + P\delta^\mu_\nu \,, \tag{2.14}$$

where u^μ is the relative velocity field of the fluid with respect to a rest-frame observer, ρ its density and P the pressure. If we consider a comoving coordinate system (which scales with $a(t)$), then the fluid is at rest with respect to the observers, i.e.

$$u^\mu = a^{-1}\delta^\mu_0 \qquad u_\mu = -a\delta^\mu_0 \,. \tag{2.15}$$

In order to completely characterize the cosmic fluid it is necessary to provide an equation of state (herein after EoS) which relates density and pressure as

$$P = w\rho \,, \tag{2.16}$$

where w is known as the EoS parameter, and whose value depends on the kind of fluid under consideration.

2.4 Conservation of the energy-momentum tensor

The conservation of the energy-momentum tensor, $\nabla_\mu T^\mu_\nu = 0$, can be studied independently of Einstein equations. Let us consider the equation coming from the $\nu = 0$ component of this law. Since the energy-momentum tensor has the non-vanishing components $T^0_0 = -\rho$, $T^i_j = P\delta^i_j$, and the Christoffel symbols are given by (2.10), the conservation law $\nabla_\mu T^\mu_0 = 0$ implies the continuity equation (mass conservation) for the fluid

$$\dot\rho + 3\mathcal{H}(\rho + P) = 0 \,. \tag{2.17}$$

Since in general the universe consist in a mixture of matter, radiation, dark energy, etc., the variables ρ and P appearing in (2.17) should be regarded as the sum of all the contributions to the total energy density and pressure. If we consider the universe as dominated by a single component, we can use (2.17) to study how each density term scales with a. Then, if each case is parametrized by an EoS, $P_i = w_i\rho_i$ (no sum), the solution to (2.17) assuming constant w is

$$\rho_i \propto a^{-3(1+w_i)} \,. \tag{2.18}$$

Let us comment on three important cases:

- **Matter:** If we consider a fluid which is made up of non-relativistic particles, then its pressure is much smaller than its energy density, i.e. $|P_m| << \rho_m$, which implies that $w_m = 0$. This case correspond to normal (baryonic) matter as well as cold dark matter, which constitutes a gas of weakly interacting particles, and thus they are usually referred to as 'dust'. For matter domination (2.18) implies that

$$\rho_m \propto a^{-3} \,, \tag{2.19}$$

which confirms the intuitive reasoning that as the universe expands, the particle density dilutes as the volume $V \propto a^{-3}$.

- **Radiation**: A radiation gas is characterized by $w_r = 1/3$, and may represent photons, neutrinos, and gravitons. Then, we have

$$\rho_r \propto a^{-4}\,. \tag{2.20}$$

We note that there is an extra factor a^{-1} with respect to the matter solution (2.19) which is a consequence of the redshifting of the wavelength of the radiation due to the expansion of the universe.

- **Cosmological Constant:** Finally, for the cosmological constant Λ we have $w_\Lambda = -1$, i.e. it acts as a fluid with negative pressure which is able to drive an accelerated expansion. This gives the scaling

$$\rho_\Lambda \propto a^0\,, \tag{2.21}$$

showing that the energy density of the cosmological constant term does not dilute at all (hence the name). This result may appear striking at first glance as this means that energy has to be created as the universe expands. However, it is the energy of the whole gravitational system the one that needs to be conserved, which is guaranteed from the start by the condition $\nabla_\mu T^{\mu\nu} = 0$.

2.5 The Friedmann Equations

We now turn our attention to write down the Einstein equations for the FLRW metric (2.4) and the energy-momentum tensor (2.14). For the 00-component of the Einstein equation (2.3) we have

$$\mathcal{H}^2 + K = \frac{8\pi G_N a^2}{3}\rho\,, \tag{2.22}$$

or, in terms of the usual Hubble parameter

$$H^2 + \frac{K}{a^2} = \frac{8\pi G_N}{3}\rho\,. \tag{2.23}$$

This equation is called the (first) Friedmann equation. The other relevant equation is the trace-part of the ij-component, i.e. $G^i_i = 8\pi G T^i_i$. Taking the trace of (2.13) and (2.14), we find

$$2\dot{\mathcal{H}} + \mathcal{H}^2 + K = -8\pi G_N a^2 P\,, \tag{2.24}$$

which is the second Friedmann equation . Prior to solving (2.23), it is convenient to introduce the concepts of critical density and dimensionless density parameters. If we consider (2.23) evaluated at the present time t_0, we can solve for $\rho(t_0)$ and impose the condition $K = 0$, so it will gives us the value needed in order to have a flat FLRW universe today

$$\begin{aligned}\rho_{\text{crit},0} &\equiv \frac{3H_0^2}{8\pi G_N} \\ &\approx 1.878 \times 10^{-26} h^2 \text{kg m}^{-3}\,,\end{aligned} \tag{2.25}$$

where $h \equiv H_0/(100\text{kms}^{-1}\text{Mpc}^{-1})$ is the reduced Hubble constant. Then, we can compare the present values of the various density terms included in ρ with respect to this critical value $\rho_{\text{crit},0}$. We introduce a set of dimensionless density parameters as

$$\Omega_{m,0} \equiv \frac{\rho_{m,0}}{\rho_{\text{crit},0}}\,, \tag{2.26}$$

$$\Omega_{r,0} \equiv \frac{\rho_{r,0}}{\rho_{\text{crit},0}}\,, \tag{2.27}$$

$$\Omega_{\Lambda,0} \equiv \frac{\Lambda}{3H_0^2}\,, \tag{2.28}$$

$$\Omega_{K,0} \equiv \frac{-K}{H_0^2}\,, \tag{2.29}$$

where we have defined an analogous 'curvature' density parameter $\Omega_{K,0}$. It should be emphasized that the '0' subscript in the Ω's is usually dropped, and the meaning of these quantities is implicitly understood to be defined in terms of today values ($t = t_0$). In the following we adopt this convention. In terms of these quantities, the Friedmann equation (2.23) evaluated at the present time implies the constraint

$$\sum_i \Omega_i = 1\,, \tag{2.30}$$

where $i = m, r, \Lambda, K$. Now, using the scaling (2.18) we can write the Friedmann equation conveniently in terms of the Ω's as

$$H^2 = H_0^2 \sum_i \Omega_i a^{-3(1+w_i)}\,. \tag{2.31}$$

Then, if we consider a universe containing all the ingredients discussed so far, i.e. matter, radiation, a cosmological constant and curvature, the previous equation is explicitly

$$H^2 = H_0^2[\Omega_r a^{-4} + \Omega_m a^{-3} + \Omega_K a^{-2} + \Omega_\Lambda]\,. \tag{2.32}$$

As before, the case of a single-component universe is of natural interest since the different scaling of radiation, matter and dark energy imply that in certain epochs of the history of the universe one of the components has dominated over the others. In fact, we know that after the big bang, the universe was first dominated by radiation, then by matter, and the late universe eventually becomes dominated by dark energy. If we restrict to a single component, the Friedmann equation (2.31) reduces to

$$H = H_0 a^{-\frac{3}{2}(1+w)}\,, \tag{2.33}$$

and solving this equation for the scale factor as a function of the physical time we find that

$$a(t) \propto \begin{cases} t^{\frac{2}{3(1+w)}} & w \neq -1\,, \\ e^{Ht} & w = -1\,. \end{cases} \tag{2.34}$$

In particular, the second line of (2.34) shows the exponential cosmic expansion driven by the cosmological constant Λ, a very similar scenario to that hypothesised in the inflationary period. Each case is shown in Table 2.1.

	w	$\rho(a)$	$a(t)$	$a(\tau)$
RD	$\frac{1}{3}$	a^{-4}	$t^{1/2}$	τ
MD	0	a^{-3}	$t^{2/3}$	τ^2
ΛD	-1	a^0	e^{Ht}	$-\tau^{-1}$

Table 2.1: Scalings of the energy density and evolution of the scale factor for radiation dominated (RD), matter dominated (MD) and cosmological constant dominated (ΛD) universes.

Finally, recalling that for photons $dr = d\tau$ (with $c = 1$), we can also use the Friedmann equation (2.31) to calculate the comoving distance to an object at redshift z as

$$r(z) = \int_0^z \frac{dz'}{H(z')} \,. \tag{2.35}$$

This last equations tells us how the comoving distance depends on cosmological parameters through the Hubble parameter H. This concludes our review on the FLRW background universe. The next section expands this picture by including inhomogeneities in the cosmic fluid.

Chapter 3

The Inhomogeneous Universe

The FLRW model studied in the previous chapter is still far from being a realistic picture of our Universe as we know that it is far richer: we can observe several cosmic structures like galaxies, clusters, voids, sheets, filaments, etc., which in this language represent inhomogeneities in the large scale distribution of matter. Nowadays, we understand that these structures originate from tiny primordial inhomogeneities which become amplified by gravitational instabilities as the universe evolves.

The theory of structure formation can be separated into two main areas:

1. **The study of the mechanism for the generation of the primordial inhomogeneities**: the most accepted picture is the inflationary theory, which states that prior to the Big Bang the Universe experienced an epoch of exponential expansion in the presence of an inflaton field φ, whose quantum fluctuations are responsible for the 'galactic seeds' from which structures grow.

2. **The study of the evolution of the primordial seeds into the present observable structure of the universe**: although this part is probably better understood that the problem of the initial conditions, as the ΛCDM model has proven to be robust up to date, it is not completely settled either since the precise nature of dark matter and dark energy is still unclear.

In this work we focus our efforts in exploring the second point by studying the large scale structure of the Universe. The main tool for this study is linear cosmological perturbation theory, which relies on the background solution set by FLRW cosmology discussed in Chapter 2.

Before introducing the formalism of general relativistic perturbation theory, it is worth to remark the main advantages of this over the so-called Newtonian approximation. In the latter approach one regards the matter content of the universe as governed by the fluid dynamics equations for a perfect fluid in presence of a gravitational field, and completely forget about General Relativity. However, this simplified picture has some drawbacks:

1. It holds only for scales deep inside the cosmological horizon, i. e. $k^{-1} << \mathcal{H}^{-1}$. In

other words, we neglect the curvature of spacetime.

2. It assumes that the fluid filling the universe is exclusively made up of non-relativistic particles, i.e. $v << c$, or equivalently, $|P| << \rho$.
3. It misses intrinsic general relativistic degrees of freedom such as gravitational waves, which may be of interest in some contexts.

Then, if we want to study perturbations near horizon scales, or if we want to consider intrinsically relativistic objects such as photons, neutrinos or cosmic strings, we need a fully general relativistic formalism. Nevertheless, due to its simplicity and accuracy at scales below the horizon the Newtonian approximation is still widely used, specially in numerical simulations, where it can effectively model the non-linear growth of structures.

3.1 Linear Relativistic Perturbation Theory

The treatment presented in this work is based on linear perturbation theory in the general relativistic regime. This formalisms allows us to expand all the fields into a background part plus a small perturbation, so we can study the distribution of galaxies by perturbing the background FLRW metric (2.4).

3.1.1 The perturbed metric

The main assumption for using a perturbative approach is that the spacetime $\mathcal{M}$ with metric $g_{\mu\nu}$ and energy momentum tensor $T_{\mu\nu}$ describing the 'real Universe' is somehow close to a background FLRW universe, i.e. a spacetime $\bar{\mathcal{M}}$ with a metric $\bar{g}_{\mu\nu}$ associated to a homogeneous and isotropic energy momentum tensor $\overline{T}_{\mu\nu}$. Under this assumption, the full metric of the real universe can be approximated up to first order as

$$g_{\mu\nu} = \bar{g}_{\mu\nu} + \delta g_{\mu\nu} \,, \tag{3.1}$$

where $\bar{g}_{\mu\nu}$ is the FLRW metric (2.4). For the rest of this work we restrict to the case of spatially flat Universe ($K = 0$). In such case the background metric (2.4) is conformally flat, i.e.

$$\bar{g}_{\mu\nu} = a^2(\tau)(-d\tau^2 + \delta_{ij}dx^i dx^j) = a^2(\tau)\eta_{\mu\nu} \,, \tag{3.2}$$

where $\eta_{\mu\nu} = \text{diag}(-1, 1, 1, 1)$ is the Minkowski metric. Furthermore, it is useful to write the perturbation appearing in (3.1) as $\delta g_{\mu\nu} = a^2 h_{\mu\nu}$, so the metric up to first order is

$$g_{\mu\nu} = a^2(\tau)(\eta_{\mu\nu} + h_{\mu\nu}) \,. \tag{3.3}$$

The main appeal of first order perturbation theory is that all the equations for fluctuations are linear, so we can use Fourier analysis and deal with each mode k of the perturbations independently. However, it is important to remark that in practice the linear expansion is valid up to scales of roughly $k \sim 0.1$ Mpc^{-1}. At shorter distances the formation of small structures is governed by nonlinear evolution which must be treated by numerical approaches such as N-body or hydrodynamical simulations. In recent years some mixed schemes have

been proposed for going beyond the nonlinear scale such as the effective field theory of large scale-structure [36], which, nonetheless, at the current stage it still lacks the robustness and consistency needed for obtaining sensible predictions as some theoretical difficulties persist.

3.1.2 The Scalar-Vector-Tensor decomposition

Since the Einstein equations (2.3) contains rank 2 symmetric tensors, in 4 dimensions in principle it governs 10 degrees of freedom. However, since this theory is covariant under general coordinate transformations, we must subtract 4 degrees which correspond to the reparametrization of each coordinate $\tilde{x}^\mu = \tilde{x}^\mu(x)$, so that only 6 degrees of freedom are physically described.

Then, before deriving the perturbation equations it is convenient to use the so-called Scalar-Vector-Tensor (SVT) decomposition, and divide the perturbations into scalar (S), vector (V) and tensor (T) each one containing 4+4+2 degrees of freedom, of which 2+2+2 are physical. In the most general case we can write the metric perturbations as,

$$h_{00} = -2A, \quad h_{0i} = -B_i, \quad h_{ij} = 2H_{ij} = 2(H_L\delta_{ij} + H_{Tij} + H_{ij})\,, \tag{3.4}$$

where A, H_L, B_i and H_{Tij} are scalar degrees of freedom, two of which can be removed by gauge transformations, and H_{ij} is the transverse traceless gravitational wave term (see Appendix A for more detail on these quantities). Then, the line element in the perturbed universe is

$$ds^2 = a^2(\tau)\{-(1+2A)d\tau^2 - 2B_i d\tau dx^i + [(1+2H_L)\delta_{ij} + 2H_{Tij} + 2H_{ij}]dx^i dx^j\}\,. \tag{3.5}$$

Since we are doing first order perturbation theory, we can use the background metric for rising and lowering indexes of the perturbed metric, i.e.

$$h^\mu_\nu = \eta^{\mu\rho}h_{\rho\nu}, \qquad h^{\mu\nu} = \eta^{\mu\rho}\eta^{\mu\sigma}h_{\rho\sigma}\,. \tag{3.6}$$

The perturbations with raised indexes are explicitly given by

$$h^{00} = -2A, \quad h^{0i} = +B_i, \quad h^{ij} = 2H_{ij} = 2(H_L\delta^{ij} + H_{Tij} + H_{ij})\,. \tag{3.7}$$

Notice that due to our metric convention the spatial indexes can be freely raised and lowered, e.g. $B^i = B_i$. Since the inverse metric must satisfy the condition $g^{\mu\rho}g_{\rho\nu} = \delta^\mu_\nu$, we find that up to first order it is given by

$$g^{\mu\nu} = a^{-2}(\bar{g}^{\mu\nu} - h^{\mu\nu})\,. \tag{3.8}$$

It can be shown that the perturbative expansion (3.1) does not mix the scalar (S), vector (V) and tensor (T) degrees of freedom, thus they can be conveniently decoupled and analyzed separately (this holds true only at the linear level). This allows us to focus on the scalar perturbations, which are associated to density perturbations. Vector perturbations are not usually predicted by inflationary models, and even if they were, these would quickly decay with the expansion of the universe. Tensor perturbations, however, are important prediction of inflation, but we will neglect them for simplicity. Then, we focus on the Einstein Equations for scalar perturbations, which are the relevant ones for the late time universe.

3.1.3 Gauge fixing

The general covariance of General Relativity implies that the arbitrary split between background and perturbed quantities introduces redundant degrees of freedom. In fact, we can use this gauge freedom to set two of the metric perturbations to zero, or, alternatively, we can define the gauge in the matter sector imposing conditions over $T^{\mu\nu}$. In GR the mathematical procedure of choosing a gauge corresponds, physically, to selecting a specific observer. The most common gauge choices used in the framework of cosmological perturbation theory are:

- **Synchronous Gauge**: This was the gauge used by Lifshitz [37] and the first cosmologists who dealt with the theory of cosmological perturbations. This is defined by the conditions $A = B_i = 0$, i.e. only the spatial h_{ij} components of the metric perturbation are manifest. The drawback of this gauge is that it is not uniquely defined by this requirement and there is still the freedom to make a further transformation and still stay within this gauge. In other words, the metric perturbations are not defined uniquely, and it is not always clear what metric perturbations are real, physical perturbations and which of them are simply coordinate artifacts. Historically, the confusion due to gauge modes motivated Bardeen to formulate alternative approaches that deal with gauge-invariant quantities [38] such as the Bardeen potentials.
- **Conformal Newtonian (or Longitudinal) Gauge**: In the Newtonian gauge one imposes that $B_i = H_{Tij} = 0$, and then $A = \Psi$ and $H_L = -\Phi$, where Ψ and Φ are the Bardeen potentials. Physically, this gauge represents the coordinate system fixed to the background universe, so that peculiar velocities and other effects caused by the inhomogeneities in the distribution of the matter-energy content of the universe are manifest. The main advantages of this gauge is that the metric is diagonal, and it is in fact the most intuitive one as it has a direct Newtonian limit. However, this gauge is restricted to scalar modes only since vector and tensor degrees of freedom are eliminated from the beginning.

In the rest of this chapter we will use the Newtonian Gauge for our derivations.

3.1.4 The perturbed Einstein equations

The perturbed metric (3.1) implies that we must expand the Einstein equations (2.3) up to first order, i.e.

$$G^\mu_\nu = \bar{G}^\mu_\nu + \delta G^\mu_\nu \,, \tag{3.9}$$
$$T^\mu_\nu = \bar{T}^\mu_\nu + \delta T^\mu_\nu \,. \tag{3.10}$$

By construction we know that the Einstein equation is satisfied at the background level by the FLRW metric, i.e. $\bar{G}_{\mu\nu} = 8\pi G_N \bar{T}_{\mu\nu}$, so that the equation for the perturbations is simply

$$\delta G^\mu_\nu = 8\pi G_N \delta T^\mu_\nu \,. \tag{3.11}$$

In order to obtain δG^μ_ν we start by computing the Christoffel symbols $\Gamma^\mu_{\alpha\beta} = \bar{\Gamma}^\mu_{\alpha\beta} + \delta\Gamma^\mu_{\alpha\beta}$ with the perturbed metric (3.5) in the Newtonian Gauge, where $\bar{\Gamma}^\mu_{\alpha\beta}$ are the background

connection coefficients (2.10). The first order contributions are

$$\delta\Gamma^0_{00} = \dot{\Psi}, \qquad \delta\Gamma^0_{0i} = \partial_i\Psi \qquad \delta\Gamma^i_{00} = \partial_i\Psi\,, \tag{3.12}$$
$$\delta\Gamma^i_{j0} = -\dot{\Phi}\delta^i_j, \quad \delta\Gamma^0_{ij} = -2\mathcal{H}(\Psi+\Phi)\delta_{ij} - \dot{\Phi}\delta_{ij}, \quad \delta\Gamma^k_{ij} = -\partial_j\Phi\delta_{ik} - \partial_k\Phi\delta_{ij} + \partial_i\Phi\delta_{jk}\,.$$

Then, we find that the first order perturbations entering into (3.11) are

$$\delta G^0_0 = 2a^{-2}[-\nabla^2\Phi + 3\mathcal{H}(\dot{\Phi} + \mathcal{H}\Psi)]\,, \tag{3.13}$$
$$\delta G^0_i = -2a^{-2}\partial_i(\dot{\Phi} + \mathcal{H}\Psi)\,, \tag{3.14}$$
$$\delta G^i_0 = 2a^{-2}\partial_i(\dot{\Phi} + \mathcal{H}\Psi)\,, \tag{3.15}$$
$$\delta G^i_j = a^{-2}[2\ddot{\Phi} + 2(2\dot{\mathcal{H}} + \mathcal{H}^2)(\Phi+\Psi) + 2\mathcal{H}(2\dot{\Phi} + \dot{\Psi}) + \nabla^2(\Psi-\Phi)]\delta^i_j + \partial^i\partial_j(\Phi-\Psi)\,. \tag{3.16}$$

We now turn our attention to the perturbed stress energy tensor needed for the right hand side of (3.11).

3.1.5 The perturbed energy-momentum tensor

Recalling our discussion on the homogeneous universe in Chapter 2, the background energy-momentum tensor of the cosmic fluid is given by

$$\bar{T}^\mu_\nu = (\bar{\rho} + \bar{P})u^\mu u_\nu + \bar{P}\delta^\mu_\nu\,, \tag{3.17}$$

where the four-velocity is

$$\bar{u}^\mu = a^{-1}\delta^\mu_0 \qquad \bar{u}_\mu = -a\delta^\mu_0\,. \tag{3.18}$$

Let us now introduce a perturbation and write the stress-energy tensor as

$$T^\mu_\nu = \bar{T}^\mu_\nu + \delta T^\mu_\nu\,. \tag{3.19}$$

Just like the metric perturbation, δT^μ_ν has 10 degrees of freedom, 6 which are physical and 4 corresponding to gauge choices. We can also perform the SVT decomposition and divide them into scalar+vector+tensor with 4+4+2 degrees of freedom, of which 2+2+2 are physical. Alternatively, they can be classified as 5+5 degrees of freedom related to a perfect fluid and non-perfect fluid, respectively. The perfect fluid degrees of freedom are those which keep the full tensor in the perfect fluid form, i.e. keeping the structure of $\bar{T}^\mu_\nu$. Then, they may correspond to perturbations in the density, pressure and velocity of the fluid, namely

$$\rho = \bar{\rho} + \delta\rho\,, \tag{3.20}$$
$$P = \bar{P} + \delta P\,, \tag{3.21}$$
$$u^i = \bar{u}^i + \delta u^i\,. \tag{3.22}$$

Here, we have not included the perturbation δu^0 since this is not and independent degrees of freedom because of the constraint $u_\mu u^\mu = -1$. Furthermore, in (3.22) we have $\bar{u}^i = 0$ since the fluid is at rest in the background universe, and we can define the peculiar velocity as

$$v^i \equiv a\delta u^i = au^i\,, \tag{3.23}$$

which represents the coordinate velocity of the fluid $v^i \equiv dx^i/d\tau$, as defined by a comoving observer.

At this point it is customary to define the relative matter density perturbation, or overdensity variable, as

$$\delta \equiv \frac{\delta\rho}{\bar{\rho}}\,. \tag{3.24}$$

This is the central variable for our analysis since it represents the fluctuation in the matter density with respect to the cosmic mean $\bar{\rho}$, and then allows to quantify the clustering of matter at galactic scales.

Then, including these perturbations related to the 5 perfect fluid degrees of freedom, the non-vanishing components of the perturbed energy momentum tensor are given by

$$T^0_0 = -(\bar{\rho} + \delta\rho)\,, \tag{3.25}$$
$$T^0_i = (\bar{\rho} + \bar{P})v_i\,, \tag{3.26}$$
$$T^i_0 = -(\bar{\rho} + \bar{P})v^i\,, \tag{3.27}$$
$$T^i_j = (\bar{P} + \delta P)\delta^i_j\,. \tag{3.28}$$

Let us now add the remaining 5 degrees of freedom which drive the base perfect fluid away from such condition. These are encoded as contributions to the spatial part of the perturbations δT^i_j as

$$\delta T^i_j = \delta P \delta^i_j + \Sigma^i_j = \bar{P}[\pi_L \delta^i_j + \Pi^i_j]\,, \tag{3.29}$$

where we have defined the overpressure perturbation variable

$$\pi_L \equiv \frac{\delta P}{\bar{P}}\,, \tag{3.30}$$

which plays an analogous role to the overdensity variable δ. The tensor $\Pi^i_j \equiv \Sigma^i_j/\bar{P}$ is called anisotropic stress, and correspond to a traceless tensor, i.e.

$$\Sigma^i_j \equiv \delta T^i_j - \frac{1}{3}\delta^i_j \delta T^k_k\,, \tag{3.31}$$
$$\delta P \equiv \delta T^k_k\,. \tag{3.32}$$

For a perfect fluid one has that $\Pi^i_j = 0$, but even if we consider the background fluid as perfect, the perturbed fluid in general is not.

Summarizing, we see that the perturbation to the energy-momentum tensor δT^μ_ν brings in the scalar perturbations $\delta\rho$ and δP, the 3-vector $\mathbf{v} = v_i$ and the traceless 3-rank tensor Π_{ij}. Analogously as for the metric perturbations, the latter two can be further decomposed following the SVT scheme. We can decompose the perturbation v_i in terms of a scalar and a vector components as

$$v_i = v^S_i + v^V_i\,, \tag{3.33}$$

which satisfy the conditions

$$v^S_i = -\partial_i v, \qquad \partial_i v^V_i = 0\,. \tag{3.34}$$

Likewise, we can decompose Π_{ij} into scalar, vector and tensor parts as

$$\Pi_{ij} = \Pi^S_{ij} + \Pi^V_{ij} + \Pi^T_{ij}\,, \tag{3.35}$$

where

$$\Pi^S_{ij} = (\partial_i\partial_j - \frac{1}{3}\delta_{ij}\nabla^2)\Pi\,, \tag{3.36}$$

$$\Pi^V_{ij} = -\frac{1}{2}(\Pi_{i,j} + \Pi_{j,i})\,, \tag{3.37}$$

$$\delta^{ik}\Pi^T_{ij,k} = 0\,. \tag{3.38}$$

Together with the SVT decomposition of the metric previously discussed, the SVT decomposition of energy-momentum tensor allows us to completely decouple the evolution of each component in first order perturbation theory.

3.1.6 Conservation of the perturbed energy-momentum tensor

Since we have the full form for the energy-momentum tensor, we may consider the equations arising from its conservation, $\nabla_\mu T^\mu_\nu = 0$. From Chapter 2 we recall that at the background level the $\nu = 0$ component of this conservation law yields the continuity equation for matter. Likewise, at the perturbation level we find the equation governing the evolution of the density perturbation variable,

$$\dot{(\delta\rho)} = -3\mathcal{H}(\delta\rho + \delta p) + (\bar\rho + \bar P)(-\partial_i v^i + 3\dot\Phi)\,. \tag{3.39}$$

In the right hand side of (3.39) we have the effect of the background expansion, then the effect of velocity divergence i.e. the local fluid expansion, and finally the effect of fluctuations in the scalar potential Φ. Similarly, from the spatial component $\nu = i$ we find the equation for the peculiar velocity

$$(\bar\rho + \bar P)\dot v_i = -(\bar\rho + \bar P)v_i + \partial_i\left[\delta P + (\bar\rho + \bar P)\Psi + \frac{2}{3}\bar P\nabla^2\Pi\right] - 4\mathcal{H}(\bar\rho + \bar P)v_i\,. \tag{3.40}$$

In the momentum perturbation equation (3.40), the left hand side and the first term on the right represent the change in inertia times velocity. The second term (in square brackets) represent forces due to gradients in pressure and gravitational potential, and the last term on the right is the effect of background expansion.

The previous equations can be manipulated using the EoS of the fluid and the background continuity equation (2.17) to write them more conveniently as

$$\dot\delta = 3\mathcal{H}\left(w\delta - \frac{\delta p}{\bar\rho}\right) + (1+w)(\nabla^2 v + 3\dot\Phi)\,, \tag{3.41}$$

and

$$\dot v = -\mathcal{H}(1-3w)v - \frac{\dot w}{1+w}v + \frac{\delta P}{\bar\rho(1+w)} + \frac{2}{3}\frac{w}{1+w}\nabla^2\Pi + \Psi\,, \tag{3.42}$$

where we have used (3.34) to write $v_i = -\partial_i v$.

3.1.7 Einstein equations for scalar perturbations

We have all the ingredients for writing down the perturbation equations for scalar, vector, and tensor perturbations, which we now that at the linear level do not mix. Here, we are interested in the scalar perturbations only. Using the perturbed Einstein tensor (3.13) and the perturbed stress-energy tensor (3.25) we can finally write the perturbed Einstein equations $\delta G^\mu_\nu = 8\pi G \delta T^\mu_\nu$. For the scalar perturbations they read

$$-\nabla^2\Phi + 3\mathcal{H}(\dot\Phi + \mathcal{H}\Psi) = -4\pi G_N a^2 \delta\rho \qquad (00)\,, \tag{3.43}$$

$$\partial_i(\dot\Phi + \mathcal{H}\Psi) = -4\pi G_N a^2(\bar\rho + \bar P)v_i \qquad (0i)\,, \tag{3.44}$$

$$\ddot\Phi + \mathcal{H}(2\dot\Phi + \dot\Psi) + (2\dot{\mathcal{H}} + \mathcal{H}^2)\Psi + \frac{1}{3}\nabla^2(\Psi - \Phi) = 4\pi G_N a^2 \delta P \qquad (ii)\,, \tag{3.45}$$

$$\partial_i\partial_j(\Phi - \Psi) = 8\pi G_N a^2 \bar P \Pi_{ij} \qquad (ij)\,. \tag{3.46}$$

We can use the $(0i)$ equation for simplifying the first one. Since in Fourier space the velocity is written as $v_i = -\partial_i v/k$, the $(0i)$ equation implies that

$$(\dot\Phi + \mathcal{H}\Psi) = 4\pi G_N a^2(\bar\rho + \bar P)\frac{v}{k} \qquad (0i)\,. \tag{3.47}$$

Substituting this expression in the (00) component, in Fourier space (3.43) reads

$$-k^2\Phi = 4\pi G_N a^2 \rho D \qquad (00)\,, \tag{3.48}$$

where we have introduced the comoving-gauge density variable

$$\rho D \equiv \delta\rho + 3\mathcal{H}(\bar\rho + \bar P)\frac{v}{k}\,. \tag{3.49}$$

Let us now consider the spatial components (3.45) and (3.46). We note that in the case of perfect fluids ($\Pi_{ij} = 0$) both Bardeen potentials coincide, while in general this is not true, $\Phi \neq \Psi$. Then, we can physically interpret their relative difference as a measure of the anisotropic stress present in the fluid. Since $\Pi_{ij} = \partial_i\partial_j\Pi$ for $i \neq j$, (3.46) implies that

$$\Phi - \Psi = 8\pi G_N a^2 \bar P \Pi \qquad (ij)\,. \tag{3.50}$$

Then, for scalar perturbations we have a set of four independent equations (4 Einstein or 2 Einstein plus 2 conservation laws) and six variables, namely $\{\Phi, \Psi, \delta, v, \pi_L, \Pi\}$. In order to obtain a closed system, we must provide two additional equations. The simplest prescription is to consider a perfect fluid, $\Pi_{ij} = 0$, which implies that we have only one degree of freedom in the scalar metric perturbation

$$\Phi = \Psi\,. \tag{3.51}$$

The final closure relation comes from relating pressure and density perturbations. In general, this is given by

$$\delta P = c_s^2\left[\delta\rho - 3(\bar\rho + \bar P)\mathcal{S}\right]\,, \tag{3.52}$$

where $\mathcal{S} \equiv \mathcal{H}(\delta P/\dot{\bar P} - \delta\rho/\dot{\bar\rho})$ is the total entropy perturbation, and

$$c_s^2 = w - \frac{\dot w}{3\mathcal{H}(1+w)}\,, \tag{3.53}$$

is the adiabatic sound speed of the fluid. Then, in the case of adiabatic fluids, or more precisely, adiabatic density perturbations[1], (3.52) implies that pressure and density fluctuations are related by

$$\delta P = c_s^2 \delta\rho \,. \tag{3.54}$$

For matter and radiation the adiabatic sound speeds are $c_s^2 = 0$ and $c_s^2 = 1/3$, respectively. Physically, a vanishing sound speed implies that density perturbations in the fluid will not propagate, allowing it to cluster. On the other hand, if $c_s^2 \neq 0$ then the cosmic fluid is capable of supporting waves which propagate due to local gradients in density and pressure. This implies the existence of a sound horizon, namely, a scale below which the matter perturbations cannot growth due to the counteracting pressure force, and thus they are instead forced to oscillate in time. This crossover scale is usually quantified by the Jeans length

$$\lambda_J = c_s \sqrt{\frac{\pi}{G_N \bar{\rho}}} \,, \tag{3.55}$$

where $\lambda = 2\pi/k$ is the wavelength of the perturbation. At large scales, i.e. $k < k_J$, gravity dominates over pressure and matter is able to cluster due to gravitational instability. When the wavenumber approaches k_J the clustering process becomes increasingly difficult due to the counteracting pressure, and at scales inside the sound horizon, i.e. $k > k_J$, the counteracting pressure is able to support waves and the perturbations can no longer grow. Instead of growing with time they behave oscillatory, just as in the process of baryon acoustic oscillations which took place in the early universe.

3.2 Evolution of linear density perturbations

Instead of going into a detailed discussion of how to solve (3.41) in order to obtain the evolution of density perturbations in different scenarios, we will introduce the concept of transfer functions. Let us start by writing down the evolution equation (3.41) in terms of the comoving-gauge density variable D. Combining (3.41) and (3.42), using (3.52) for the adiabatic case, after a Fourier transform and some manipulations we can obtain the second order differential equation governing the evolution of D [39]

$$\ddot{D} + (1 + 3c_s^2 - 6w)\mathcal{H}\dot{D} - \left[\frac{3}{2}\mathcal{H}^2\left(1 + 8w - 3w^2 - 6c_s^2\right) - c_s^2 k^2\right] D = 0 \,. \tag{3.56}$$

The fact that this is a second order differential equation in the time coordinate τ implies two things. First, this equation has in general two solutions

$$D(\tau, k) = D_1(\tau, k) + D_2(\tau, k) \tag{3.57}$$

representing growing and decaying modes, respectively. Since we are interested in the clustering of matter, we discard the decaying mode and focus our attention in the growing one, usually called linear growth rate and denoted by D_1. It can be shown that dark matter

[1] In cosmology, it is customary to speak about adiabatic perturbations referring to perturbations which were initially adiabatic. Such perturbations do not usually stay adiabatic as the universe evolves.

perturbations grow logarithmically with the scale factor during radiation domination (i.e. in the early universe) and when matter domination starts they grow linearly (hence the name for D_1). This era spans most of the universe history, and most of the cosmic structures that we see today forms during it. Finally, in the late universe dark energy eventually takes over, and even if virialized structures are already decoupled from the cosmic expansion, the growth rate of matter perturbations is suppressed with respect to matter domination era.

In terms of (3.56) we can explicitly identify modes below and above the sound horizon by analyzing the sign of the term in square brackets. We assert that

$$k << \mathcal{H}/c_s \quad \text{modes above sound horizon (can grow).} \tag{3.58}$$
$$k >> \mathcal{H}/c_s \quad \text{modes below sound horizon (cannot grow).} \tag{3.59}$$

Then, when a mode is above the sound horizon the fluid may cluster and form structures, but if the mode falls inside it then the perturbations cannot grow due to pressure support. In this picture the Hubble horizon plays an analogous role by establishing a causal horizon above which no perturbation can grow since it is impossible for them to connect larger spacetime regions than $(\mathcal{H}/c)^{-1}$, where c is the speed of light.

The other important consequence of the linear, second order nature of (3.56) is that in the case of adiabatic modes ($\mathcal{S} = 0$), according to linear response theory we can isolate the time dependence in $D(\tau, k)$ and relate its value at a particular time to a single initial metric perturbation by means of a transfer function which evolves (or 'processes') some initial random variable $\Psi_{\rm in}$ up to a given time. In fact, we can do the same for the other physical fields as long as we consider first order perturbation theory. Then, we can write

$$D(\tau, \mathbf{k}) = T_D(\tau, k)\Psi_{\rm in}(\mathbf{k})\,, \tag{3.60}$$
$$V(\tau, \mathbf{k}) = T_V(\tau, k)\Psi_{\rm in}(\mathbf{k})\,, \tag{3.61}$$
$$\Psi(\tau, \mathbf{k}) = T_\Psi(\tau, k)\Psi_{\rm in}(\mathbf{k})\,, \tag{3.62}$$
$$\Phi(\tau, \mathbf{k}) = T_\Phi(\tau, k)\Psi_{\rm in}(\mathbf{k})\,, \tag{3.63}$$

We may regard the statistical (quantum) fluctuations of this primordial field $\Psi_{\rm in}$ as the 'seeds' from which the present observable universe evolved from. The prevailing paradigm for describing this primordial field is the inflationary theory. In the simplest case, its power spectrum is characterized in terms of a spectral index n_s and an amplitude A_s as

$$k^3\langle\Psi_{\rm in}(\mathbf{k})\Psi^*_{\rm in}(\mathbf{k}')\rangle = (2\pi)^3 A_s(k\tau_o)^{n_s-1}\delta(\mathbf{k}-\mathbf{k}')\,. \tag{3.64}$$

Here, we have multiplied by the constant $\tau_o^{n_s-1}$ (the actual comoving size of the horizon) in order to keep A_s dimensionless for any value of n_s. Then, A_s represents the amplitude of the metric perturbations at horizon scales today, $k = 1/\tau_o$. The shape of the power spectrum (3.64) will become relevant when we study the matter power spectrum in Chapter 7.

On the other hand, the actual expressions for the different transfer functions (3.60)-(3.62) depend on the theory of gravity which relates matter and metric degrees of freedom. As we previously discussed, the simplest case is to assume Einstein GR and to neglect the anisotropic stress. Assuming a matter dominated era, the Einstein equations (3.48), (3.47)

and (3.50) transforms into

$$T_D(z,k) = -\frac{2a}{3\Omega_m}\left(\frac{k}{\mathcal{H}_0}\right)^2 T_\Psi \qquad (00)\,, \tag{3.65}$$

$$T_V(z,k) = \frac{2a}{3\Omega_m}\frac{k}{H_0^2}\left(\mathcal{H}T_\Psi + \dot{T}_\Psi\right) \qquad (0i)\,, \tag{3.66}$$

$$T_\Phi(z,k) = T_\Psi(z,k) \qquad (ij)\,, \tag{3.67}$$

where we have used (2.26). From this set of equations we can obtain T_D, T_V and T_Φ as a function of T_Ψ. Furthermore, within the linear approach we can decompose the transfer function T_Ψ for the initial metric perturbation in terms of a growth function G and a time-independent transfer function $T(k)$ as [40]

$$T_\Psi(z,k) = G(a,k)T(k)\,. \tag{3.68}$$

Here, the growth function parametrizes the growth of structures, which is sensitive to the presence of a dark energy component in the energy-density of the Universe (or the fact that our theory of gravity needs to be modified on large scales). Then, in order to encompass a wide class of models, we can adopt the growth index formalism and use a fit for G in terms of the growth index $\gamma(k,a)$ as [41]

$$G(a,k) \equiv \frac{D_1}{a} = \exp\left(\int_1^a da' \frac{\Omega_m(a')^\gamma - 1}{a'}\right)\,, \tag{3.69}$$

where

$$\Omega_m(a) \equiv \frac{\Omega_m a^{-3}}{(H/H_0)^2}\,. \tag{3.70}$$

In ΛCDM, the growth index takes the constant value $\gamma \sim 0.545$, and then G depends only on the scale factor, i.e. $G = G(a)$. In alternative models, however, γ may be both scale and time dependent, and allows to parametrize possible deviations from the standard evolution. In general, the growth factor can either be modified at the background level by considering a different background cosmology, which leads to a different expansion history, or at the perturbative level, where the gravitational potentials might be altered by the presence of extra degrees of freedom in the modified gravity or dark energy model, which ultimately impact the growth rate of dark matter.

Chapter 4

Relativistic Effects in the Large Scale Structure

Relativistic effects in the large scale structure appear naturally if one realizes that when measuring the distribution of galaxies in the universe we do not observe the actual positions, but rather redshifted photons coming from a particular direction in the sky. Then, one obtains the fluctuations in the number of galaxies across the sky in terms of this information by pixelising galaxy maps in bins of redshift and solid angle.

Since the photons experiment several distortions when travelling across the universe, the volume elements constructed using the observed redshift and observed angle might differ from the real physical volume that the observed galaxies actually occupy, and the observed flux and redshift of the source galaxies also differ from their intrinsic properties. Therefore, the observed galaxy number density contains additional contributions arising from the distortion in the observable quantities in comparison to the standard description where galaxies simply trace the underlying matter distribution with a bias factor.

In this Chapter we show a detailed derivation and discussion of the results obtained in Ref. [26] and Ref. [28], which serve as the basis for our analysis in the following Chapters.

4.1 Galaxy number density fluctuations

In order to consistently relate theoretical predictions to observable quantities, we follow the approach discussed in Ref. [26, 28]. The starting point is to consider that in a generic galaxy survey the sky is pixelised in bins of redshifts and solid angles, in which one then count the number of galaxies that lie inside (within a certain luminosity range). In such case, the positions of the source galaxies is determined by a unit directional vector $\hat{\mathbf{n}}(\theta,\varphi) = (\sin\theta\cos\varphi, \sin\theta\sin\varphi, \cos\theta)$ and a given redshift z. Then, one can construct a quantity that measures the overdensity in the number of galaxies in the sky when observing in a particular

direction $\hat{\mathbf{n}}$ at some redshift z as

$$\Delta(z,\hat{\mathbf{n}}) \equiv \frac{N(z,\hat{\mathbf{n}}) - \overline{N}(z)}{\overline{N}(z)}\,, \tag{4.1}$$

where $N(z,\hat{\mathbf{n}})$ is the number of galaxies detected in a pixel centered at $(z,\hat{\mathbf{n}})$ of size dz and solid angle $d\Omega$, and $\overline{N}(z)$ correspond to its average over all directions in the sky at a fixed redshift. Since we want to relate the *observed* density variable $\Delta(z,\hat{\mathbf{n}})$ to the *underlying* dark matter overdensity, we express the number of galaxies as $N(z,\hat{\mathbf{n}}) = \rho(z,\hat{\mathbf{n}})V(z,\hat{\mathbf{n}})$, where ρ is the galaxy number density and V the volume of a pixel. Then, we can expand both ρ and V around their background values at a given redshift as

$$\rho(z,\hat{\mathbf{n}}) = \bar{\rho}(z) + \delta\rho(z,\hat{\mathbf{n}})\,, \tag{4.2}$$
$$V(z,\hat{\mathbf{n}}) = \bar{V}(z) + \delta V(z,\hat{\mathbf{n}})\,, \tag{4.3}$$

which substituted into (4.1) yields, up to first order,

$$\Delta(z,\hat{\mathbf{n}}) = \frac{\delta\rho}{\bar{\rho}} + \frac{\delta V}{\bar{V}}\,. \tag{4.4}$$

Now, we can also consider fluctuations in the observed redshift with respect to a background redshift, i.e. $z = \bar{z} + \delta z$, so that we can write a Taylor expansion for the density term appearing in the denominator as

$$\bar{\rho}(z) \approx \bar{\rho}(\bar{z}) + \frac{d\bar{\rho}}{d\bar{z}}\delta z = \bar{\rho}(\bar{z}) + 3\frac{\delta z}{(1+\bar{z})}\,, \tag{4.5}$$

where we have used that in the background universe the matter density evolves as $\bar{\rho}(\bar{z}) \propto a^{-3} \propto (1+\bar{z})^3$. Using this expansion in (4.4) and identifying the matter density fluctuation as

$$\delta(z,\hat{\mathbf{n}}) \equiv \frac{\rho(z,\hat{\mathbf{n}}) - \bar{\rho}(\bar{z})}{\bar{\rho}(\bar{z})}\,, \tag{4.6}$$

one finds that the observed matter fluctuation is given up to first order by

$$\Delta(z,\hat{\mathbf{n}}) = \delta_z(z,\hat{\mathbf{n}}) + \frac{\delta V(z,\hat{\mathbf{n}})}{\overline{V}}\,, \tag{4.7}$$

where we have defined

$$\delta_z(z,\hat{\mathbf{n}}) \equiv \delta - 3\frac{\delta z}{1+z}\,. \tag{4.8}$$

The previous equation shows that Δ is not only connected to the underlying dark matter distribution but it is also sensitive to possible fluctuations in the observed redshift and observed volume of each pixel. The last two contributions are a direct consequence of the perturbed photon propagation; they are encoded in the time component ($\mu = 0$) and spatial components ($\mu = i$) of the geodesic equation, respectively. In particular, the observed volume element is constructed in terms of the observed redshift and angles in a homogeneous universe, while the real physical volume element needs to be constructed by tracing backwards the photon geodesic in an inhomogeneous universe.

4.2 Photon propagation in a perturbed Friedmann Universe

Since the FLRW universe in the $K = 0$ case is conformally flat as shown in (3.2), the null geodesics are straight lines. However, when departing from this background, photons travelling through a inhomogeneous universe towards our detectors follow perturbed trajectories, resulting in various observable effects. In this analysis we consider the metric in the full representation (3.5), i.e. without fixing the gauge, so we can distinguish physically measurable quantities.

Let us study the motion of massless particles in the perturbed universe. In any metric theory of gravity, the trajectories $x^\mu = (\tau, x^1, x^2, x^3)$ followed by particles are solutions to the geodesic equation

$$\frac{dn^\mu}{d\tau} + \Gamma^\mu_{\alpha\beta} n^\alpha n^\beta = 0\,, \tag{4.9}$$

where

$$n^\mu = \frac{dx^\mu}{d\lambda} \tag{4.10}$$

is the vector tangent to the particle trajectory, and λ is the affine parameter. Since we are interested in photons, one also need to consider the dispersion relation for massless particles $n^\mu n_\mu = 0$, or equivalently

$$ds^2 = g_{\mu\nu} dx^\mu dx^\nu = 0\,, \tag{4.11}$$

which characterizes the null geodesics and serves as a constraint for the photon momenta. Notice that the four-momenta of particles are usually denoted by k^μ, but in order to avoid confusion we reserve the letter k for the wavenumber appearing later in Fourier transforms.

Instead of directly studying the photon propagation in the perturbed FLRW universe, we can exploit the fact that null geodesics are conformally invariant. Since this kind of geodesic satisfies the null condition $ds^2 = 0$, we can always use a conformally related metric $\hat{g}_{\mu\nu} = a^2 g_{\mu\nu}$ and still automatically satisfy the null geodesic condition in this spacetime, i.e. $d\hat{s}^2 = 0$. This means that both metrics share the same families of null geodesics $\hat{x}^\mu(\hat{\lambda}) = x^\mu(\lambda)$, which only differ on the affine parameter used to describe them, related by $\lambda = a\hat{\lambda}$. This simple observation allows us to swap our FLRW background universe for Minkowski spacetime, which is particularly convenient since it has a reference frame where all Christoffel symbols vanish.

Then, splitting terms as background plus first order contributions, at zeroth order (4.9) reduces to

$$\frac{d\bar{n}^\mu}{d\lambda} = -\bar{\Gamma}^\mu_{\alpha\beta} \bar{n}^\alpha \bar{n}^\beta = 0\,. \tag{4.12}$$

Then, the components of $\bar{n}^\mu = (\bar{n}^0, \bar{n}^i)$ are constant along the photon trajectories. Since we also have the condition for massless particles $\bar{n}^\mu \bar{n}_\mu = -(\bar{n}^0)^2 + \bar{n}^i \bar{n}_i = 0$, the background four-momenta can be chosen such that

$$\bar{n}^0 = 1, \qquad \bar{n}^i \bar{n}_i = 1\,. \tag{4.13}$$

Next, for the first order part of the geodesic equation (4.9) we have

$$\frac{d\delta n^\mu}{d\lambda} = -\delta\Gamma^\mu_{\alpha\beta}\bar{n}^\alpha\bar{n}^\beta\,, \tag{4.14}$$

which can be directly integrated between some initial and final values of the affine parameter

$$\delta n^\mu = \int_{\lambda_i}^{\lambda_f} d\lambda\delta\Gamma^\mu_{\alpha\beta}\bar{n}^\alpha\bar{n}^\beta\,. \tag{4.15}$$

In general, we are interested in computing fluctuations between the source position $r = r_s$, parametrized by $\lambda_i = 0$, and the observer position $r = 0$, parametrized by $\lambda_f = r_s$. We will use the result (4.15) exhaustively in the following discussion.

4.2.1 Calculation of redshift fluctuations

We now focus our attention in the calculation of the redshift fluctuation δz appearing in (4.7), which is connected to the observed frequency of the incoming photons. We know that the temperature of a black body distribution is proportional to the average frequency of photons ω. If they are emitted by a body moving with velocity u_μ relative to us, the temperature we measure is proportional to $-n^\mu u_\mu = \omega$, where n^μ is the four-momentum of incoming photons. Then, if a photon is emitted at the time τ_s and it is received at τ_o, the emission (intrinsic) temperature T_s and the observed temperature T_o are related to each other via

$$\frac{T_o}{T_s} = \frac{\omega_o}{\omega_s} = \frac{(n^\mu u_\mu)_o}{(n^\mu u_\mu)_s} = \frac{a(\tau_s)}{a(\tau_o)} = \frac{1}{1+z}\,, \tag{4.16}$$

where $a(\tau_s)$ and $a(\tau_o)$ are the scale factors of the universe at the time of emission and observation, respectively. Taking variations on both sides and rearranging terms we obtain that the redshift fluctuation is given in terms of the four velocity of the fluid and photon momentum as

$$\delta z = -(1+z)\left[\frac{\delta(n^\mu u_\mu)}{(n^\mu u_\mu)}\right]_s^o\,. \tag{4.17}$$

Expanding the last factor up to first order, and lowering indexes so that $u_0 = g_{0\nu}u^\nu = -(1+A)$ and $u_i = g_{i\nu}u^\nu = -B_i + v_i$, we find that the redshift fluctuation is given by

$$\delta z = -(1+z)\left[\delta n^0 + A + \bar{n}^i B_i - \bar{n}^i v_i\right]_s^o\,. \tag{4.18}$$

This last equation shows that redshift fluctuations depends on perturbations in the time component of the photon four-momenta, δn^0. Its expression in terms of the metric perturbations is derived using (4.15). Substituting back into (4.18) and using the explicit form for A, after some calculations (see Appendix B) we arrive at our final expression for the redshift fluctuation

$$\delta z = -(1+z)\left[-\Psi|_s^o + \mathbf{V}\cdot\mathbf{n}|_s^o - \int_s^o d\lambda(\dot{\Phi}+\dot{\Psi})\right]\,, \tag{4.19}$$

where $V \equiv v - k^{-1}\dot{H}_T$ is the gauge invariant velocity potential. This result coincides with that of [26] when working in the Newtonian gauge. The first term appearing in (4.19) is the Sachs-Wolfe (SW) effect, while the last one is known as the integrated Sachs-Wolfe (ISW) effect for

obvious reasons, though they probe different physics. Finally, the $\mathbf{V}\cdot\mathbf{n}$ term correspond to a dipole contribution.

Now we can go back to the matter density fluctuation (4.7) and make use of the result (4.19). In this way we find

$$\delta_z(z,\hat{\mathbf{n}}) = D_s - 3\mathbf{V}\cdot\hat{\mathbf{n}} + 3\Psi + 3\int_0^r dr'(\dot{\Phi}+\dot{\Psi})\,. \tag{4.20}$$

Here, D_s and V correspond to gauge invariant variables describing the galaxy density and peculiar velocity in the longitudinal gauge, respectively (see Appendix A).

4.2.2 Calculation of volume fluctuations

The next step to obtain $\Delta(z,\hat{\mathbf{n}})$ in terms of observable quantities is computing the volume fluctuation $\delta V(z,\hat{\mathbf{n}})$ appearing in (4.7), which is naturally related to the spatial components of the geodesic deviation, i.e. we need the spatial deviations in the photon trajectories δx^i, which are obtained through the spatial components of the geodesic equation. To see this connection we start by writing the volume element in terms of the photon geodesic, the four velocity u^μ and the observation coordinate system $(\theta_o,\phi_o)\equiv(\theta,\phi)$. This is given by [24]

$$\begin{aligned} dV &= \sqrt{-g}\varepsilon_{\mu\nu\alpha\beta}u^\mu\frac{\partial x^\nu}{\partial z}\frac{\partial x^\alpha}{\partial\theta_s}\frac{\partial x^\beta}{\partial\phi_s}|J|dzd\theta_o d\phi_o \\ &\equiv v(z,\theta_o,\phi_o)dzd\theta_o d\phi_o\,, \end{aligned} \tag{4.21}$$

where $|J|$ is the determinant of the Jacobian of the coordinate transformation going from the angles at the source (θ_s,ϕ_s) to the angles at the observer (θ_o,ϕ_o), and $\varepsilon_{\mu\nu\alpha\beta}=\varepsilon_{[\mu\nu\alpha\beta]}$ is the Levi-Civita symbol. In the second line of (4.21) we have introduced the density v which determines the actual volume perturbation appearing in (4.7), i.e.

$$\frac{\delta V}{\bar{V}} = \frac{v(z)-\bar{v}(z)}{\bar{v}(z)} = \frac{\delta v}{\bar{v}}\,. \tag{4.22}$$

As previously discussed, in a homogeneous and isotropic FLRW universe, photons propagates on straight lines, so that $\theta_o=\theta_s$ and $\phi_o=\phi_s$. However, in the perturbed universe the observation and emission angles do not coincide. We can write the fluctuation in the observation angles up to first order as

$$\theta_s = \theta_o + \delta\theta\,, \tag{4.23}$$

$$\phi_s = \phi_o + \delta\phi\,. \tag{4.24}$$

Then, the volume element v defined in the second line of (4.21) is given by (see Appendix B for detailed calculations)

$$v(z) = a^3(1+A+3H_L)\left[\frac{dr}{dz}r^2\sin\theta_s\left(1+\frac{\partial\delta\theta}{\partial\theta}+\frac{\partial\delta\phi}{\partial\phi}\right)-\left(A\frac{d\bar{r}}{d\bar{z}}+v_r\frac{d\tau}{dz}\right)\bar{r}^2\sin\theta_o\right]\,. \tag{4.25}$$

In addition to the first order expansions (4.23) and (4.24), we can write the perturbation in the comoving distance as $r = \bar{r} + \delta r$. Then, after some calculations (4.25) becomes

$$v(z) = \frac{a^4 \bar{r}^2 \sin\theta}{\mathcal{H}} \times \left[1 + 3H_L + \left(\cot\theta + \frac{\partial}{\partial\theta}\right)\delta\theta + \frac{\partial\delta\phi}{\partial\phi} - \mathbf{v}\cdot\mathbf{n} + 2\frac{\delta r}{r} - \frac{d\delta r}{d\lambda} + \frac{1}{\mathcal{H}(1+\bar{z})}\frac{d\delta z}{d\lambda}\right] . \tag{4.26}$$

where we have dropped the subscript for θ_o and ϕ_o (herein after these coordinates are just θ and ϕ). According to (4.22), for obtaining the actual fluctuation in the volume element we need to subtract the unperturbed part $\bar{v}(z)$. Writing the observed redshift as a perturbation with respect to a background quantity as $z = \bar{z} + \delta z$, the second term in the numerator of (4.22) can be expanded in Taylor series. We find that the volume element perturbation up to first order is given by

$$\frac{\delta v}{\bar{v}} = \left(\frac{\delta v}{v}\right)_\Omega + 3H_L - \mathbf{v}\cdot\mathbf{n} + 2\frac{\delta r}{r} - \frac{d\delta r}{d\lambda} + \frac{1}{\mathcal{H}(1+\bar{z})}\frac{d\delta z}{d\lambda} - \frac{1}{1+\bar{z}}\left(-4 + \frac{2}{r\mathcal{H}} + \frac{\dot{\mathcal{H}}}{\mathcal{H}^2}\right)\delta z\,, \tag{4.27}$$

where we have defined the angular part of the volume perturbation as

$$\left(\frac{\delta v}{v}\right)_\Omega \equiv \left(\cot\theta + \frac{\partial}{\partial\theta}\right)\delta\theta + \frac{\partial\delta\phi}{\partial\phi}\,. \tag{4.28}$$

Then, in order to construct the final expression for the volume perturbation (4.27) in terms of observable quantities we need to compute every perturbation appearing in the right hand side of the above equations. We have already computed the redshift fluctuation δz in (4.19), so we are left with the spatial fluctuations δr, $\delta\theta$ and $\delta\phi$.

In order to express quantities in terms of the perturbed metric and peculiar velocities we need to compute the deviation $\delta x^\mu(\lambda) = x^\mu(\lambda) - \bar{x}^\mu(\lambda)$. In the spherical coordinate system in which we perform the observation this translates into

$$\delta r \equiv \delta x^i e_{ri}\,, \tag{4.29}$$

$$\delta\theta \equiv \frac{\delta x^i e_{\theta i}}{r_s}\,, \tag{4.30}$$

$$\delta\phi \equiv \frac{\delta x^i e_{\phi i}}{r_s \sin\theta}\,. \tag{4.31}$$

As we mentioned, we have already dealt with the time component of the perturbed photon propagation n^0 in the derivation of (4.19). Then, for obtaining the spatial components of the deviation we can conveniently use the following expression

$$\frac{dx^\mu}{d\tau} = \frac{dx^\mu}{d\lambda}\frac{d\lambda}{d\tau} = \frac{n^\mu}{n^0}\,, \tag{4.32}$$

which can be integrated on both sides from the emission time τ_s to the observation time τ_o. Separating the time and spatial components and recalling that the affine parameter is chosen such that $r(\lambda = 0) = r_s$ and $r(\lambda = r_s) = 0$, up to first order we find that

$$x^0(\tau_s) = \tau_s - \tau_o = r_s, \tag{4.33}$$

$$x^i(\tau_s) = (\tau_s - \tau_o)\bar{n}^i - \int_0^{r_s} d\lambda(\delta n^i - \bar{n}^i\delta n^0). \tag{4.34}$$

In the second equation, the integral is carried out along the unperturbed photon path, which is adequate within the first order regime (which is known as Born approximation). Then, after computing δn^i using (4.15), the spatial fluctuation δx^i is given by

$$\delta x^i = \int_0^{r_s} dr\left(h_{i\alpha}\bar{n}^\alpha + h_{0\alpha}\bar{n}^i\bar{n}^\alpha\right) + \frac{1}{2}\int_0^{r_s} dr(r_s - r)\left(h_{\alpha\beta,i} + \dot{h}_{\alpha\beta}\bar{n}^i\right)\bar{n}^\alpha\bar{n}^\beta\,. \tag{4.35}$$

We can now compute $\delta r \equiv \delta x^i e_{ri} = -\delta x^i \bar{n}_i$. Then, after some calculations (see Appendix B) we find

$$\delta r = \int_0^{r_s} dr(\Psi + \Phi) + \frac{B}{k} + \frac{1}{k^2}\left(\frac{dH_T}{d\lambda} - 2\dot{H}_T\right)\,. \tag{4.36}$$

Similarly, for computing the angular perturbations $\delta\theta$ and $\delta\phi$ using (4.30) and (4.31) we take into account that $\bar{n}^i e_{\theta i} = \bar{n}^i e_{\varphi i} = 0$ since the background geodesics are radial. Hence, projecting (4.35) we find that

$$\delta\theta = \frac{1}{r_s}\int_0^{r_s} dr\frac{(r_s - r)}{r}\partial_\theta(h_{\alpha\beta}\bar{n}^\alpha\bar{n}^\beta) + \frac{1}{r_s}\int_0^{r_s} dr\frac{1}{r}h_{i\alpha}e^i_\theta\bar{n}^\alpha\,. \tag{4.37}$$

Analogously for the azimuthal projection we have

$$\delta\varphi = \frac{1}{r_s\sin^2\theta}\int_0^{r_s} dr\frac{(r_s - r)}{r}\partial_\varphi(h_{\alpha\beta}\bar{n}^\alpha\bar{n}^\beta) + \frac{1}{\sin\theta}\int_0^{r_s} dr\frac{1}{r}h_{i\alpha}e^i_\theta\bar{n}^\alpha\,. \tag{4.38}$$

Notice that the displacements δr, $\delta\theta$ and $\delta\varphi$ are all gauge dependent and hence not measurable by themselves. Finally, substituting the expressions for the angular fluctuations (4.37) and (4.38) we find that the angular volume fluctuation, after some calculations, is

$$\left(\frac{\delta v}{v}\right)_\Omega = -\frac{1}{r_s}\int_0^{r_s} d\lambda\frac{(r_s - r)}{r}\Delta_\Omega(\Phi + \Psi) - \frac{\Delta_\Omega H_T(\tau_s)}{k^2 r_s^2}\,. \tag{4.39}$$

We identify the first term appearing in the previous equation is the standard expression for weak gravitational lensing in a perturbed FLRW universe [42]. Since this effect depends only on the angular fluctuations of the metric perturbations along the line-of-sight, it is clear that a constant gravitational field results in no observable effect.

4.3 The observed matter overdensity variable

We can now add up all the terms for obtaining the total volume perturbation. Combining the result (4.39) with (4.27) and the previous expressions we obtain our final result for the observed overdensity of matter,

$$\begin{aligned}\Delta(z,\hat{\mathbf{n}}) = {} & D_s + \frac{1}{\mathcal{H}}\partial_r(\mathbf{V}\cdot\mathbf{n}) + \frac{1}{\mathcal{H}}\dot{\mathbf{V}}\cdot\mathbf{n} + \left(\frac{\dot{\mathcal{H}}}{\mathcal{H}^2} + \frac{2}{r\mathcal{H}} - 1\right)\mathbf{V}\cdot\mathbf{n} + \frac{1}{\mathcal{H}}\partial_r\Psi \\ & - \frac{1}{r_s}\int_0^{r_s} d\lambda\frac{r_s - r}{r}\Delta_\Omega(\Phi + \Psi) + \left(\frac{\dot{\mathcal{H}}}{\mathcal{H}^2} + \frac{2}{r\mathcal{H}}\right)\left(\Psi + \int_0^{r_s} d\lambda(\dot{\Phi} + \dot{\Psi})\right) \\ & + \frac{2}{r_s}\int_0^{r_s} dr(\Phi + \Psi) + \Psi - 2\Phi + \frac{1}{\mathcal{H}}\dot{\Phi}\,.\end{aligned} \tag{4.40}$$

Here, the first term on the right hand side correspond to the true fluctuation in the distribution of matter, related to the fact that baryons trace the underlying dark matter distribution (up to a bias factor). As our previous derivation shows, all other terms in (4.40) represent distortions in the observed redshift and incoming direction of photons, i.e. in the coordinate system in which we are making our observations. The second term in the first line of (4.40) correspond to the Redshift-space distortion effect, which depends on the spatial gradient of peculiar velocities projected along the line-of-sight [19]. The second and third terms in the first line of (4.40) correspond to Doppler effect (analogous to sound waves) which depends directly on $\mathbf{V}$ projected along the line-of-sight. The rest of terms depend on the metric perturbations Ψ and Φ. The first effect in the second line of (4.40) correspond to weak gravitational lensing, as noted after (4.39). This set of effects is known as the *standard effects*.

The remaining terms are directly proportional to the Bardeen potentials Φ and Ψ, and represent the so-called *relativistic effects*[1]. These depend either locally on the source redshift z, such as gravitational redshift and Sachs-Wolfe effect, or are integrated from source to observer along the line-of-sight, similar to gravitational lensing. Following the convention adopted in the literature [26, 43] we group the first class of effects as *local potential terms*, while the integrated terms correspond to the Shapiro time-delay effect (third line) and the Integrated Sachs-Wolfe effect. The former reflects the fact that photons takes longer to travel through potential wells compared to flat space, which implies that we receive them slightly delayed and consequently more redshifted. The ISW effect on the other hand shows that photons can gain or lose energy (and hence redshift) due to the time evolution of the scalar potentials as they travel from the source up to $z = 0$.

The relativistic effects are suppressed by a factor $(\mathcal{H}/k)^2$ with respect to the leading terms as can be seen from Poisson equation (3.48), and by $\mathcal{H}/k$ with respect to velocities as can be seen from (3.47). Then, the magnitude of these effects is negligible on scales much smaller than the horizon with respect to the standard terms, $k >> \mathcal{H}$, while they become relevant on large scales, $k \sim \mathcal{H}$ (i.e. approaching the horizon).

According to our previous discussion, we can regard the result for the observed galaxy overdensity (4.40) as

$$\Delta(z, \hat{\mathbf{n}}) = \sum_{i=1}^{7} \Delta_i \,, \tag{4.41}$$

[1]In strict sense gravitational lensing is also relativistic in nature, but we will stick to the usual convention.

Symbol	Effect	Scaling	z-dep.	Eq.
Δ_D	Intrinsic clustering	$\left(\frac{k}{\mathcal{H}}\right)^2 \delta g_{\mu\nu}$	local	(4.42)
Δ_z	Redshift-space distortion	$\left(\frac{k}{\mathcal{H}}\right)^2 \delta g_{\mu\nu}$	local	(4.43)
Δ_L	Gravitational lensing	$\left(\frac{k}{\mathcal{H}}\right)^2 \delta g_{\mu\nu}$	integrated	(4.45)
Δ_V	Doppler effect	$\left(\frac{k}{\mathcal{H}}\right) \delta g_{\mu\nu}$	local	(4.44)
Δ_{lp}	Potentials	$\delta g_{\mu\nu}$	local	(4.46)
Δ_{std}	Shapiro time delay	$\delta g_{\mu\nu}$	integrated	(4.47)
Δ_{isw}	Integrated Sachs-Wolfe	$\delta g_{\mu\nu}$	integrated	(4.48)

Table 4.1: Different contributions to the observed matter overdensity 4.40, indicating their scaling and whether the effect is local or it is integrated from observer to source along the line-of-sight.

where the different contributions can be identified as follows:

$$\Delta_D = D_s \,, \tag{4.42}$$

$$\Delta_z = \frac{1}{\mathcal{H}} \partial_r (\mathbf{V} \cdot \mathbf{n}) \,, \tag{4.43}$$

$$\Delta_V = \left(\frac{\dot{\mathcal{H}}}{\mathcal{H}^2} + \frac{2}{r\mathcal{H}} - 1 \right) \mathbf{V} \cdot \mathbf{n} + \frac{1}{\mathcal{H}} \dot{\mathbf{V}} \cdot \mathbf{n} \,, \tag{4.44}$$

$$\Delta_L = -\frac{1}{r_s} \int_0^{r_s} d\lambda \frac{r_s - r}{r} \Delta_\Omega (\Phi + \Psi) \,, \tag{4.45}$$

$$\Delta_{lp} = \frac{1}{\mathcal{H}} \partial_r \Psi + \left(\frac{\dot{\mathcal{H}}}{\mathcal{H}^2} + \frac{2}{r\mathcal{H}} + 1 \right) \Psi - 2\Phi + \frac{1}{\mathcal{H}} \dot{\Phi} \,, \tag{4.46}$$

$$\Delta_{std} = \frac{2}{r_s} \int_0^{r_s} dr (\Phi + \Psi) \,, \tag{4.47}$$

$$\Delta_{isw} = \left(\frac{\dot{\mathcal{H}}}{\mathcal{H}^2} + \frac{2}{r\mathcal{H}} \right) \int_0^{r_s} d\lambda (\dot{\Phi} + \dot{\Psi}) \,. \tag{4.48}$$

A summary of all these contributions is included in Table 4.1, showing their nomenclature, relative scaling and redshift dependence.

Finally, for complementing our discussion we can introduce by hand one last contribution to (4.40) which is useful for practical purposes but it does not arise naturally in the previous derivation (and we will not use it in the following Chapters). By construction, the observed matter overdensity (4.40) does not take into account the fact that real galaxy surveys are limited in magnitude, namely, only galaxies above a given luminosity threshold are detected. Thus, there exist an intrinsic magnification bias, which can be introduced by adding an additional fluctuation to the right hand side of (4.40) as

$$\Delta_{\rm mb} = 5s\kappa \,, \tag{4.49}$$

where s is the effective number count slope and κ is the observed convergence, which contains additional perturbations [23, 25, 26] that can be obtained solving the geodesic deviation equation for following neighbouring rays of a light beam travelling from source to observer.

In Ref. [23] it is shown that the fully relativistic expression for the convergence at linear order reads

$$\kappa = \frac{1}{2r}\int_0^r dr' \frac{r-r'}{r'}\Delta_\Omega(\Phi+\Psi) + \left(\frac{1}{r\mathcal{H}}-1\right)\mathbf{V}\cdot\hat{\mathbf{n}} - \frac{1}{r}\int_0^r dr'(\Phi+\Psi) \qquad (4.50)$$
$$- \left(\frac{1}{r\mathcal{H}}-1\right)\int_0^r dr'(\dot{\Phi}+\dot{\Psi}) - \left(\frac{1}{r\mathcal{H}}-1\right)\Psi + \Phi\,.$$

Combining (4.40), (4.49) and (4.50) we have the full expression for the observed density fluctuations at the linear order including magnification bias. It is worthwhile to emphasize that this result is valid in any metric theory of gravity (e.g. GR, $f(R)$, DGP, etc.), as we have not used any particular equation of motion our derivation. We have only used the fact that the perturbed universe can be described as a departure from the background FLRW metric (i.e. the Cosmological Principle), and that photons travel along null geodesics.

The previous expression for $\Delta(z,\hat{\mathbf{n}})$ given by (4.40) can be further simplified if we restrict to cosmological models in which the particles move along geodesics, i.e. the matter components satisfy the Euler equation

$$\dot{\mathbf{V}}\cdot\hat{\mathbf{n}} + \mathcal{H}\mathbf{V}\cdot\hat{\mathbf{n}} + \partial_r\Psi = 0\,. \qquad (4.51)$$

We note that this can be violated in special classes of scalar-tensor theories, such as chamaleons or symmetrons [44], in which screened objects follow trajectories determined by some effective metric involving the extra scalar field which mediates the fifth force responsible for such mechanism. However, violations to (4.51) are strongly suppressed in most scalar-tensor theories of cosmological interest [43], where modifications to ΛCDM enter only through the different relations between gravitational potentials and matter distribution.

For the rest of the analysis we assume that (4.51) is satisfied. In addition, for the sake of simplicity we will also ignore magnification bias (4.49), i.e. we set $s = 0$ in our work and take (4.40) as our full expression for the observed matter overdensity at linear order.

Chapter 5

The ΛCDM model and alternatives

In the previous Chapters we have settled the theoretical basis of our current cosmological models. We will now discuss the concordance cosmological model, ΛCDM, which has attained such status thanks to a significant and impressive body of observational evidence that continuously supports its theoretical predictions. This standard model is now well established, and there seems to be little room left for any dramatic revision of this paradigm as it has been demonstrated over the last decade how difficult it is to formulate convincing alternatives. We next give an overview of ΛCDM model, discussing its virtues, problems and possible alternatives.

5.1 The Concordance cosmological model

Observations have led to a prevailing cosmological model, now called ΛCDM, which represents one of the major achievements of physics during the XX century. In this paradigm, the Universe is spatially flat at large scales ($K = 0$), the gravitational interaction is described by Einsten's GR, and about 95% of the Universe is composed of dark energy (Λ) and cold dark matter (CDM). The Universe begins ~ 13.8 Gyrs ago with a spacetime singularity, followed by a period of accelerated cosmic expansion which amplifies primordial curvature fluctuations that are adiabatic and gaussian. In the recombination epoch, around $z \sim 1100$ (380,000 yrs), the CMB photons decouple from matter and are free to stream through the universe. After matter starts dominating the background energy density the clustering process becomes efficient, but it is not until $z \sim 20$ (400 millions yrs) that the Dark Ages ends with the formation of the first stars, which begin to form gravitationally bound objects that decouple from the overall cosmic expansion. This leads to a picture of hierarchical structure formation with small-scale structures (like stars and galaxies) forming first and then merging into larger structures (clusters and superclusters of galaxies), thus forming the Cosmic Web. Since matter density decays as the universe expands, around $\mathcal{O}(z) \sim 1$ the negative pressure dark energy component starts to dominate the universe and the growth of structure is suppressed due to the accelerated cosmic expansion.

Many of the key cosmological parameters have been determined to an accuracy of one

or two significant figures. Particularly prominent are measurements of cosmic microwave background (CMB) anisotropies, with the highest precision observations being those of the Planck Satellite [45] which for temperature anisotropies supersede the iconic WMAP results [46]. However, a robust and accurate model of the Universe requires consideration of a range of different types of observation, with complementary probes providing consistency checks, lifting parameter degeneracies, and enabling the strongest constraints to be placed.

The ΛCDM model has survived more than a decade of increasingly stringent precision tests. In many ways the Planck 2015 cosmological results [45] highlight the successes of the ΛCDM model, a summary of which is included in Table 5.1. The good fit of ΛCDM with Planck 2015 data implies that there no convincing evidence for simple extensions to the model yet. Nonetheless, there are still some tensions with other data, particularly those considering observations in the local universe [47], which may give some clues in the near future.

parameter	symbol	68% limits
Physical baryon density today	$\Omega_b h^2$	0.02230 ± 0.00014
Physical cold dark matter density today	$\Omega_m h^2$	0.1188 ± 0.0010
Expansion rate today	H_0	67.74 ± 0.46
Optical depth due to reionization	τ	0.066 ± 0.012
Scalar spectrum index	n_s	0.9667 ± 0.0040
Primordial curvature perturbation	$10^9 A_s$	2.142 ± 0.049
Dark energy density today	Ω_Λ	0.6911 ± 0.0062
Matter density today	$\Omega_m h$	0.3089 ± 0.0062
Age of the Universe (Gyr)	t_0	13.799 ± 0.0021

Table 5.1: Cosmological parameters values for ΛCDM model from Planck 2015, considering the temperature (TT), temperature-polarization spectrum (TE) and the polarization power (EE) power spectra, as well as lensing reconstruction and external data set.

Despite the sequence of observational successes of ΛCDM there is a persistent interest in extending or studying alternatives to this cosmological model. This is motivated by a range of apparently deep theoretical issues, involving questions such as the cosmological constant problem, the particle nature of cold dark matter, the validity of general relativity on large scales, the anomalies in the CMB on small scales, and the predictability and testability of the inflationary paradigm. We next briefly discuss the first issue of the previous list, which is arguably the most common motivation for studying modified dark energy models.

5.1.1 The Cosmological Constant Problem

The success of the ΛCDM model to explain our observable Universe with a high degree of accuracy is in deep contrast with our ignorance about the physical nature of the dark components in the foundations of this model. In one hand, we are still lacking a direct detection of dark matter, and there is still room for some alternatives to the standard cold, non-interacting particle model.

On the other hand, the interpretation of dark energy as a cosmological constant Λ is not completely satisfactory. The so-called Cosmological Constant problem can be divided into two major issues:

1. **The fine-tuning problem**: An estimation of the total vacuum energy density ρ_Λ using particle physics gives a result that is way off the observed value

$$\frac{\rho_\Lambda}{\rho_{\text{obs}}} \sim 10^{120} \,. \tag{5.1}$$

   This discrepancy of 120 orders of magnitude between theoretical expectations and the observational value has been called 'the worst theoretical prediction in the history of physics!' [48]. One may try to overcome this issue by adjusting the 'bare' cosmological constant of the theory, but nonetheless it requires to fix such value with extremely high precision (120 orders of magnitude), i.e. it transforms into a fine-tuning problem since there is no physical reason supporting this ad-hoc choice.

2. **The coincidence problem**: The different scaling of the energy density given by (2.18) implies that at early times the cosmological constant would be negligible, while at later times the density of matter will approach to zero and the Universe will be mostly empty. If Dark Energy were to dominate earlier in the history of the Universe, it is possible that all cosmic structures that we observe today would not have had enough time to form. The fact that the present value of Ω_Λ is comparable to the present matter energy density Ω_m requires some explanation since in principle these two quantities should be unrelated. We can compute the redshift at which both components become equal as

$$z_c = \left(\frac{\Omega_\Lambda}{\Omega_m}\right)^{1/3} - 1 \approx 0.3 \,, \tag{5.2}$$

   which shows that the cross-over happened not to far into the past. The question of *why* the phase of accelerated cosmic expansion began in the late Universe and not before that is sometimes answered just by invoking the Anthropic principle.

The persistence of these issues until today makes the nature of the dark energy one of the most challenging open puzzles in modern cosmology and encourages to revise the standard cosmological model and propose feasible alternatives.

5.2 Alternatives to ΛCDM

The open problems of the standard cosmology leave room to explore alternative theories that aim to describe the cosmic accelerated expansion by other mechanisms. Even if in principle there exist several ways to look for alternatives, all of them ultimately rely on modifying one side of the Einstein equations (2.3), as we have seen that the contribution of the matter-energy content of the universe appears on the right hand side of the Einstein equation, whereas the left hand side represents the geometrical description of the gravitational interaction. Then, one may either argue that GR needs to be modified at large scales (where the cosmic expansion drives the dynamics) or that Λ needs to be replaced by a new kind of

dark energy component. In a fundamental approach, the Einstein Equations of GR can be derived from a least action principle using the action

$$S = \frac{c^4}{16G_N\pi}\int dx^4\sqrt{-g}(R-2\Lambda) + S_M\,, \tag{5.3}$$

where

$$S_{EH} = \frac{c^4}{16G_N\pi}\int dx^4\sqrt{-g}R \tag{5.4}$$

is the so-called Einstein-Hilbert action, which provides the left hand side of (2.1), and S_M accounts for the matter fields appearing in the theory, i.e. it defines $T_{\mu\nu}$. The Einstein-Hilbert action (5.4) represents a minimal one in the sense that the Ricci scalar R appears linearly, but in principle this does not need to be the case.

The study of possible modifications and extensions of this action has received a lot of attention in the last decade as a possible way to explain the accelerated cosmic expansion of our Universe without the need to include Λ in the theory. However, since ΛCDM has proven to be so robust all alternative models are strongly constrained, specially on Solar System scales, where GR has been tested up to a high degree of accuracy. Moreover, the recent 'multimessenger' detection of the binary neutron star merger [49] through a gravitational wave signal (GW170817) followed by a gamma ray burst (GRB170817A) has put strong constraints on the speed of propagation of tensor modes, $|c_T/c-1| < 4.5\times10^{-16}$, thus ruling out a class of dark energy models where $c_T \neq c$ such as quartic/quintic Galileons and Gauss-Bonnet gravity, among others [50].

We next give a non-exhaustive list and a brief description of some of the most popular alternative models:

- $f(R)$ **gravity**: Since there is no a priori reason to consider a gravitational Lagrangian as a linear function of the Ricci scalar as GR does (5.4), this class of theories generalize the action to

$$S = \frac{c^4}{16G_N\pi}\int dx^4\sqrt{-g}f(R)\,, \tag{5.5}$$

  where the function f may include higher order terms built from R and $R_{\mu\nu}$ (and their derivatives), and also minimally and non-minimally coupled terms between scalar fields and geometry, e.g. ϕ^2R. In this class of theories the Einstein equations are now replaced by the field equations

$$f_{,R}R_{\mu\nu} - \frac{1}{2}f(R)g_{\mu\nu} - [\nabla_\mu\nabla_\nu - g_{\mu\nu}\Box]f_{,R} = \frac{8\pi G_N}{c^4}T_{\mu\nu}\,, \tag{5.6}$$

  where $f_{,R} = df/dR$ and $\Box = g^{\mu\nu}\nabla_\mu\nabla_\nu$ is the d'Alembert operator. This proposal is interesting because one may explain the accelerated expansion without the need for dark energy. In addition, it is sufficiently general to include all of the basic features of modified gravity models and make connection with observations. However, since GR works extremely well within the Solar System, the new degrees of freedom need to be somehow hidden at small scales (or high density environments) in order to accommodate the existing constraints. This implies the action of 'screening mechanism', in which

the mass of an effective scalar field degree of freedom depends on the density of its environment. Then, if the matter density is sufficiently high, the field acquires a heavy mass about the potential minimum and it cannot be excited, whereas in low density environments, i.e. large scales, it is capable of driving the accelerated cosmic expansion. The most popular model designed to recover GR sufficiently fast at Solar System scales is the Hu-Sawicki $f(R)$ model [51], which has the form

$$f(R) = -m^2 \frac{c_1 \left(\frac{R}{m^2}\right)^2}{c_2 \left(\frac{R}{m^2}\right)^n + 1}\,, \tag{5.7}$$

where m is a new mass scale related to the scalar field mass.

- **Dvali-Gabadadze-Porrati (DGP) braneworld model**: In this model [15] a 4-dimensional brane is embedded in a 5-dimensional Minkowski bulk with an infinitely large extra dimension. Matter is then confined in the 4-dimensional brane and only gravity can propagate in the 5-dimensional bulk, leaking off the 4-dimensional brane into the 5-dimensional bulk only on large scales. On small scales gravity is effectively bound to the brane and 4-dimensional dynamic is recovered with very good approximation. Then, in this model the gravity leakage leads to the observed late-time cosmic acceleration. The modified Friedmann equation for a flat universe in DGP is

$$H^2 = \pm \frac{H}{r_c} + \frac{8\pi G_N}{3}\rho_m\,, \tag{5.8}$$

where r_c is the crossover scale separating 4D and 5D regimes. Then, we can consider an effective dark energy component with density

$$\rho_{\text{eff}} \equiv \frac{3H}{8\pi G_N r_c}\,, \tag{5.9}$$

which leads to the DGP expansion history. In other words, the cosmic acceleration in this model is not due to the presence of a dark energy component but rather to the weakening of gravity parametrized by r_c. In spite of its attractive features, the DGP model suffers from observational disfavor and ghost instabilities. In addition, SN Ia, BAO and CMB data show that the modified Friedmann equation is less consistent with observations than the standard Friedmann equation from ΛCDM.

- **Quintessence model**: This model suggests that a canonical scalar field ϕ with a potential $V(\phi)$ might be responsible for the late time acceleration. The quintessence model is described by the action:

$$S = \int dx^4 \sqrt{-g}\left[\frac{c^4}{16\pi G_N}R + \mathcal{L}_\phi\right] + S_M\,, \tag{5.10}$$

where $\mathcal{L}_\phi$ is the scalar field Lagrangian given by

$$\mathcal{L}_\phi = -\frac{1}{2}g^{\mu\nu}\partial_\mu\partial_\nu\phi - V(\phi)\,. \tag{5.11}$$

It can be shown that, in order to have an accelerated cosmic expansion, the potential $V(\phi)$ needs to be shallow enough for the field to evolve slowly along with it, i.e. this situation is very similar to inflationary cosmology, and slow-roll conditions must be

satisfied. As a result, quintessence models are very constraint because it is difficult to find a corresponding model in particle physics due to the low energy scale (in the context of particle physics)

$$m_\phi = \sqrt{V''(\phi)} \sim H_0 \sim 10^{-33}\ \text{eV}\,. \tag{5.12}$$

Moreover, such a light scalar field could in principle interact with ordinary matter, which could lead to observable long-range forces and time dependence on the constants of nature [52].

- **Dark energy fluids:** Besides considering scalar fields, an entire class of models exists involving perfect fluids. At background level a perfect fluid is characterized by its equation of state parameter $w(a)$, which gives rise to the generic scaling

$$\rho \propto a^{-3(1+\hat{\omega})}\,, \tag{5.13}$$

where

$$\hat{\omega}(a) = \frac{1}{\ln a}\int_1^a \frac{w(a')}{a'}da'\,. \tag{5.14}$$

There is now the problem to parametrize $w(a)$. As realized from the previous discussions, there are different possibilities: according to the preferred model the equation of state parameter can be a constant (as for the cosmological constant) or it can be a function of time (as for scalar field models). There is no unique general expression for w if we consider the dark energy as being a fluid. The easiest alternative, called the Chevallier-Polarski-Linder (CPL) parametrization [53, 54], is to Taylor expand $w(a)$ around $a_0 = 1$

$$w(a) = w_0 + w_a(1-a)\,, \tag{5.15}$$

where w_0 is the value of the parameter of equation of state today and w_a gives the variation on time of $w(a)$. The values of the parameters are usually assumed to be $w_0 \sim -1$ because observations tell us that the value of the parameter of equation of state today has to be close to -1 and $w_a << 1$ because we do not have any strong evidence that the dark energy varies so much over time. Moreover, the previous expression is very convenient because it also avoids possible complication of having unrealistic behavior. e.g., $w << -1$.

- **Effective field theory of dark energy:** Finally, it is worth to mention the effective field theory (EFT) approach to dark energy [55], which is not a model by itself but rather tries to provide a unified phenomenological description of dark energy and modified gravity, similar to Horndeski theory. It is inspired by the EFT of inflation, with the main difference that in this case matter species are present and coupled to the metric. In this framework one assumes a generic scalar field ϕ in the dark sector, which is responsible for the late time accelerated expansion, and which allows to establish a preferred time foliation (i.e. a 3+1 decomposition of the spacetime). The general gravitational action in this framework is

$$S = \int d^4x\sqrt{-g}\left[\frac{M_*^2}{2}f(t)R - \Lambda(t) - c(t)g^{00}\right] + S_{DE}^{(2)}\,. \tag{5.16}$$

Here, M_* is the 'bare' Planck mass (or bare gravitational Constant), and the time dependant functions f, Λ and c reflect the broken time-invariance due to the (implicit)

presence of the scalar field ϕ, which is behind the mechanism for accelerated expansion but no longer appears in the action (but can be made manifest by performing the so-called Stückelberg trick [56]). In this approach, Λ and c are fixed by the FLRW background model, while f depends on the actual dark energy model. In addition, quadratic and higher-order terms in the perturbations are contained in $S^{(2)}_{DE}$, and will vary from one dark energy model to the other, allowing to effectively describe and match different theories.

Chapter 6

Phenomenological parametrization of dark energy models

We now go beyond ΛCDM by considering alternative dark energy models. As we discussed in Chapter 5, they are an appealing alternative for explaining the late-time accelerated cosmic expansion, although they are very constrained from current observations. Then, since there are no preferred candidates at this point, we choose to parametrize potential deviations from GR in a phenomenological, model independent approach, which is next introduced.

The present Chapter discusses the ideas of Ref. [32] and Ref. [32] which we implement to derive our results in the next Chapters.

6.1 The (Q, η) parametrization

This approach was first discussed in Ref. [32] as a framework that is general enough to represent both modified gravity models and alternative forms of dark energy. The key idea is to introduce two new phenomenological parameters into the Einstein equations (3.48) and (3.51) which directly modify the evolution of the potentials Ψ and Φ to account for possible deviations from ΛCDM.

We know that when dark energy starts dominating the universe the potential Φ starts to decay. Moreover, as we move into the late time universe a generic (non-smooth) dark energy fluid is also able to clump. Then, we can introduce an effective clustering parameter Q which takes into account deviations in Φ from the standard ΛCDM evolution and also parametrizes the additional clustering due to the perturbations in a dark energy fluid, so that the generalized Poisson equation (3.48) becomes

$$-k^2\Phi = 4\pi G_N a^2 Q(a,k)\bar{\rho}_m D_m \,, \tag{6.1}$$

where $D_m = \delta + 3\mathcal{H}V/k$ is the comoving matter density contrast (often denoted by Δ_m). Clearly, this parametrization is such that, if the dark energy or modified gravity model

does not contribute to the gravitational potential (e.g. if the dark energy is a cosmological constant), then $Q = 1$. Otherwise Q will deviate from unity, and in general it is a function of both scale and time. In the context of modified gravity models, the function Q represents a mass screening effect due to local modifications of gravity and effectively modifies Newton's constant, i.e. we can properly interpret $G_{\rm eff}(a,k) \equiv Q(a,k)G_N$ in the previous modified Poisson equation [33, 35].

Furthermore, in order to take into account a general class of modified gravity and dark energy models we also need to allow for a possible non-vanishing anisotropic stress [57]. Then, we can introduce a second parameter to the model, η, this time going into (3.51), as

$$\Psi = [1 + \eta(a,k)]\Phi \,. \tag{6.2}$$

Then, η can be regarded as a gravitational slip parameter which is non-zero only when anisotropic stress is present, implying that the metric perturbations Ψ and Φ are no longer equivalent at some scales and/or times. Currently, there is no sign for a non-vanishing anisotropic stress beyond that generated by the free streaming of photons and neutrinos. However, it is expected to be non-zero in a wide class of theories, such as anisotropic dark energy fluids [58], models including topological defects such as cosmic strings, among others.

By construction, the introduction of two new degrees of freedom in the (Q,η) approach allows to represent a wide class of theories such as $f(R)$ gravity, the DGP model and other scalar-tensor theories. Likewise, it also allows to consider effective dark energy components beyond Λ. In this thesis we will focus our attention in a dynamical, quintessence-like dark energy fluid model which is discussed in the next section.

6.2 Effective dark energy fluid with time-independent properties

A possible alternative to a cosmological constant description is a dark energy fluid which is not necessarily homogeneously distributed in the universe. Namely, dark energy could be a kind of fluid which may also cluster over time, just as matter, and which in general may exhibit some degree of anisotropic stress. We parametrize this kind of fluid by introducing three constants in the model; an equation of state parameter w, a sound speed c_s^2 and a viscosity term c_v^2, which parametrizes the anisotropic stress. Even if most models of dark energy are based on classical scalar fields, in which case no anisotropic stress appears [59], it is nevertheless interesting to consider such a possibility since in fact very little is known about the true nature of dark energy, and new degrees of freedom may eventually arise. Moreover, many modified gravity models present anisotropic stress, and they can be reformulated as effective dark energy fluids.

As we discussed in the previous section, in the context of dark energy fluids the clustering parameter Q appearing in the modified Poisson equation (6.1) can be regarded as describing the possible clustering of the dark energy fluid, i.e.

$$Q = 1 + \frac{\rho_{\rm DE} D_{\rm DE}}{\rho_m D_m} \,, \tag{6.3}$$

where $\rho_{\rm DE}$ represents the dark energy background density (which not necessarily constant in time) and $D_{\rm DE}$ its corresponding density contrast in the comoving gauge, as defined for matter in (3.49). For the class of models in which both sound speed c_s^2 and equation of state parameter w are constant in time, but still may depend on the scale k, the following expression for $Q(a,k)$ has been derived [33]

$$Q(a,k) = 1 + \frac{1-\Omega_m}{\Omega_m}(1+w)\frac{a^{-3w}}{1-3w+\frac{2k^2\hat{c}_s^2 a}{3H_0^2\Omega_m}}\,, \tag{6.4}$$

where, in general, $\hat{c}_s^2$ is regarded as an effective sound speed of the fluid, which is given by

$$\hat{c}_s^2 = c_s^2 + \frac{8}{3}\frac{(c_s^2-w)}{(1+w)}c_v^2\,. \tag{6.5}$$

Here, c_s^2 is the intrinsic sound speed and c_v^2 is a possible viscosity contribution appearing in this dark energy model parameterizing the coupling of the anisotropic stress to the (gauge invariant) velocity perturbation V via

$$w\left(\dot{\Pi}+3\mathcal{H}\Pi\right) = 4c_v^2 kV\,. \tag{6.6}$$

This idea is based on the 'generalized dark matter' concept proposed in [60], and suggest that sound speed and viscosity have a similar damping effect on density perturbations. According to (6.6), this parametrization does not take into account models in which stress fluctuations are not derived from density and velocity perturbations.

The expression for Q in (6.4) shows that in order to cluster, this kind of fluid needs to have an EoS parameter $w \neq -1$. Also, from (6.5) we note that the effect of c_v^2 is enhanced with respect to that of c_s^2 by a factor of $8(c_s^2-w)/3(1+w)$, which is approximately 10 for $w=-0.8$ and very small c_s^2, and then these are the situations where viscosity effects are expected to more clearly observed.

Furthermore, it has been shown that the anisotropy parameter introduced in (6.2) for this particular dark energy fluid model is given by [58]

$$\eta = -\frac{9}{2}H_0^2(1-\Omega_m)(1+w)\frac{a^{-(1+3w)}}{k^2 Q}\left(1-\frac{c_s^2}{\hat{c}_s^2}\right)\,. \tag{6.7}$$

As shown in (6.4) and (6.7), both Q and η grow with the scale factor (in terms of absolute values), and then their effects are more noticeable at late times since dark energy is able to cluster, see Fig 6.1. Various test show that, even assuming a matter dominated Universe, these parametrizations for (Q,η) are well approximated by numerical results even at late times, when dark energy starts dominating [58].

Besides the explicit form for (Q,η), we still need one more input for totally describing our model. As we remarked at the end of Chapter 3, the growth index is also a convenient way of parametrize alternative models. Naturally, in this particular case it becomes modified with respect to ΛCDM due to the presence of dark energy perturbations. In this class of effective

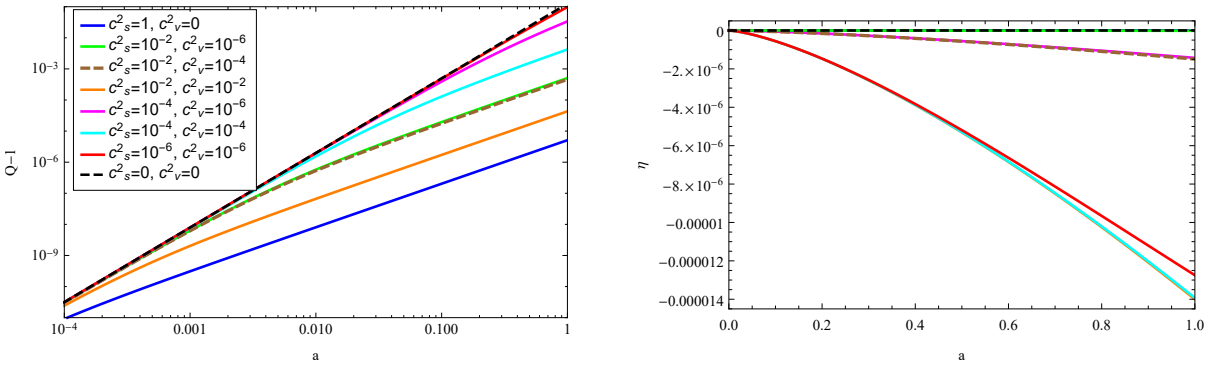

Figure 6.1: Clustering and anisotropy parameters for various combinations of intrinsic and viscous sound speeds. Left: Plot of $Q-1$. Right: Plot of η. All lines correspond to $w=-0.8$ and $k=200H_0$, with $h=0.67$.

fluid models γ depends on the dark energy clustering parameter Q and anisotropy parameter η as [61]

$$\gamma(a,k)=\frac{3}{5-6w}\left(1-w-\frac{(1+\eta)Q-1}{1-\Omega_m(a)}\right)\,, \tag{6.8}$$

where $\Omega_m(a)=\Omega_m a^{-3}H_0^2/H^2$. This implies that the growth function G defined in (3.69) now acquires a k-dependence which is due to the presence of a sound horizon dampening the perturbations below that characteristic scale. While dark energy perturbations themselves are difficult to measure unless dark energy has very low sound speed and viscosity, the growth index on itself has proven to be a more easily detectable parameter and several ongoing and future experiments are built to measure its value [34].

It is worthwhile to classify three characteristic regimes appearing in this particular dark energy fluid model:

1. **The case $c_s^2=c_v^2=0$**

   Naturally, the simplest case in this class of models is to consider negligible viscosity effects, i.e. $c_v^2=0$ which into (6.7) implies a vanishing anisotropic stress, $\eta=0$. If in addition we consider $c_s^2=0$, then the clustering parameter (6.4) as well as the growth index (6.8) depend only on the scale factor, $Q=Q(a)$ and $\gamma(a)$. Then

   $$Q(a)=1+\frac{1-\Omega_m}{\Omega_m}\frac{1+w}{1-3w}a^{-3w}\equiv 1+Q_0a^{-3w}\,. \tag{6.9}$$

   In this case there is no sound horizon, and the perturbations are free to growth at all scales inside the Hubble horizon.

2. **The case $c_s^2\neq 0$ and $c_v^2=0$**

   In this case we allow the dark energy fluid to have a non-vanishing sound speed but we still restrict its viscosity effects so that no anisotropic stress is present, i.e. $\eta=0$. Then, the clustering parameter and growth index are both scale and time dependent,

i.e. $Q = Q(a,k)$ and $\gamma = \gamma(a,k)$. In this scenario the fluid will have a sound horizon set by $\mathcal{H}/c_s$ below which perturbations can no longer grow.

3. **The case $c_s^2 \neq 0$ and $c_v^2 \neq 0$**

   The most general behaviour parametrized by this model is a fluid with a non-vanishing sound speed and also viscosity effects, which contributes to $\hat{c}_s^2$ through the relation (6.5). Then, all three parameters depend on both scale factor and scale, i.e. $\eta(a,k) \neq 0$, $Q = Q(a,k)$ and $\gamma(a,k)$. In this case the dark energy will also have an effective sound horizon set by $\mathcal{H}/\hat{c}_s$ below which pressure support is able to dampen the perturbations.

In the next chapter we will present our power spectrum calculations considering both modified Einstein equations (6.1) and (6.2), so that the result will be valid for any model encompassed by the (Q,η) parametrization. This correspond to consider the third case in the previous list, i.e. we will not make any additional assumptions on the nature of the dark energy fluid discussed in this section.

Chapter 7

Angular power spectrum in dark energy models

One of the most fundamental tools to compare observations against theoretical models of large scale structure having stochastic initial fluctuations are power spectra. They are the 'harmonic transforms' of the two point correlation functions, which are a measure of the degree of clustering in either the spatial or angular distribution of galaxies. If the initial perturbations in the model under consideration are Gaussian (a relatively generic prediction from inflationary models), then the power spectra contain the full statistical information, i.e. there is no need to consider correlation functions of higher orders (such as the bispectrum).

We next focus our attention on writing down a general expression for the matter power spectrum using the full observed density perturbation variable (4.40). At a fixed redshift, Δ is a function on the sphere, so it is most natural to expand it in terms of spherical harmonics as

$$\Delta(z, \hat{\mathbf{n}}) = \sum_{\ell m} a_{\ell m}(z) Y_\ell(\hat{\mathbf{n}}) \,. \tag{7.1}$$

The angular power spectrum C_ℓ then corresponds to the amplitude of the coefficients when Δ is decomposed in such a base of functions, namely

$$\delta_{\ell\ell'}\delta_{mm'} C_\ell = \langle a_{\ell m} a^*_{\ell' m'} \rangle \,, \tag{7.2}$$

where the brackets indicate ensemble average and the star complex conjugation. This statistical quantity has the advantage of being optimally adapted to our coordinate system in which we perform the measurements as it exploits the statistical isotropy upon which the cosmic metric is constructed. The expansion coefficients $a_{\ell m}$ can be computed by inverting the previous expression through the orthogonality property of the spherical harmonics as

$$a_{\ell m}(z) = \int d\Omega_{\hat{\mathbf{n}}} Y^*_{\ell m}(\hat{\mathbf{n}}) \Delta(z, \hat{\mathbf{n}}) \,. \tag{7.3}$$

For calculating these coefficients we consider the fact that according to (4.41)-(4.48) the observed density fluctuation consists in the sum of various terms Δ_i, whose k-dependence are given by either a perturbation variable evaluated at the source position $r_s = \tau_o - \tau_s$

(i.e. at redshift $z = z_s$) or an integral of a perturbation variable over the unperturbed photon trajectory (due to Born approximation). The various variables in these terms are then decomposed in terms of a set of transfer functions, as discussed at the end of Chapter 3, and we use the primordial power spectrum (3.64) in order to calculate the ensemble average in (7.2). The details of the calculations are presented in the Appendix C. The final expression for power spectrum (7.2) is

$$C_\ell(z) = \frac{2A_s}{\pi}\int_0^\infty \frac{dk}{k}(k\tau_0)^{n_s-1}|\Delta_\ell(z,k)|^2\,, \tag{7.4}$$

where

$$\begin{aligned}\Delta_\ell(z,k) = j_\ell(kr_s)\left[T_D + \left(1+\frac{\dot{\mathcal{H}}}{\mathcal{H}^2}+\frac{2}{r_s\mathcal{H}}\right)T_\Psi + T_\Phi + \frac{1}{\mathcal{H}}\dot{T}_\Phi\right] + j'_\ell(kr_s)\left(\frac{\dot{\mathcal{H}}}{\mathcal{H}^2}+\frac{2}{r_s\mathcal{H}}\right)T_V \\ + \frac{k}{\mathcal{H}}j''_\ell(kr_s)T_V + \frac{1}{r_s}\int_0^{r_s} d\lambda j_\ell(k\lambda)\left(2+\frac{r_s-\lambda}{\lambda}\ell(\ell+1)\right)(T_\Psi+T_\Phi) \\ + \left(\frac{\dot{\mathcal{H}}}{\mathcal{H}^2}+\frac{2}{r_s\mathcal{H}}\right)\int_0^{r_s} d\lambda j_\ell(k\lambda)(\dot{T}_\Psi+\dot{T}_\Phi)\,.\end{aligned} \tag{7.5}$$

Here, $j_l(x)$ represents a spherical Bessel function which appear due to the Rayleigh formula for plane waves (see Appendix C), and $j'_\ell(x) \equiv dj_\ell(x)/dx$. In addition, we have already used the Euler equation (4.51) which simplifies some of the terms originally present in (4.40). Now, tracking the various contributions in Δ, we can write $\Delta_\ell = \sum \Delta^i_\ell$, where we identify each one as

$$\Delta^D_\ell = j_\ell T_D\,, \tag{7.6}$$

$$\Delta^z_\ell = \frac{k}{\mathcal{H}}j''_\ell T_V\,, \tag{7.7}$$

$$\Delta^L_\ell = \frac{1}{r_s}\int_0^{r_s} d\lambda j_\ell(k\lambda)\frac{r_s-\lambda}{\lambda}\ell(\ell+1)(T_\Psi+T_\Phi)\,, \tag{7.8}$$

$$\Delta^V_\ell = j'_\ell g T_V\,, \tag{7.9}$$

$$\Delta^{lp}_\ell = j_\ell\left[(g+1)T_\Psi + T_\Phi + \frac{1}{\mathcal{H}}\dot{T}_\Phi\right]\,, \tag{7.10}$$

$$\Delta^{std}_\ell = \frac{2}{r_s}\int_0^{r_s} d\lambda j_\ell(k\lambda)(T_\Psi+T_\Phi)\,, \tag{7.11}$$

$$\Delta^{isw}_\ell = g\int_0^{r_s} d\lambda j_\ell(k\lambda)(\dot{T}_\Phi+\dot{T}_\Psi)\,, \tag{7.12}$$

and $g(z) \equiv \left(\dot{\mathcal{H}}/\mathcal{H}^2 + 2/r_s\mathcal{H}\right)$. Then the total power spectrum C_ℓ is given by

$$C_\ell = \sum_{ij} C^{ij}_\ell\,, \tag{7.13}$$

where ij labels any pair of effects, i.e. it includes autocorrelations as well cross-correlations. Then, the different contributions can be systematically computed as

$$C^{ij}_\ell = \frac{2A_s}{\pi}\int_0^\infty \frac{dk}{k}(k\tau_0)^{n_s-1}\Delta^i_\ell\Delta^j_\ell\,. \tag{7.14}$$

This last set of equations gives the generic structure of the power spectrum, regardless of the relation between the metric and energy-matter degrees of freedom. These expressions depend explicitly on the background cosmology through the expansion terms $\mathcal{H}$, $\dot{\mathcal{H}}$ and the comoving distance r_s, which are given by (2.22), (2.24) and (2.35), respectively.

At the perturbation level, the C_ℓ's depend on the relation among the various transfer functions $\{T_D, T_V, T_\Psi, T_\Phi\}$, which are given by the actual Einstein (or field) equations of the theory.

7.1 Angular power spectrum in the (Q, η) parametrization

The modified Einstein equations in the (Q, η) parametrization (6.1) and (6.2) imply modified relations at the level of transfer functions with respect to GR. It is straightforward to show that the set of relations (3.65)-(3.67) derived from the Einstein equations now takes the form

$$T_D(z,k) = -\frac{2a}{3\Omega_m}\left(\frac{k}{H_0}\right)^2 \frac{T_\Psi}{Q(1+\eta)} \qquad (00)\,, \tag{7.15}$$

$$T_V(z,k) = \frac{2a}{3\Omega_m}\frac{k}{H_0^2}\mathcal{H}\left[\left(1 - \frac{a}{(1+\eta)^2}\frac{\partial\eta}{\partial a}\right)T_\Psi + \frac{a}{1+\eta}\frac{\partial T_\Psi}{\partial a}\right] \qquad (0i)\,, \tag{7.16}$$

$$T_\Phi(z,k) = \frac{T_\Psi}{(1+\eta)} \qquad (ij)\,, \tag{7.17}$$

where we have used the identity

$$\frac{1}{\mathcal{H}}\frac{d}{d\tau} = a\frac{d}{da}\,. \tag{7.18}$$

Naturally, in the case $Q = 1$ and $\eta = 0$ the above set of equations reduces to (3.65)-(3.67). According to our discussion in Chapter 3, we decompose the transfer function T_Ψ for the initial metric perturbation in terms of a growth rate G and a time-independent transfer function $T(k)$ as

$$T_\Psi(a,k) = G(a,k)Q(a,k)T(k)\,, \tag{7.19}$$

where both G and T are influenced by the effective dark energy model. In general, the transfer function at zero redshift $T(k)$ needs to be computed with numerical codes such as MGCAMB[1][62] . Using these expressions we can write the various $C_\ell(z)$'s using our general result (7.14). The autocorrelations of the different contributions, as well as their correlations with density are next given. Notice that we have omitted the (a,k) dependence in most terms to avoid cluttered notation. We also denote $j'_\ell(x) = dj_\ell(x)/dx$ and $\nu = \ell + 1/2$ for the Limber-approximated terms [63].

1. Density:

   The dominant term in the observed matter power spectrum is the intrinsic density fluctuation, which is enhanced by a factor of $(k/\mathcal{H})^2$ with respect to the relativistic

[1] we are explicitly including the factor $Q(a,k)$ in (7.19) so that $T(k)$ correspond to the actual transfer function at $z = 0$ from CAMB codes.

terms (see Table 2.1). The autocorrelation is given by:

$$C_\ell^{DD} = \frac{8A_s\tau_0^{n_s-1}a^2}{9\pi H_0^4\Omega_m^2}\int_0^\infty dk k^{2+n_s}\frac{j_\ell^2(kr_s)G^2T^2(k)}{(1+\eta)^2}\,. \tag{7.20}$$

2. Redshift-space distortion:

   2.1 The autocorrelation is

$$C_\ell^{zz} = \frac{8A_s\tau_0^{n_s-1}a^2}{9\pi H_0^4\Omega_m^2}\times \int_0^\infty dk k^{2+n_s}\left[\left(1-\frac{a}{(1+\eta)^2}\frac{\partial\eta}{\partial a}\right)GQ+\frac{a}{1+\eta}\frac{\partial(GQ)}{\partial a}\right]^2(j_\ell''(kr_s))^2T^2(k)\,. \tag{7.21}$$

   2.2 Correlation between RSD and density:

   This cross-correlation is particularly important since it scales in the same way as the autocorrelations of density and RSD. This is given by

$$C_\ell^{Dz} = -\frac{8A_s\tau_0^{n_s-1}a^2}{9\pi H_0^4\Omega_m^2}\int_0^\infty dk k^{2+n_s}\left[\left(1-\frac{a}{(1+\eta)^2}\frac{\partial\eta}{\partial a}\right)GQ+\frac{a}{1+\eta}\frac{\partial(GQ)}{\partial a}\right] \times\frac{j_\ell(kr_s)j_\ell''(kr_s)GT^2(k)}{(1+\eta)}\,. \tag{7.22}$$

3. Doppler effect:

   3.1 Autocorrelation of Doppler effect is

$$C_\ell^{VV} = \frac{8A_s\tau_0^{n_s-1}a^2}{9\pi H_0^4\Omega_m^2}\left(\frac{\dot{\mathcal{H}}}{\mathcal{H}}+\frac{2}{r_s}\right)^2 \times\int_0^\infty dk k^{n_s}\left[\left(1-\frac{a}{(1+\eta)^2}\frac{\partial\eta}{\partial a}\right)GQ+\frac{a}{1+\eta}\frac{\partial(GQ)}{\partial a}\right]^2(j_\ell'(kr_s))^2T^2(k)\,. \tag{7.23}$$

   3.2 Correlation of Doppler effect and density:

$$C_\ell^{VD} = -\frac{8A_s\tau_0^{n_s-1}a^2}{9\pi H_0^4\Omega_m^2}\left(\frac{\dot{\mathcal{H}}}{\mathcal{H}}+\frac{2}{r_s}\right)\times \int_0^\infty dk k^{1+n_s}\left[\left(1-\frac{a}{(1+\eta)^2}\frac{\partial\eta}{\partial a}\right)GQ+\frac{a}{1+\eta}\frac{\partial(GQ)}{\partial a}\right]j_\ell'(kr_s)j_\ell(kr_s)\frac{GT^2(k)}{(1+\eta)}\,. \tag{7.24}$$

4. Gravitational lensing:

   4.1 Using Limber approximation [63] (see Appendix) the autocorrelation is

$$C_\ell^{LL} = \frac{A_s\tau_0^{n_s-1}\ell^2(\ell+1)^2}{r_s^2\nu^{4-n_s}}\int_0^{r_s}drT^2\left(\frac{\nu}{r}\right)\frac{(r_s-r)^2}{r^{n_s}}G^2\left(r,\frac{\nu}{r}\right)Q^2\left(r,\frac{\nu}{r}\right) \times\left(\frac{2+\eta(r,\nu/r)}{1+\eta(r,\nu/r)}\right)^2\,. \tag{7.25}$$

4.2 The correlation of lensing and density after using Limber approximation is

$$C_\ell^{LD} = -\frac{8A_s(\tau_0\nu)^{n_s-1}\ell(\ell+1)a}{3r_s\Omega_m H_0^2}\sqrt{\frac{\nu}{2\pi}}\int_0^{r_s} dr\frac{(r_s-r)}{r^{2+n_s}}\frac{j_\ell\left(\frac{\nu r_s}{r}\right)G(a,\nu/r)}{[1+\eta(a,\nu/r)]} \times\left[G\left(r,\frac{\nu}{r}\right)Q\left(r,\frac{\nu}{r}\right)\left(1+\frac{1}{1+\eta(\nu/r)}\right)\right]T^2\left(\frac{\nu}{r}\right). \tag{7.26}$$

5. Local potentials:

5.1 The autocorrelation of the local potential terms is

$$C_\ell^{PP} = \frac{2A_s\tau_0^{n_s-1}}{\pi}\int_0^\infty dk k^{n_s-2}j_\ell^2(kr_s)T^2(k) \times\left[GQ\left(\frac{\dot{\mathcal{H}}}{\mathcal{H}^2}+\frac{2}{r_s\mathcal{H}}+\frac{2+\eta}{1+\eta}-\frac{a}{(1+\eta)^2}\frac{\partial\eta}{\partial a}\right)+\frac{a}{1+\eta}\frac{\partial(GQ)}{\partial a}\right]^2. \tag{7.27}$$

5.2 Correlation with density:

$$C_\ell^{PD} = -\frac{4A_s\tau_0^{n_s-1}}{3\pi\Omega_m H_0^2}\int_0^\infty dk k^{n_s}j_\ell^2(kr_s)\frac{GT^2(k)}{(1+\eta)} \times\left[GQ\left(\frac{\dot{\mathcal{H}}}{\mathcal{H}^2}+\frac{2}{r_s\mathcal{H}}+\frac{2+\eta}{1+\eta}-\frac{a}{(1+\eta)^2}\frac{\partial\eta}{\partial a}\right)+\frac{a}{1+\eta}\frac{\partial(GQ)}{\partial a}\right]. \tag{7.28}$$

6. Shapiro time-delay:

6.1 After using Limber approximation, the autocorrelation term is

$$C_\ell^{std} = \frac{4A_s\tau_0^{n_s-1}}{r_s^2\nu^{4-n_s}}\int_0^{r_s} dr r^{2-n_s}T^2\left(\frac{\nu}{r}\right)G^2(r,\nu/r)Q^2(r,\nu/r)\left(\frac{2+\eta(r,\nu/r)}{1+\eta(r,\nu/r)}\right)^2. \tag{7.29}$$

6.2 The correlation with density is

$$C_\ell^{stdD} = -\frac{8A_s(\tau_0\nu)^{n_s-1}a}{3r_s\Omega_m H_0^2}\sqrt{\frac{\nu}{2\pi}}\int_0^{r_s}\frac{dr}{r^{1+n_s}}\frac{j_\ell\left(\frac{\nu r_s}{r}\right)G(a,\nu/r)}{1+\eta(a,\nu/r)} \times\left(\frac{G(r,\nu/r)[2+\eta(r,\nu/r]}{1+\eta(r,\nu/r)}\right)T^2\left(\frac{\nu}{r}\right). \tag{7.30}$$

7. Integrated Sachs-Wolfe effect:

7.1 After using Limber approximation, the autocorrelation term is

$$C_\ell^{isw} = \frac{A_s\tau_0^{n_s-1}}{\nu^{4-n_s}}\left(\frac{\dot{\mathcal{H}}}{\mathcal{H}^2}+\frac{2}{r_s\mathcal{H}}\right)^2\times \int_0^{r_s} dr r^{3-n_s}T^2\left(\frac{\nu}{r}\right)\left\{\mathcal{H}(r)a(r)\frac{\partial}{\partial a}\left[G\left(r,\frac{\nu}{r}\right)Q\left(r,\frac{\nu}{r}\right)\left(\frac{2+\eta(r,\nu/r)}{1+\eta(r,\nu/r)}\right)\right]\right\}^2. \tag{7.31}$$

7.2 The correlation with density using Limber approximation is

$$C_\ell^{iswD} = -\frac{4A_s(\tau_0\nu)^{n_s-1}a}{3\Omega_m H_0^2}\sqrt{\frac{\nu}{2\pi}}\left(\frac{\dot{\mathcal{H}}}{\mathcal{H}^2}+\frac{2}{r_s\mathcal{H}}\right)\int_0^{r_s}\frac{dr}{r^{1+n_s}}T^2\left(\frac{\nu}{r}\right)\times \tag{7.32}$$
$$\frac{j_\ell(\nu r_s/r)G(a_s,\nu/r)}{1+\eta(a_s,\nu/r)}\mathcal{H}(r)a(r)\frac{\partial}{\partial a}\left[G\left(r,\frac{\nu}{r}\right)Q\left(r,\frac{\nu}{r}\right)\left(\frac{2+\eta(r,\nu/r)}{1+\eta(r,\nu/r)}\right)\right].$$

In the limit $Q=1$ and $\eta=0$, all the previous expressions reduce to those calculated in [26] for a ΛCDM cosmology considering a scale-invariant primordial power spectrum ($n_s=1$). In the next Chapter we discuss these power spectra for ΛCDM and the effective dark energy fluid.

Chapter 8

Results and Discussion

In this chapter we use our general result (7.20)-(7.32) for the galaxy power spectrum in the (Q, η) parametrization to study the predictions of the dark energy fluid model discussed at the end of Chapter 5. Since we are interested in the Universe on late times, we will assume that it contains only two components; a matter fluid with $w = \delta p = 0$ (i.e. mostly composed by cold dark matter) and an effective dark energy fluid which is parametrized by two degrees of freedom: an equation of state parameter $w \sim -1$ and sound speed c_s^2.

For testing this model we consider the cases $c_s^2 = \{0, 10^{-6}, 10^{-4}, 10^{-2}, 1\}$ and the results for each one are compared with respect to a fiducial ΛCDM cosmology (at this stage we ignore viscosity terms, i.e. $\eta = 0$). The cosmological parameters used are shown in Table 8.1. For the ΛCDM case we consider the same set of parameters except for the EoS parameter, which is replaced by $w = -1$ in order to actually describe a cosmological constant Λ.

parameter	symbol	value
Baryon density today	Ω_b	0.05
Cold dark matter density today	Ω_c	0.27
Dark energy density today	Ω_Λ	0.68
Optical depth due to reionization	τ	0.1
Scalar spectrum index	n_s	0.96
Primordial curvature perturbation	$10^9 A_s$	2.1
Expansion rate today	H_0	67
Equation of state parameter	w	-0.8

Table 8.1: Cosmological parameters used for the effective dark energy fluid model. For the fiducial ΛCDM cosmology we consider the same set except for the equation of state parameter, which is replaced by $w = -1$.

Notice that the transfer functions at zero redshift $T(k)$ are the only numerical input entering in the C_l's (7.20)-(7.32) . We compute these with MGCAMB code [62] for the dark energy model, and with CAMB code [64] for ΛCDM, both in the linear regime (no Halofit). We also normalize the growth function in all cases to be unity during matter domination era,

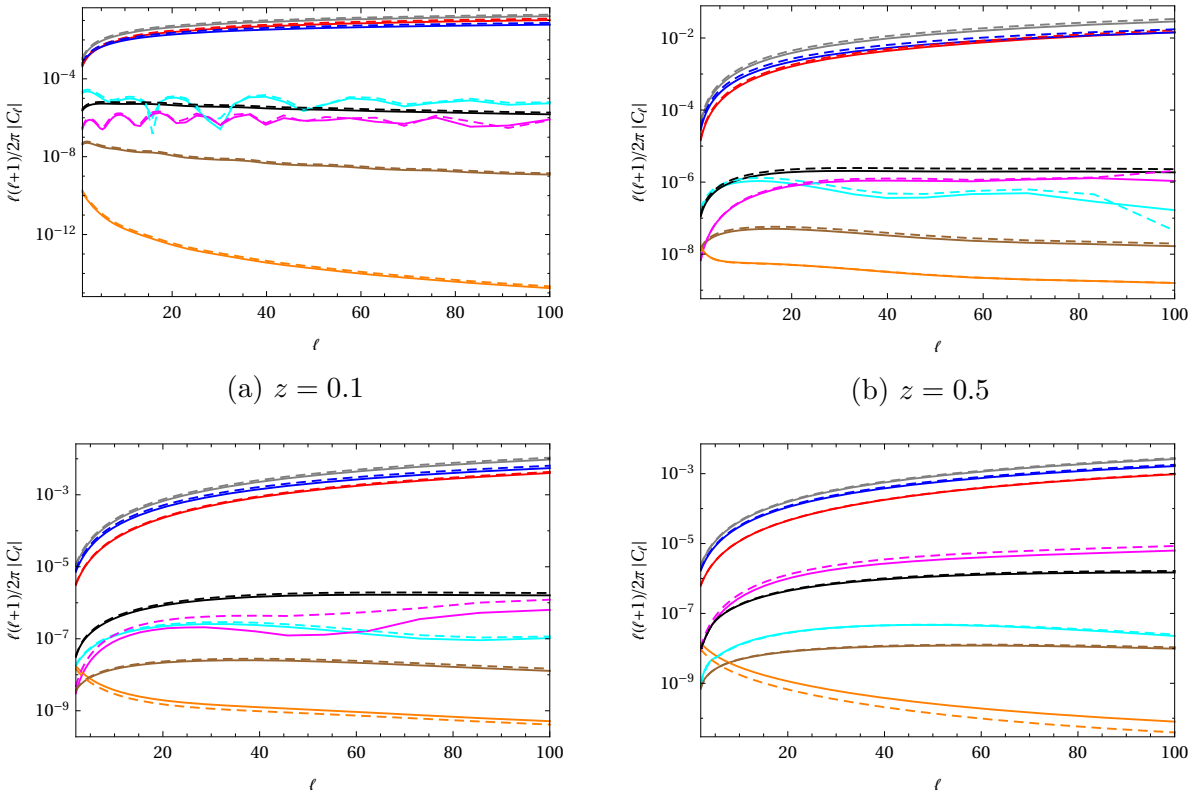

(a) $z = 0.1$ (b) $z = 0.5$

(c) $z = 1$ (d) $z = 2$

Figure 8.1: Angular power spectrum for $c_s^2 = 1$ (solid line) and ΛCDM (dashed line) using (8.1). The different colours represent each effect: red (density), blue (RSD), cyan (Doppler), magenta (lensing), black (local potentials), brown (Shapiro time-delay) and black (ISW). The apparent spikes are due to the C_ℓ's crossing zero (we plot absolute values).

where the features of the dark energy fluid have not yet manifested[1], i.e. $G(a = 10^{-3}, k) = 1$.

In order to build some intuition about the angular power spectra let us start by plotting all the contributions (7.20)-(7.32) at different redshifts for the various sound speed cases together with ΛCDM. For any given effect shown in Fig. 8.1 we plot its autocorrelation as well as the cross-correlation with the intrinsic density fluctuation, i.e.

$$C_\ell^i = C_\ell^{ii} + 2C_\ell^{iD}\,, \tag{8.1}$$

where i labels any effect except for D itself. Unlike autocorrelations, cross-correlations may take negative values, and these are responsible for the spikes that appear in some of the effects, where $C_\ell^i < 0$.

Figure 8.1 (and the subsequent figures up to Fig 8.5) shows a clear hierarchy in the different contributions to the total power spectrum. The intrinsic density fluctuation and redshift-space distortion represent the largest contributions at all redshifts, while the rest of

[1]Alternatively, one may choose to normalize the growth rate of structures at the present.

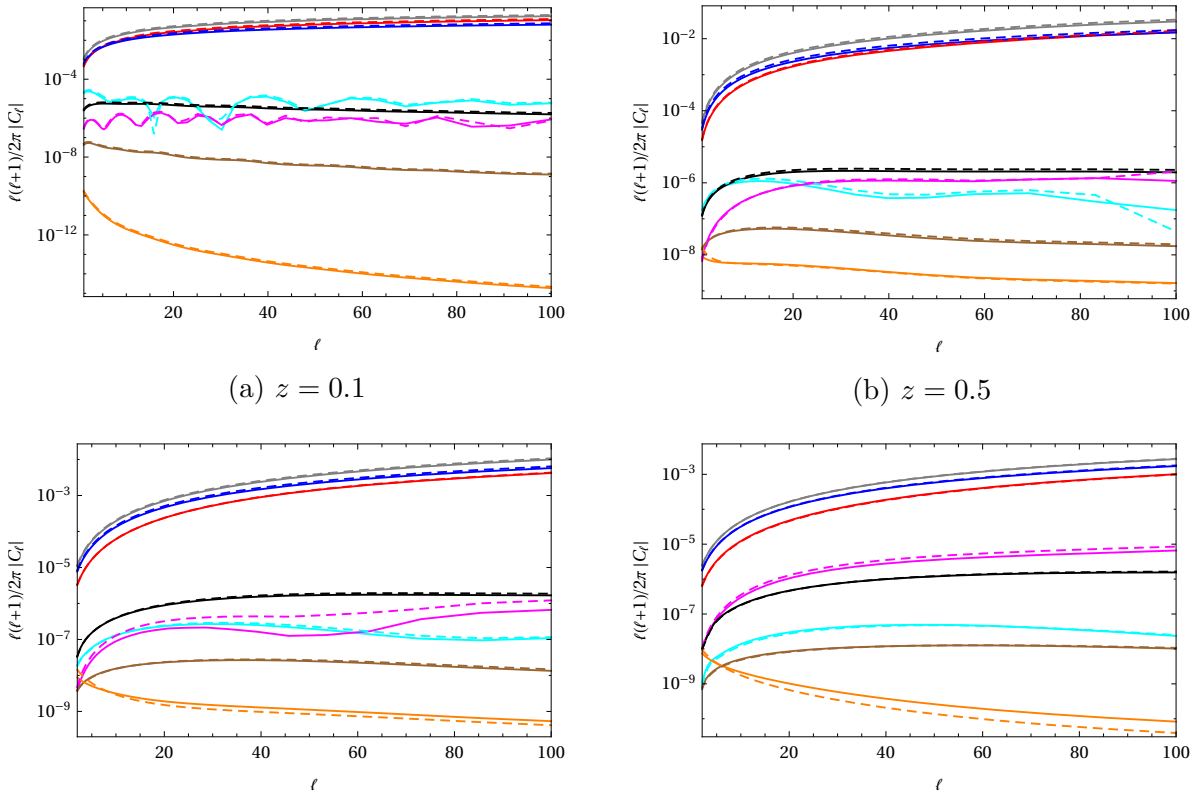

(a) $z = 0.1$ (b) $z = 0.5$

(c) $z = 1$ (d) $z = 2$

Figure 8.2: Angular power spectrum for $c_s^2 = 10^{-2}$ (solid line) and ΛCDM (dashed line) using (8.1). The different colours represent each effect: red (density), blue (RSD), cyan (Doppler), magenta (lensing), black (local potentials), brown (Shapiro time-delay) and black (ISW). The apparent spikes are due to the C_ℓ's crossing zero (we plot absolute values).

the terms remain subdominant in every case, although their relative magnitudes change. We find that the least prominent contributions to the total power spectrum come from terms related to the metric perturbations, i.e. the relativistic effects, which we have divided into local potential terms, Shapiro time-delay effect and ISW effect, the latter two corresponding to integrated terms.

Naturally, the amplitude of the matter density fluctuations decreases with z since the universe is more homogeneous in the past. Since in Figs 8.1 to 8.5 every term includes its cross-correlation with density, this implies that their overall amplitudes are also smaller for increasing z. However, the autocorrelation of some of the effects can be more relevant in the past, and then its interplay with the cross-correlation may cause that, even if the total amplitude of such contributions decrease, their relative weight with respect to density fluctuations in fact increases, as shown in Fig 8.1.

We remark that terms which are integrated along the line of sight, i.e. gravitational lensing, Shapiro time-delay and ISW effect are suppressed at low redshift with respect to

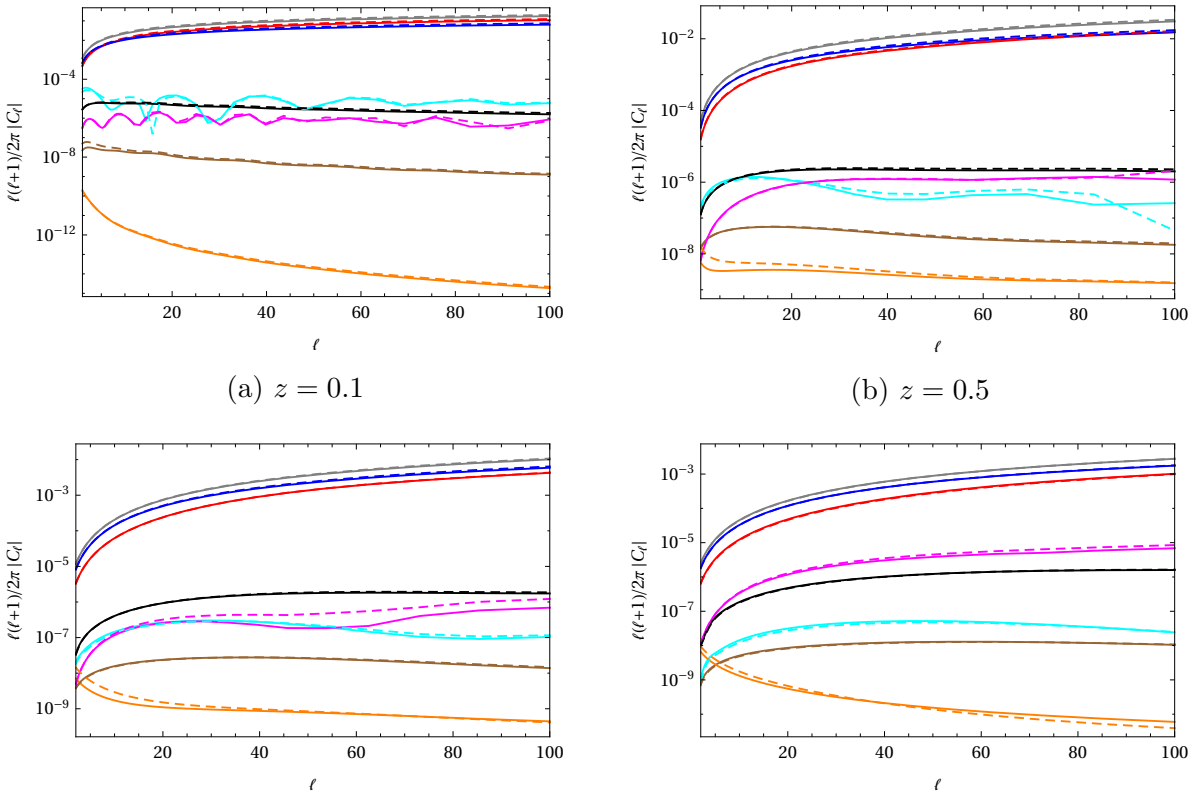

(a) $z = 0.1$ (b) $z = 0.5$

(c) $z = 1$ (d) $z = 2$

Figure 8.3: Angular power spectrum for $c_s^2 = 10^{-4}$ (solid line) and ΛCDM (dashed line) using (8.1). The different colours represent each effect: red (density), blue (RSD), cyan (Doppler), magenta (lensing), black (local potentials), brown (Shapiro time-delay) and black (ISW). The apparent spikes are due to the C_ℓ's crossing zero (we plot absolute values).

local terms, which dominate the total matter clustering signal. In fact, Fig 8.1 shows that the local potentials term is the more prominent effect among the relativistic terms at all redshifts, and it even surpasses Doppler at $z = 3$, while the Shapiro time-delay and ISW effect are the weakest signals and remain several orders of magnitude below the others at all redshifts.

At low redshift we find that the Doppler effect dominates over the local potentials and gravitational lensing signals, since the peculiar velocities are more relevant for nearby objects. However, at $z = 0.5$ the former only dominates at very large scales (small ℓ) and the amplitude of these three effects becomes comparable at $\ell \sim 35$. At $z = 1$ they are of similar order even at small ℓ, and for $z = 3$ the lensing signal dominates over Doppler effect at all scales. Since gravitational lensing is an integrated effect it grows toward higher redshift as the source is more distant and the light is more likely to be deflected by the presence of inhomogeneities.

Since we can identify this clear hierarchy of contributions to the power spectrum spanning several orders of magnitude, we will study the imprints of the dark energy fluid model in the

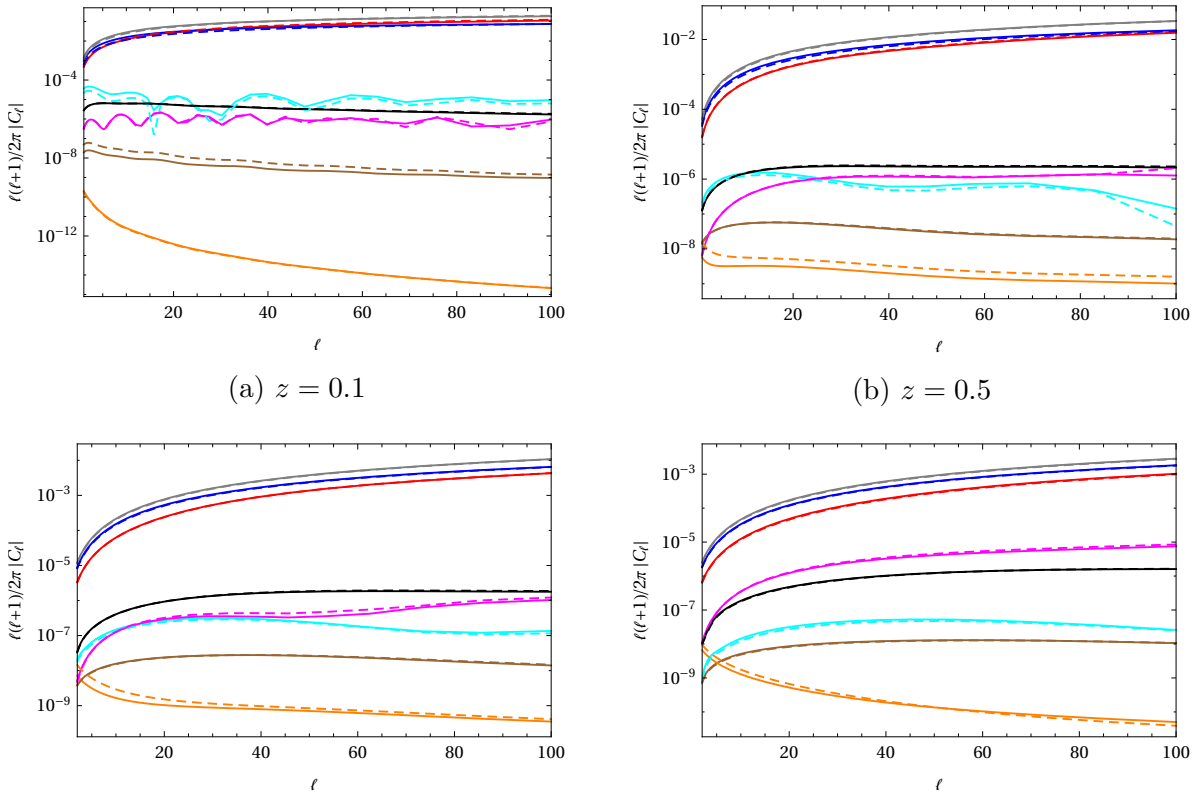

(a) $z = 0.1$ (b) $z = 0.5$

(c) $z = 1$ (d) $z = 2$

Figure 8.4: Angular power spectrum for $c_s^2 = 10^{-6}$ (solid line) and ΛCDM (dashed line) using (8.1). The different colours represent each effect: red (density), blue (RSD), cyan (Doppler), magenta (lensing), black (local potentials), brown (Shapiro time-delay) and black (ISW). The apparent spikes are due to the C_ℓ's crossing zero (we plot absolute values).

power spectrum by analyzing each effect individually. In order to quantify possible deviations from ΛCDM, we define the relative power spectrum of each effect as

$$\Delta C_\ell^i = 1 - \frac{C_\ell^i(\mathrm{DE})}{C_\ell^i(\Lambda)}\,, \tag{8.2}$$

where $C_\ell^i(\mathrm{DE})$ and $C_\ell^i(\Lambda)$ are the power spectra for a given effect calculated with the dark energy model and ΛCDM, respectively. We note that, as a way to disentangle the origin of possible deviations from ΛCDM, in (8.2) we only consider pure effects, i.e. without including its cross-correlation with density, contrary to Figs 8.1 to 8.5.

At this point it is worthwhile to remark that, as shown in Figure 8.1, the angular power spectrum of the $c_s^2 = 1$ model is not completely equivalent to that of ΛCDM as one might expect in principle. Even if in both models the dark energy component is completely homogeneous, the dark energy fluid has $w = -0.8$ and then the expansion history of this cosmology is different from ΛCDM ($w = -1$). As a consequence, at the background level the comoving

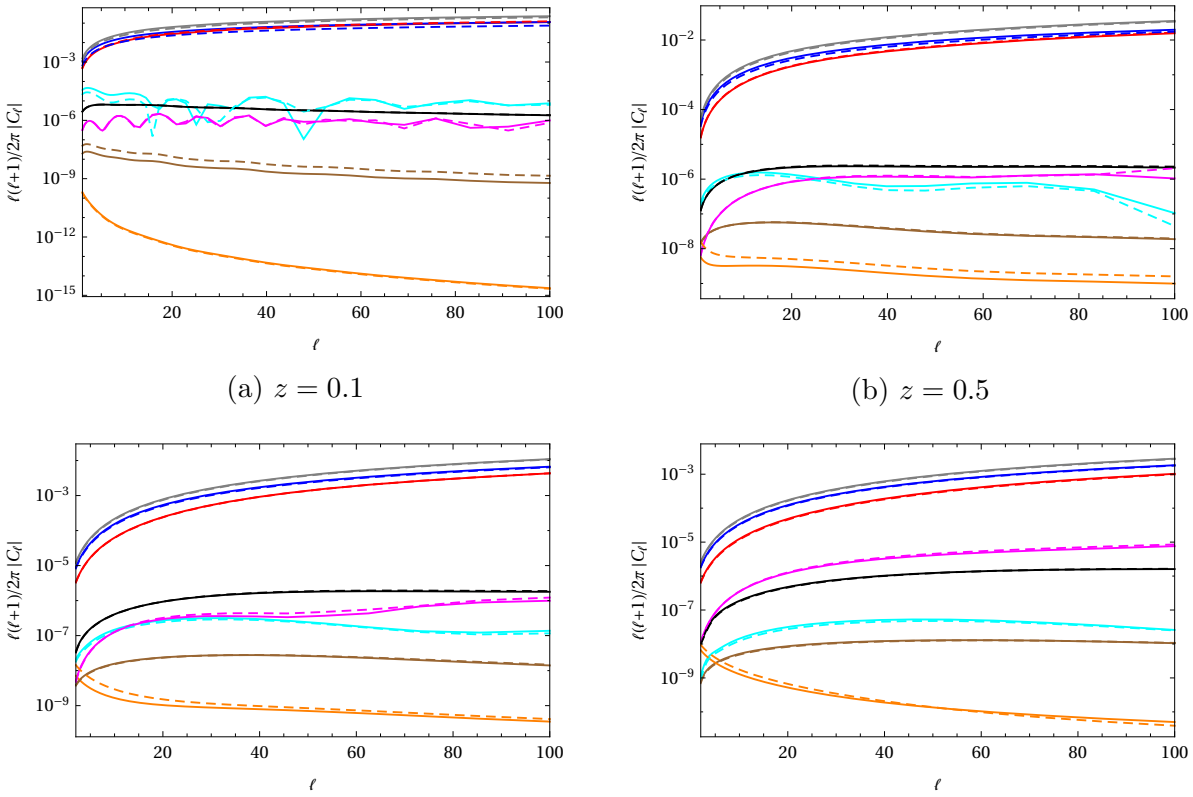

(a) $z = 0.1$ (b) $z = 0.5$

(c) $z = 1$ (d) $z = 2$

Figure 8.5: Angular power spectrum for $c_s^2 = 0$ (solid line) and ΛCDM (dashed line) using (8.1). The different colours represent each effect: red (density), blue (RSD), cyan (Doppler), magenta (lensing), black (local potentials), brown (Shapiro time-delay) and black (ISW). The apparent spikes are due to the C_ℓ's crossing zero (we plot absolute values).

distance to the source $r(z_s)$ differ in $\sim 1\%$ at $z = 0.1$ (nearby objects), and about $\sim 4\%$ at $z = 2$, since at this redshift we are completely taking into account the different dark energy domination eras. On the other hand, the estimates on the (conformal) age of the universe τ_0 differ in $\sim 3\%$, but since all the C_ℓ's (7.20)-(7.32) depend on $\tau_0^{n_s-1}$, the deviation arising from this factor becomes less than 0.1% (for $n_s = 0.96$).

At the perturbative level, the amplitude of the transfer function at $z = 0$ (or equivalently the matter power spectrum today $P(k)$) represents the major source of relative difference with respect ΛCDM which also arise from the different equation of state parameters. This amplitude is suppressed for greater w (i.e. closer to zero), as in such case the universe has less time to evolve and form new structures. Naturally, the different sound speeds are also imprinted in $T(k)$ since the matter power spectrum is enhanced by the presence of dark fluid clustering. In general, even if the interplay of Q, G and $T(k)$ might approximate the behaviour of ΛCDM in some cases, background differences arising from $r(z)$ and τ_0 will persist.

In order to keep track of the relative intensity of possible deviations it is also useful to quantify the relative power spectrum of each effect with respect to the total signal predicted

by ΛCDM. Following (8.1), this is given by

$$\Delta C_\ell^{i-\mathrm{tot}} = \frac{C_\ell^i(\mathrm{DE}) - C_\ell^i(\Lambda)}{C_\ell^{\mathrm{tot}}(\Lambda)}\,, \tag{8.3}$$

where the terms in the numerator represent the contributions coming from a given effect, but this time we include their respective cross-correlations with density, and $C_\ell^{\mathrm{tot}}(\Lambda)$ correspond to the power spectrum of ΛCDM with all contributions in (7.20)-(7.32).

Figure 8.6 shows the fractional deviations obtained with (8.3) for the five different sound speed cases using the same colour nomenclature for each effect as in Fig 8.1. We find that the intrinsic density fluctuations (red) and redshift-space distortion (blue) represent the largest weighted deviations in all cases. At $z = 0.1$ the strongest contributions come from the latter effect, specially at large scales, where the cases $c_s^2 = 0$ and $c_s^2 = 10^{-6}$ show the strongest departures. At higher z the redshift-space distortions represent a larger contribution to the total signal than density in models with sound speeds close to unity. On the other hand, the relative weight of deviations in Doppler and lensing terms remain small at all redshifts.

Regarding the relativistic effects, we find that the local potential terms (black) contribute more strongly at small ℓ (large scales), and their relative weight decays quickly towards small scales. The other two relativistic effects, i.e. Shapiro time-delay (brown) and ISW (orange) remain completely subdominant with respect to the full signal at all redshifts, which implies that they are the most difficult to extract from the total power spectrum.

8.1 Standard Effects

In this section we start by discussing the angular power spectra of the standard terms, i.e. those for the intrinsic density fluctuations, redshift-space distortions, Doppler effect and gravitational lensing. Figure 8.7 shows the relative deviations with respect to ΛCDM for each pure effect, as obtained with (8.2), for the extreme cases $c_s^2 = 1$ and $c_s^2 = 0$. Other sound speed cases lie within the shown curves.

Figure 8.7a shows that from the standard terms, the Doppler effect (cyan) and redshift-space distortion (blue) are the most susceptible to deviations from ΛCDM, but gravitational lensing deviations (magenta) can become considerable at higher redshifts.

8.1.1 Matter density

Let us next analyze each standard effect separately. The first term in this set is the intrinsic density fluctuations, which is the leading contribution to the total signal. Its angular power spectrum is shown in Fig 8.8.

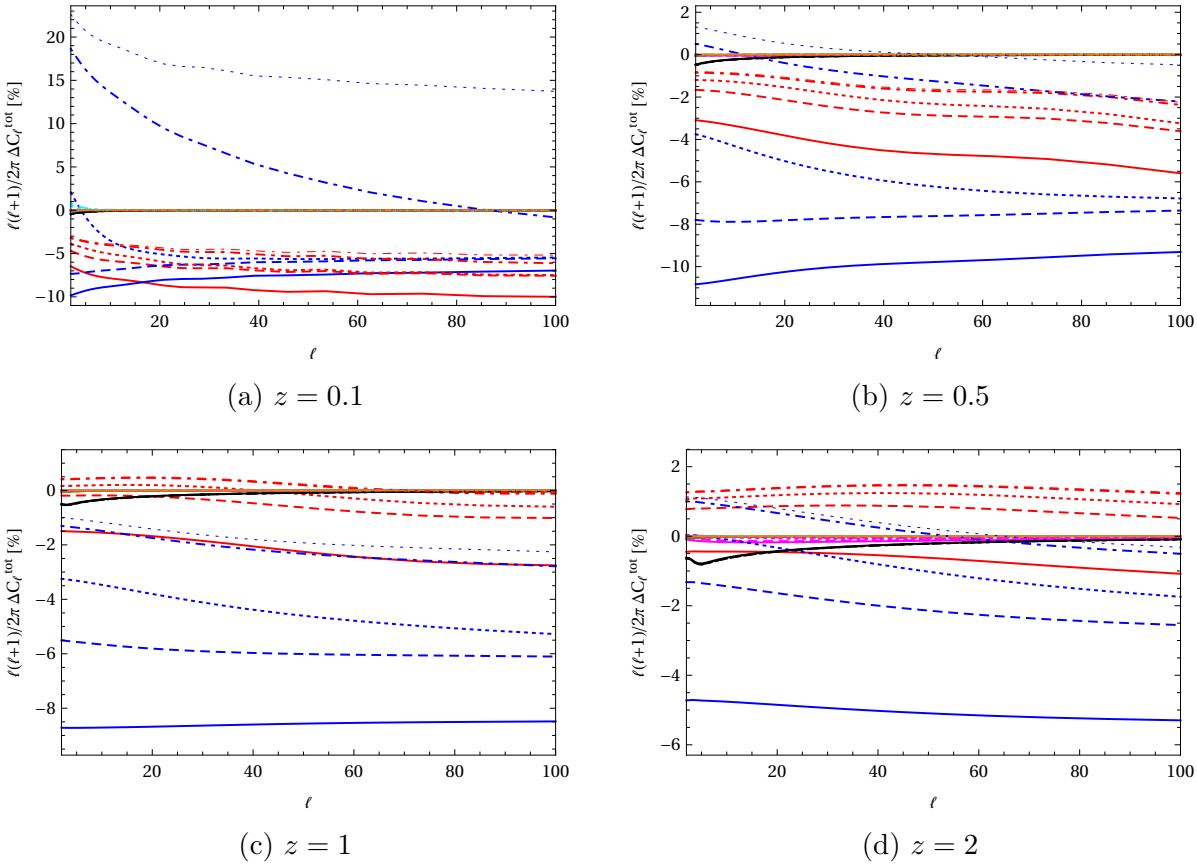

(a) $z = 0.1$ (b) $z = 0.5$

(c) $z = 1$ (d) $z = 2$

Figure 8.6: Relative power spectrum for all effects (including cross-correlations with density) with respect to the total ΛCDM signal obtained with (8.3). Each model is represented by a different line style: solid ($c_s^2 = 1$), dashed ($c_s^2 = 10^{-2}$), dotted ($c_s^2 = 10^{-4}$), dot-dashed ($c_s^2 = 10^{-6}$), thin-dashed ($c_s^2 = 0$). The different colours represent each effect: red (density), blue (RSD), cyan (Doppler), magenta (lensing), black (local potentials), brown (Shapiro time-delay) and black (ISW).

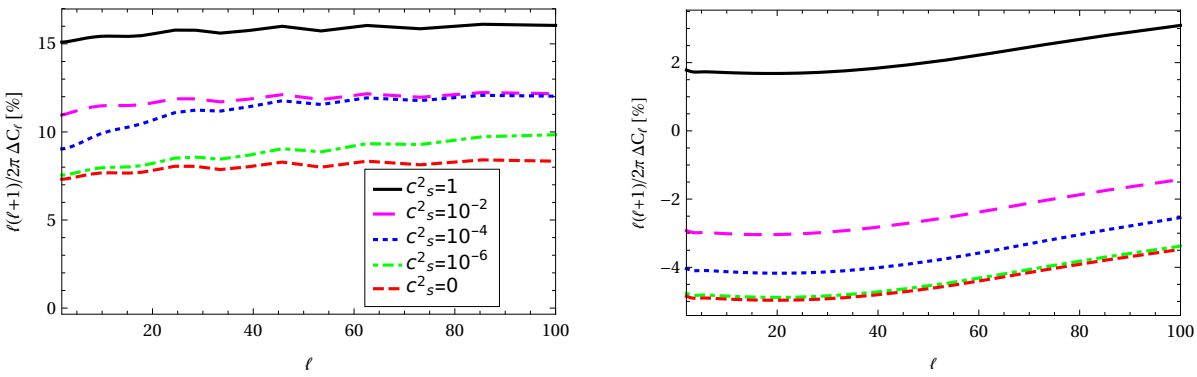

(a) $z = 0.1$ (b) $z = 2$

Figure 8.8: Relative matter density power spectrum at different source redshifts.

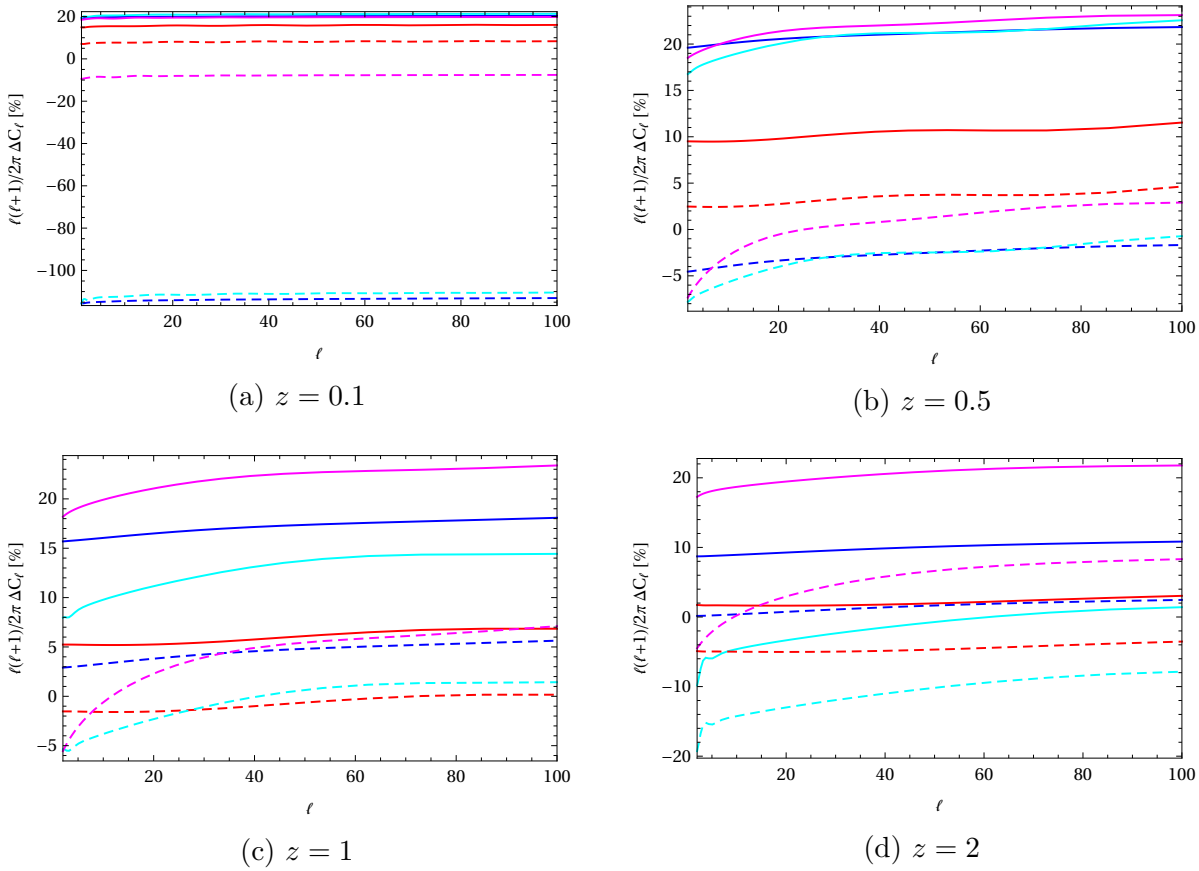

(a) $z = 0.1$ (b) $z = 0.5$

(c) $z = 1$ (d) $z = 2$

Figure 8.7: Relative power spectrum for the standard (pure) effects at different source redshifts for $c_s^2 = 1$ (solid line) and $c_s^2 = 0$ (dashed line). The different colors represent each effect: red (density), blue (RSD), cyan (Doppler) and magenta (lensing).

Figure 8.8a shows that at $z = 0.1$, the amplitude of the matter power spectrum is smaller than in ΛCDM (corresponding to a positive ΔC_ℓ due to our sign convention in (8.2)). As it is expected, the case of dark energy with $c_s^2 = 1$ deviates the most from ΛCDM since the amplitudes of both present growth rate $G(z = 0, k)$ and $T(k)$ are the smallest for this model. At this point we can remark that a lower sound speed implies more clustering of the dark energy fluid, which tend to compensate the suppression of $T(k)$ for $w = -0.8$ at low z. Consequently, for low c_s^2 the amplitude of the matter power spectrum becomes closer to ΛCDM than for high sound speeds.

The general picture can be understood considering Fig 8.9, which shows the evolution of the growth function G and the dark energy density $\Omega_{DE}(a) = (1 - \Omega_m)a^{-3(1+w)}/(H/H_0)^2$. Recall that the growth rate of structures G becomes suppressed when the universe leaves the matter domination era and dark energy start to take over, as Fig 8.9b shows for different models. Since the dark energy fluid has $w = -0.8$ the dark energy domination era begins earlier than in ΛCDM, as shown in Fig 8.9a, which results in less time for structures in the universe to form, and consequently lower $T(k)$ and $P(k)$ at the present day. From Fig 8.8a we find that at $z = 0.1$ the cases $c_s^2 = 10^{-2}$ and $c_s^2 = 10^{-4}$ are very similar, while the behaviour

of $c_s^2 = 10^{-6}$ is closer to $c_s^2 = 0$. As it is shown in Fig 8.9b, towards higher redshift the gap among growth rates reduces and deviations from ΛCDM are smaller. However, the difference in comoving distance with respect to $w = -1$ is greater than at $z = 0.1$, which imprints a sizeable contribution to deviations at $z = 2$, as shown in Fig 8.8b.

The presence of wiggles in the relative power spectrum in Fig 8.8a for scales $\ell \gtrsim 15$ are due to the misalignments of baryon acoustic oscillations (BAOs) in the dark energy fluid model with respect to ΛCDM caused by the different expansion histories, as also pointed out in [43]. In fact, if we consider the BAO scale $r_{\rm BAO} \approx 110$ Mpc/h [65], we expect this to be imprinted in the multipoles $\ell_{\rm BAO}(z) = 2\pi r(z)/r_{\rm BAO}$, which at $z = 0.1$ correspond to $\ell_{\rm BAO} \sim 12$, while at $z = 2$ we find $\ell_{\rm BAO} \sim 150$, i.e. beyond the range of our analysis.

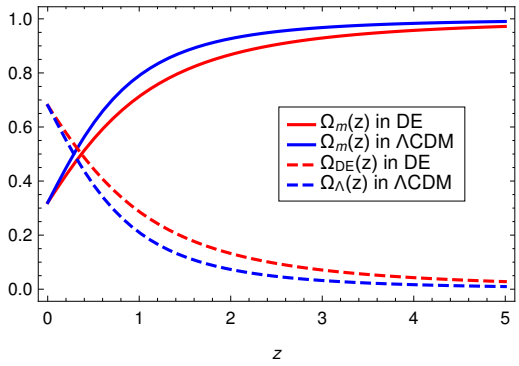

(a) Matter and dark energy density.

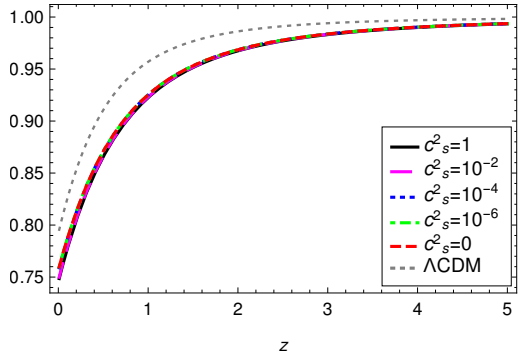

(b) Growth function for $k = 0.01$ Mpc^{-1}.

Figure 8.9: Comparison of matter-energy densities and growth functions for dark energy ($w = -0.8$) and ΛCDM. In all cases the latter is normalized to unity during matter domination era.

8.1.2 Redshift-space Distortion

Let us now analyze deviations in Redshift-space distortion, which is the next to leading contribution to the total power spectrum.

From Fig 8.10a we find that at $z = 0.1$ the deviations in this effect are strongly sensitive to the clustering properties of the dark energy fluid. For the extreme cases $c_s^2 = 1$ and $c_s^2 = 0$ we observe the same deviations at all scales since the fluid does not single out any k in these particular cases, but for $0 < c_s^2 < 1$ the deviations are higher at larger scales (small ℓ), where the dark fluid can cluster. This extra clustering then enhances the peculiar velocities of normal matter, causing a greater redshift-space distortion than in ΛCDM.

However, contrary to density fluctuations shown in Fig 8.8a,we note that the RSD power spectrum of some models is larger that in ΛCDM (i.e. $\Delta C_\ell < 0$). This is due to the fact that

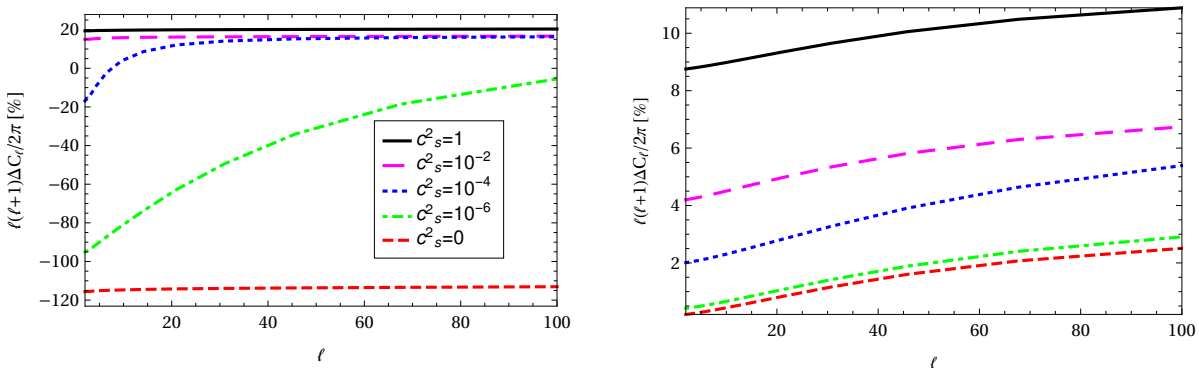

(a) $z = 0.1$ (b) $z = 2$

Figure 8.10: Relative redshift-space distortion power spectrum at different source redshifts.

if the sound speed is too high the previous effect is not enough to counterbalance the fact that normal matter has had less time to cluster in the dark fluid model (due to $w = -0.8$), and then the RSD power spectrum in this case is still lower than in ΛCDM, as Fig 8.10a shows for $c_s^2 = 1$ and $c_s^2 = 10^{-2}$.

On the other hand, unlike C_ℓ^{DD}, the redshift-space distortion is sensitive to the growth factor G and the clustering parameter Q through both $GQ > 0$ and $\partial(GQ)/\partial a < 0$, which then compete against each other, see (7.21). At low redshift the term $\partial(GQ)/\partial a$ has its biggest impact, since the dark energy fluid start to cluster at late times and the growth rate of structures keeps decreasing. At high redshift, G tends to approach a constant value (recall that $G \to 1$ as we move into matter domination era), so that $\partial(GQ)/\partial a$ is smaller, and the contribution coming from the product GQ is greater. Then, at $z = 2$ the deviations predicted for redshift space distortions are considerably smaller than at low redshift, as shown in Fig 8.10b.

8.1.3 Doppler Effect

The next contribution to the total power spectrum in the hierarchy comes from the Doppler effect. Its relative power spectrum is shown in Fig 8.11. Figure 8.11a shows that at $z = 0.1$ deviations in this effect behave very similar to redshift-space distortions for the same redshift (Fig 8.10a), which is not completely unexpected since both effects probe the peculiar velocities of the matter distribution.

As shown in (7.23), the Doppler effect is sensitive to both GQ and $\partial(GQ)/\partial a$, similarly to redshift-space distortions, but it also depends on the expansion rate of the universe through the overall factor $(\dot{\mathcal{H}}/\mathcal{H} + 2/r_s)^2$. In fact, at $z = 2$ the combination $\dot{\mathcal{H}}/\mathcal{H}$ has a relative difference of about 17% with respect to ΛCDM, which enhances deviations in all models at higher redshifts with respect to redshift-space distortions, as shown in 8.11b, since such feature is not present in the latter effect. Then, it is clear that at $z = 0.1$ the structure of

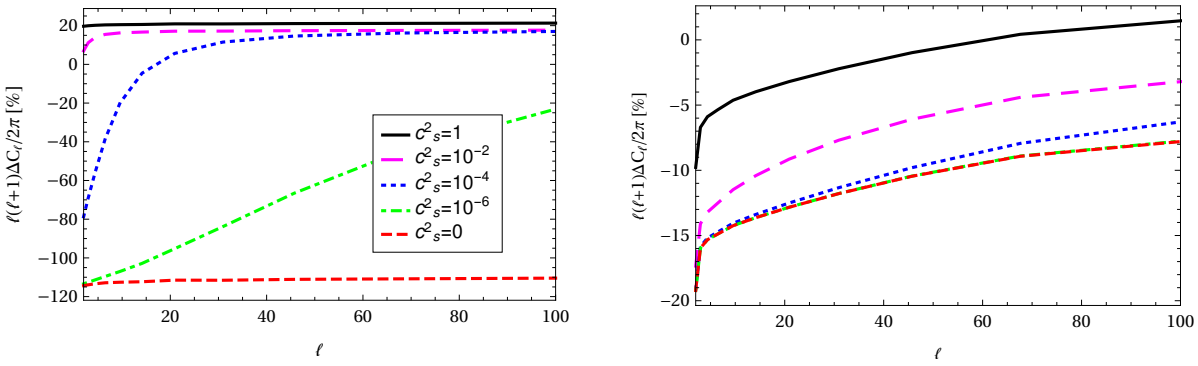

(a) $z = 0.1$ (b) $z = 2$

Figure 8.11: Relative Doppler effect power spectrum at different source redshifts.

each curve in Fig 8.11a is very similar to RSD in Fig 8.10a, since deviations in the previous terms become suppressed at such low redshift.

8.1.4 Lensing

The last standard effect in the hierarchy is the gravitational lensing signal, whose power spectrum is shown in Fig 8.12.

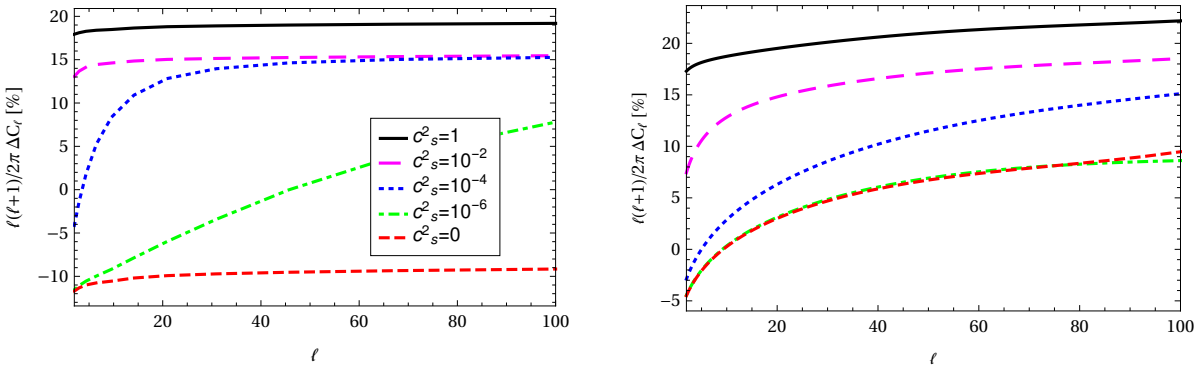

(a) $z = 0.1$ (b) $z = 2$

Figure 8.12: Relative lensing power spectrum at different source redshifts.

From Fig 8.12a we find that at low redshift deviations in lensing behave in a qualitative similar way to redshift-space distortion and Doppler effect, see Fig 8.11a. However, the amplitudes of lensing fluctuations are considerably smaller than the previous effects for the lowest sound speed cases; $c_s^2 = 0$, $c_s^2 = 10^{-6}$ and $c_s^2 = 10^{-4}$, i.e. it is not strongly enhanced by the dark energy fluid clustering. We can understand this by noting that, contrary to the effects discussed so far, lensing is not a local effect but it tracks the gravitational potentials between source and observer. Then, for nearby sources (small z) we can only explore a

relatively small portion of the late time universe. In contrast, for redshift-space distortions and Doppler, the peculiar velocities are more important at low z, and then deviations are expected to be higher.

On the other hand, comparing Fig 8.12a and Fig 8.12b we find that deviations in lensing do not decrease in amplitude as quickly as in the previous effects. Since this effect integrates along the line of sight, increasing z allows this effect to probe a larger portion of the universe. In particular, by choosing $z = 2$ we are taking into account all dark energy domination era, where deviations between the dark energy fluid and Λ are more prominent, and then we expect to find sizeable deviations in the lensing power spectrum such as in Fig 8.12b.

8.2 Relativistic effects

In this section we continue our discussion of each effect in the total power spectrum, this time considering the imprints of the dark energy model in the relativistic effects, which are the subdominant contributions to the full signal. Figure 8.13 shows deviations at various source redshifts for the extreme cases $c_s^2 = 1$ and $c_s^2 = 0$.

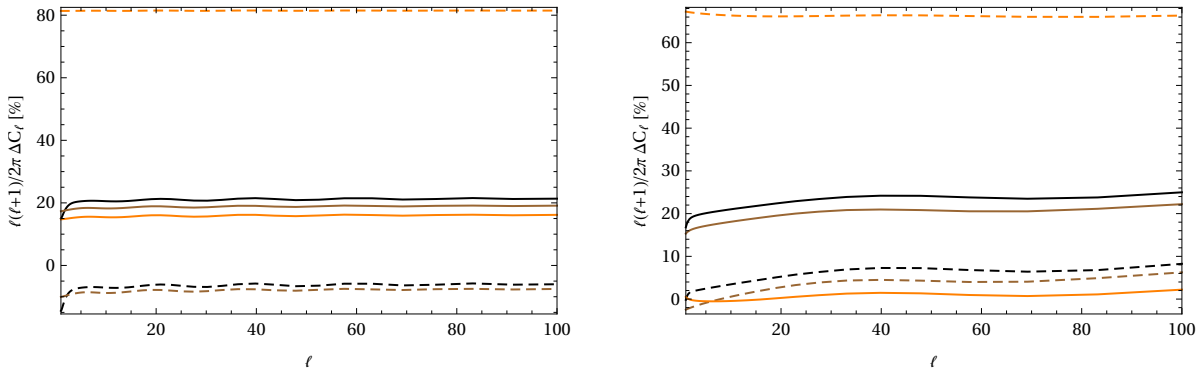

(a) $z = 0.1$ (b) $z = 0.5$

(c) $z = 1$ (d) $z = 2$

Figure 8.13: Power spectrum for the standard effects at different source redshifts for $c_s^2 = 1$ (solid line) and $c_s^2 = 0$ (dashed line). The different colors represent each effect: black (local potentials), brown (Shapiro time-delay) and orange (ISW effect).

We can clearly observe that the ISW effect (orange) is very sensitive to deviations from ΛCDM, as also remarked in previous studies on scalar-tensor theories [43]. Naturally, if the source is located at a higher redshift the ISW effect is able to track the evolution of $\dot{\Psi}$ and $\dot{\Phi}$ over a larger period of time, although the contributions are successively smaller beyond higher redshifts since the potentials stay constant in the matter-dominated era. On the other hand at small redshift the ISW effect is able to probe only a fraction of the dark energy dominated universe, and the magnitude of its deviations are comparable to the other relativistic effects.

It is interesting to note that, despite that the Shapiro time-delay (brown) also correspond to an integrated effect between source and observer, it does not show deviations as large as ISW at any redshift, which means that the power spectrum is more sensitive to how the potentials vary over time, i.e. their rates of change $(\dot{\Phi}+\dot{\Psi})$, rather than their evolution alone probed by the Shapiro time-delay through $(\Phi+\Psi)$. In fact, deviations in the local potential terms (black) are of roughly the same magnitude as in the Shapiro time-delay at all redshifts.

8.2.1 Local Potentials

We now consider each relativistic effect individually, as we did in the previous Section to study the standard effects. The relative power spectrum for the local gravitational potential terms is shown in Fig 8.14, which is the most dominant signal from this class.

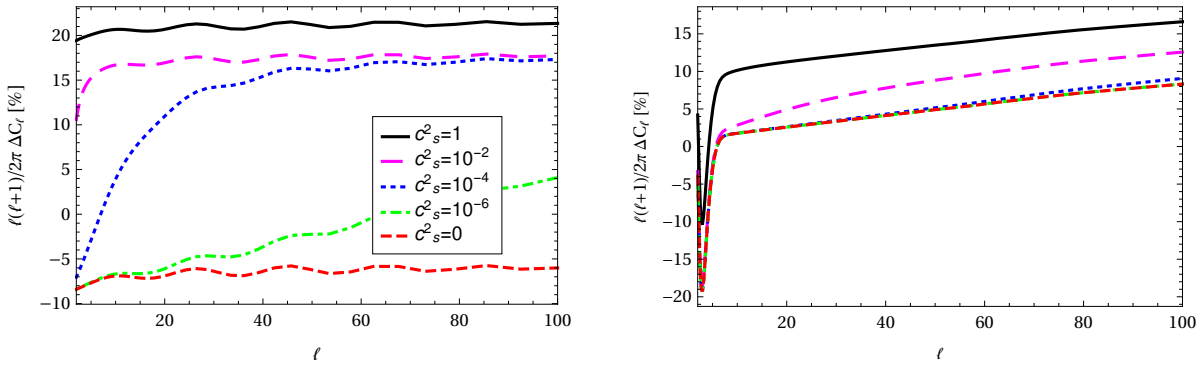

(a) $z = 0.1$ (b) $z = 2$

Figure 8.14: Relative local gravitational potentials power spectrum at different source redshifts.

Comparing Fig 8.14a with Fig 8.10a and Fig 8.11a, we find that the local potentials behave in a qualitative similar way to redshift-space distortion and Doppler effect at $z = 0.1$. In fact, this effect also depends on GQ and $\partial(GQ)/\partial a$, although in a different combination, see (7.27). However, deviations observed in this case are not as strong as in these standard effects since contrary to terms that depend on peculiar velocities, the local potential terms probe Ψ and Φ directly (and not their spatial variations). On the other hand, Fig 8.14b shows that at

$z = 2$ deviations in the potential terms spike at ultra-large scales ($\ell \sim 3$). While this would be a clear signal of departures from ΛCDM, it does not allow to clearly discriminate between the lowest sound speed cases.

8.2.2 Shapiro time-delay effect

We next consider the gravitational time delay effect, whose relative power spectrum at various redshifts is shown in Fig 8.15.

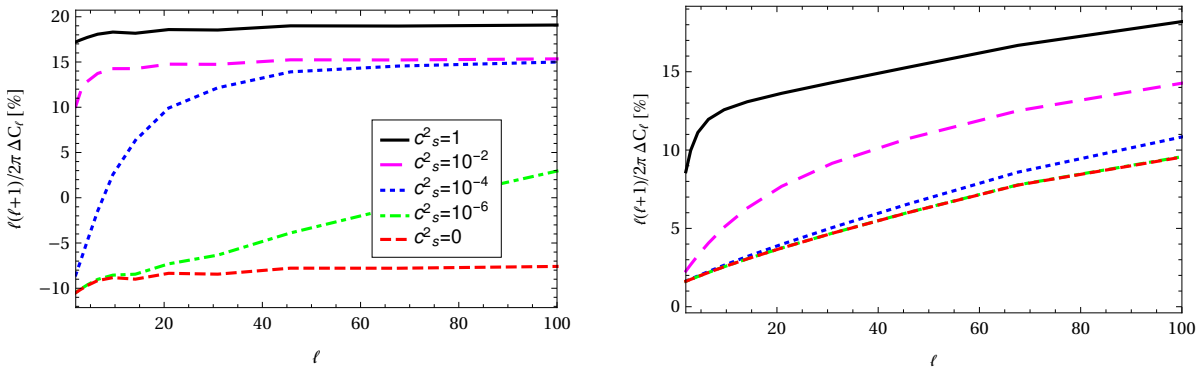

(a) $z = 0.1$ (b) $z = 2$

Figure 8.15: Relative Shapiro time-delay power spectrum at different source redshifts.

We recall that this effect probes the combination $(\Phi + \Psi) = 2\Phi$ (in absence of anisotropic stress) integrated along the line of sight. From Fig 8.15a we find that at low redshift this effect closely resembles the potential terms shown in Fig (8.14a). This is because the latter also probes 2Φ, but locally, and then for nearby sources both effects carry roughly the same information.

Despite of looking at a more distant source, Fig 8.15b shows that at higher redshift deviations in this effect do not increase considerably, and in fact there is an overall decrease. Even if for higher z the Shapiro time-delay is larger in absolute magnitude since photons travel more distance and are consequently more delayed by the presence of gravitational potentials, the relative deviation with respect to ΛCDM gets nonetheless smaller since the differences in the cosmological models reduce towards matter domination era, i.e. deviations in the time-delay arising by the dark energy model at late times lose weight when we integrate over a larger redshift range. On the other hand, if we consider the late time universe, where both dark energy models are different the relative deviation becomes higher.

8.2.3 Integrated Sachs-Wolfe Effect

The last contribution in the hierarchy of effects comes from the Integrated Sachs-Wolfe effect. Its relative power spectrum is shown in Fig 8.16.

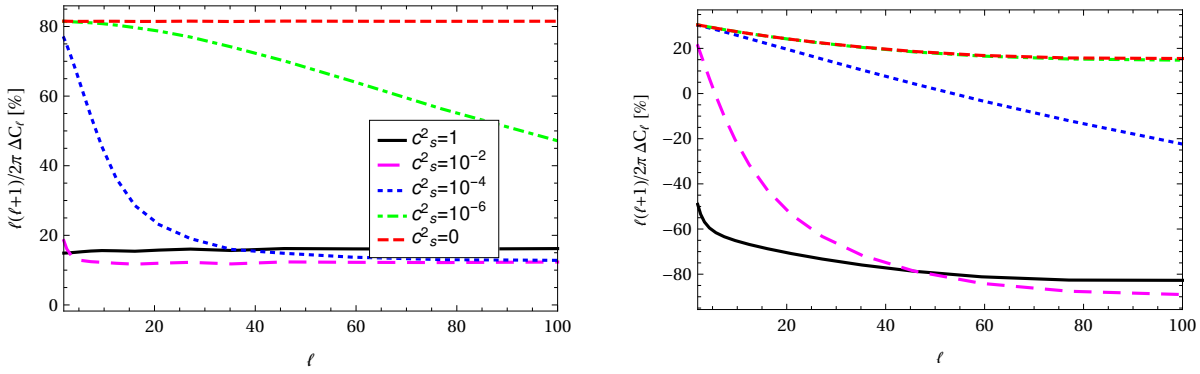

(a) $z = 0.1$ (b) $z = 2$

Figure 8.16: Relative power spectrum for the Integrated Sachs-Wolfe effect at different source redshifts.

We find that deviations in the ISW effect at $z = 0.1$ can be considerably larger than those in the previous two relativistic effects, despite that we are integrating in a relatively small redshift range. This is because that, just like the growth rate, the metric potentials are quickly changing in the late time universe due to the extra dark energy clustering, and then the power spectrum is more sensitive to the rate of change $(\dot{\Phi} + \dot{\Psi}) = 2\dot{\Phi}$ than to Φ itself.

At high redshift we find large deviations from ΛCDM, despite of ISW being the smallest contribution to the total power spectrum, reaching up to $\sim 90\%$ of relative difference for $z = 2$. The high sensitivity in this effect is due to the combination of the next two facts; firstly, from all the effects, this is the only one that probes directly the combination $\partial(GQ)/\partial a$, whose deviations with respect to ΛCDM are stronger than those from GQ itself, as we have discussed for redshift-space distortions and Doppler effect. In fact, it has been remarked that the rate of change $\partial G/\partial a$ is an excellent discriminator of dark energy models [66], as well as $\partial Q/\partial a$ [33, 58]. Secondly, as shown in (7.31), deviations in the ISW effect also become enhanced by the presence of $\mathcal{H}$ and $\dot{\mathcal{H}}$, similar to our remarks on the Doppler effect in Sec 8.1.3. This means that ISW also receives a direct background contribution which depends on the cosmological model.

Since in ΔC_ℓ we compare the dark energy angular power spectrum relative to ΛCDM, according to (7.31) the overall enhancement of the ISW effect at the perturbative level is governed by the magnification parameter

$$\mathcal{A} \equiv \frac{\partial(G(a,k)Q(a,k))/\partial a}{\partial G/\partial a} = Q + \frac{\partial Q}{\partial a}\frac{G}{\partial G/\partial a}\,. \tag{8.4}$$

By construction, in ΛCDM (or any smooth dark energy model) we have $\mathcal{A} = 1$ since $Q_\Lambda = 1$

and $\partial Q_\Lambda/\partial a = 0$. We plot the magnification parameter (8.4) in Fig 8.17 for the different sound speed cases.

For high sound speeds the perturbations in the dark energy fluid enter the sound horizon at early times and stay small until today, while at low sound speeds most modes stay outside the sound horizon and the fluid can cluster. In the latter case, the dark energy perturbations change $\mathcal{A}$ by about $\sim 70\%$ for $z \sim 0.1$, consistently with the ISW deviations shown in Fig 8.16a. Clearly, this effect cannot come from Q alone since this quantity deviates about 16% with respect to Λ at $z \sim 0.1$. In fact, we find that, for relatively large sound speeds, the 'clustering rate' $\partial Q/\partial a$ appearing in the second term of (8.4) can have an impact greater than the clustering parameter Q itself when we compare the ISW power spectrum with respect to a smooth dark energy component.

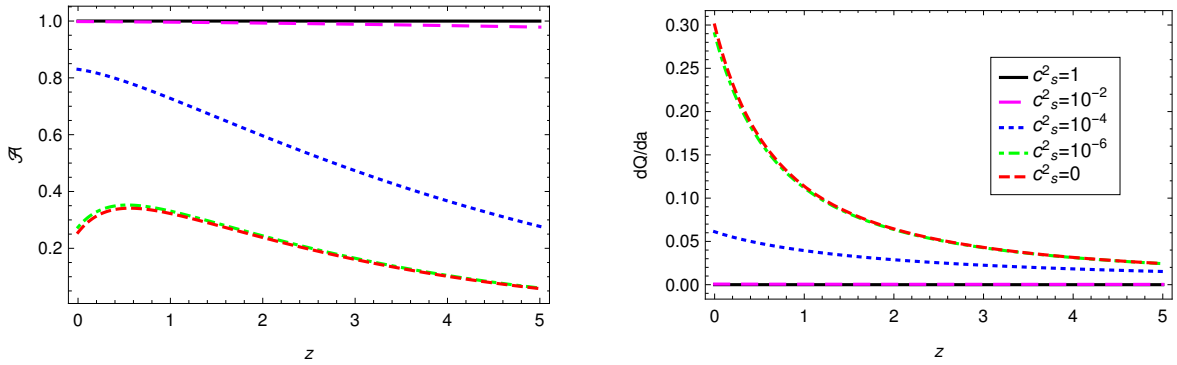

Figure 8.17: Left: Evolution of the magnification parameter $\mathcal{A}$ for the various sound speed cases. Right: Clustering rate $\partial Q/\partial a$ of dark energy perturbations. Both plots correspond to the mode $k = 200H_0$.

From the definition of Q in (6.4) we have that $\partial Q/\partial a \approx (Q-1)/a$, so that this factor grows at low redshift, as shown in Fig 8.17. On the other hand, even if this term decreases towards high redshift, it gets substantially enhanced by the factor $(G^{-1}\partial G/\partial a)^{-1}$ appearing in (8.4). From the growth factor fit formula (3.69) we know that

$$\frac{1}{G}\frac{dG}{da} = \frac{\Omega_m(a)^\gamma - 1}{a}\,. \tag{8.5}$$

Then, at high redshift we have $\partial G/\partial a << G$, so that the contribution coming from $\partial Q/\partial a$ gets strongly boosted by the inverse of the factor (8.5). On the other hand, at low redshift (8.5) implies that $|\partial G/\partial a| \approx G$ but now the clustering rate $\partial Q/\partial a$ increases, so we also find a sizeable contribution to $\mathcal{A}$.

Notice that, as shown in Fig 8.17, in terms of sound speed the magnification parameter behaves in opposite way to $T(k)$, i.e. lower c_s^2 implies stronger deviations with respect to ΛCDM. Since the ISW power spectrum (7.31) depends on the product $T\mathcal{A}$, the hierarchy of sound speed cases is broken in this effect. In fact, at every redshift included in Fig 8.16 we can observe that ISW deviations for $0 < c_s^2 < 1$ do not lie between $c_s^2 = 0$ and $c_s^2 = 1$. In

particular, we find that the case $c_s^2 = 10^{-2}$ is below $c_s^2 = 1$ at all redshifts, and shows the largest deviations from ΛCDM at $z = 2$.

In order to have an overview of the results shown in the two previous Sections we include Table 8.2, which gives a summary of the maximum deviations found in each effect for the effective dark energy fluid model relative to ΛCDM. For complementing the $w = -0.8$ case considered in the previous discussion we also show the results for the $w = -0.95$ case, which is a more realistic value if we consider observational constraints on the EoS parameter [45] and also that upcoming galaxy surveys like DESI and Euclid aim at testing the power spectrum at the $\sim 1\%$ level accuracy.

	$w = -0.8$		$w = -0.95$	
effect	$z = 0.1$	$z = 2$	$z = 0.1$	$z = 2$
Density	15	4	3	1
RSD	115	9	25	1
Doppler	115	15	25	5
Lensing	18	17	4	5
Local P.	20	15	5	3
Shapiro	20	18	4	4
ISW	80	80	27	18

Table 8.2: Summary of maximum relative deviations (rough percentages) with respect to ΛCDM in standard and relativistic effects for the effective dark energy fluid model considering $w = -0.8$ and $w = -0.95$.

8.3 Viscosity effects

To finish our discussion, in this Section we will briefly comment about the imprints of a potential dark energy fluid viscosity on the angular power spectrum. Following our discussion in Sec. 6.2, in term of our parametrization this implies the presence of a new sound speed parameter c_v^2 which give rise to a non-vanishing anisotropic stress, $\eta \neq 0$, so that the metric potentials Φ and Ψ are no longer equivalent. Mathematically, this case takes full advantage of our calculations (7.20)-(7.32) which were derived generically.

Equation (6.5) shows that the viscosity term introduces an effective sound speed $\hat{c}_s^2$ given by a combination of c_s^2 and c_v^2, which increases the possible cases to explore the degrees of freedom in our model. Here we consider two scenarios: the combination $(c_s^2, c_v^2) = (10^{-6}, 10^{-3})$ and $(c_s^2, c_v^2) = (0, 10^{-5})$, corresponding to the effective sound speeds $\hat{c}_s^2 \approx 10^{-2}$ and $\hat{c}_s^2 \approx 10^{-4}$, respectively. As we discussed in Sec. 6.2, the cases where $c_s^2 << c_v^2$ are more likely to exhibit the potential behaviour of the viscosity term in the fluid.

Figure 8.18 shows the relative power spectra for the standard effects with respect to ΛCDM for the two cases above mentioned, as well as for the cases $c_s^2 = 10^{-2}$ and $c_s^2 = 10^{-4}$ (which were included in the previous Sections). In this way we can compare the viscosity cases to their equivalent counterparts with $\eta = 0$ but featuring the same effective sound speed c_s^2.

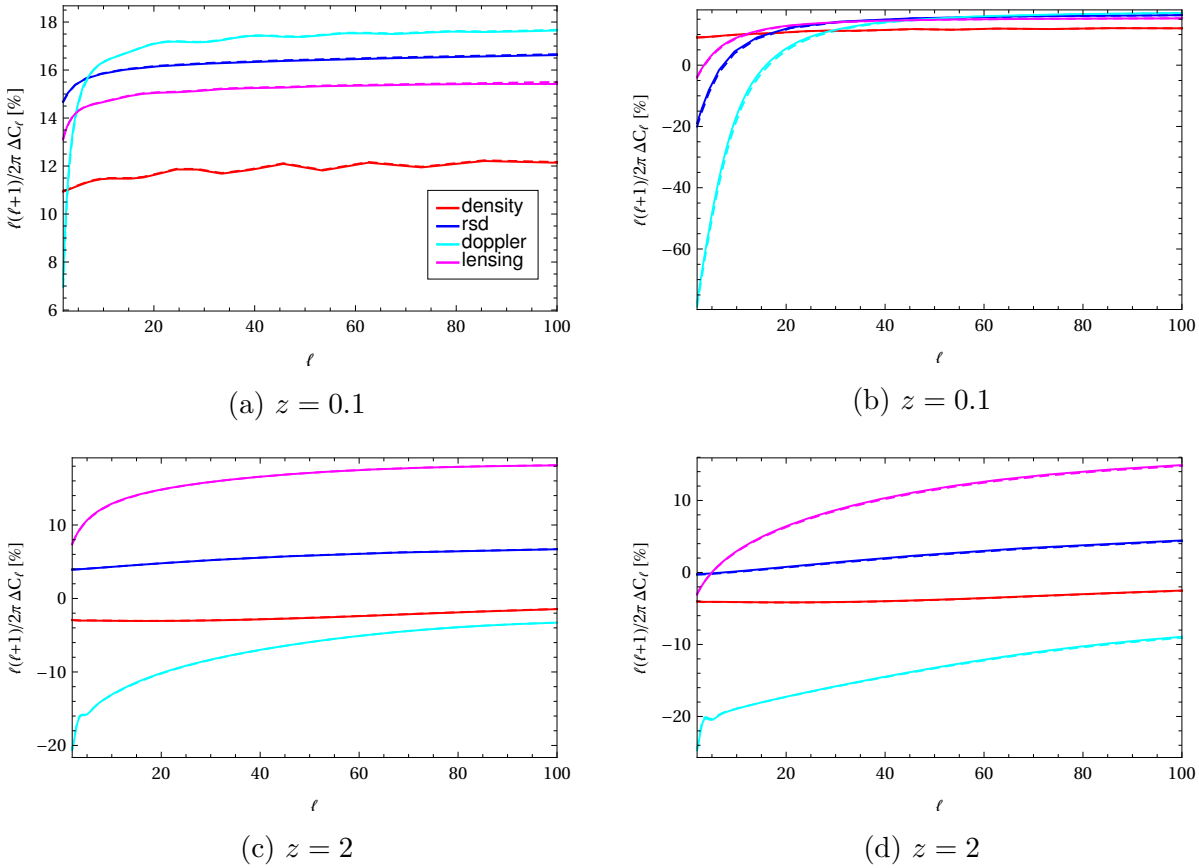

(a) $z = 0.1$ (b) $z = 0.1$

(c) $z = 2$ (d) $z = 2$

Figure 8.18: Deviations in standard effects with respect to ΛCDM. Left panels: $(c_s^2, c_v^2) = (10^{-6}, 10^{-3})$ (solid line) and $c_s^2 = 10^{-2}$ (dashed line). Right panels: $(c_s^2, c_v^2) = (0, 10^{-5})$ (solid line) and $c_s^2 = 10^{-4}$ (dashed line).

Notice that according to (6.4) the clustering parameter Q does not depend on the intrinsic sound speeds but on $\hat{c}_s^2$, so that it is degenerated with respect to c_s^2 and c_v^2. However, (6.8) shows that the growth index γ (which appears in the growth rate G) does depend directly on c_v^2 through η. From Fig 8.18 we find that, nonetheless, the standard effects cannot distinguish between viscosity and non-viscosity scenarios as the power spectra for the same effective sound speeds are completely equivalent, exhibiting no appreciable deviation at any redshift.

On the other hand, Fig 8.19 shows that the ISW effect is partially sensitive to the viscosity term c_v^2 and is able to reveal its features at high redshift and very large scales. In the same fashion as we discussed in the previous Section, this effect has the advantage of probing the term rate of change in the anisotropic stress $\partial\eta/\partial a$ in a cumulative way. Since in ΛCDM we have $\eta = 0$ this new contribution, despite being small, is able to enhance the ISW power spectrum in combination with the magnification factor $\mathcal{A}$ given in (8.4), thus introducing sizeable deviations from the case where $\hat{c}_s^2 = c_s^2$. Comparing both cases shown in Fig 8.19 we find that for $c^s = 0$ the presence of viscosity is best detected, even if deviations with respect to ΛCDM are lower than for $\hat{c}_s^2 = 10^{-2}$.

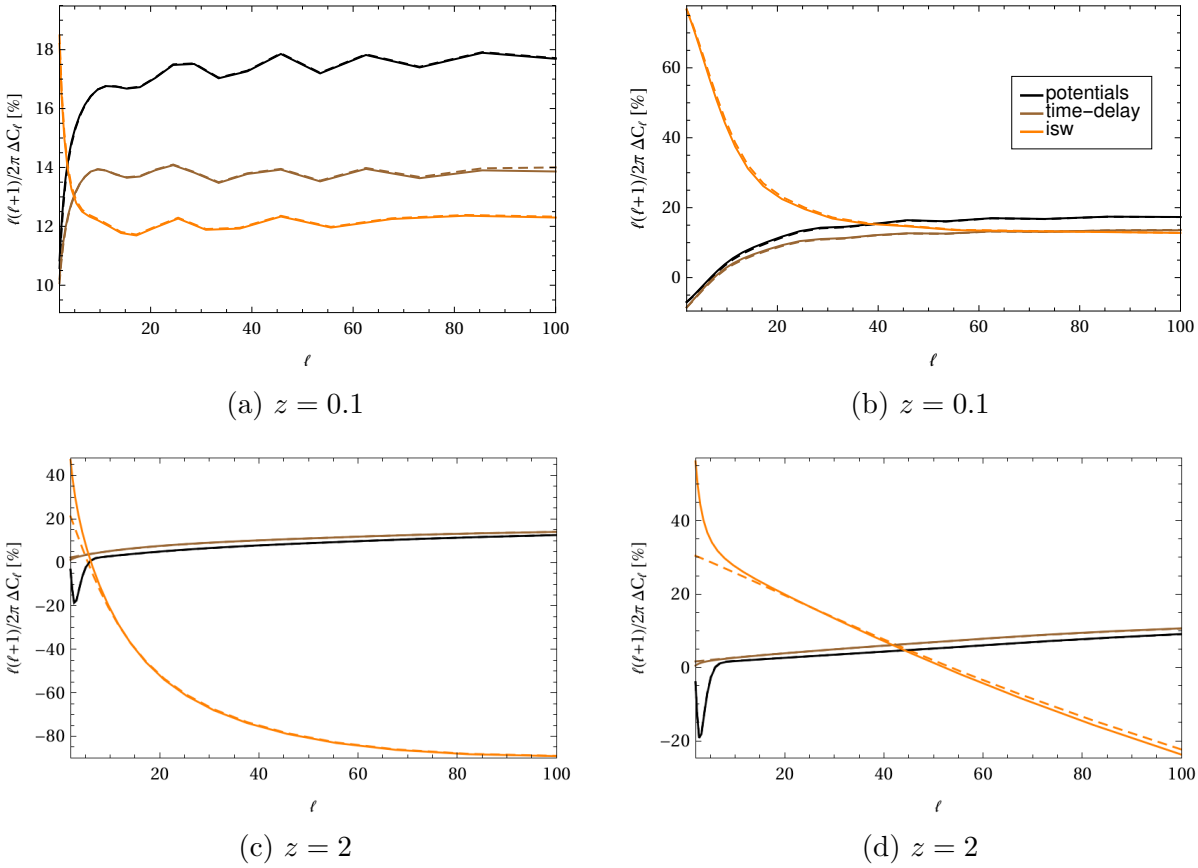

(a) $z = 0.1$ (b) $z = 0.1$

(c) $z = 2$ (d) $z = 2$

Figure 8.19: Deviations in relativistic effects with respect to ΛCDM. Left panels: $(c_s^2, c_v^2) = (10^{-6}, 10^{-3})$ (solid line) and $c_s^2 = 10^{-2}$ (dashed line). Right panels: $(c_s^2, c_v^2) = (0, 10^{-5})$ (solid line) and $c_s^2 = 10^{-4}$ (dashed line).

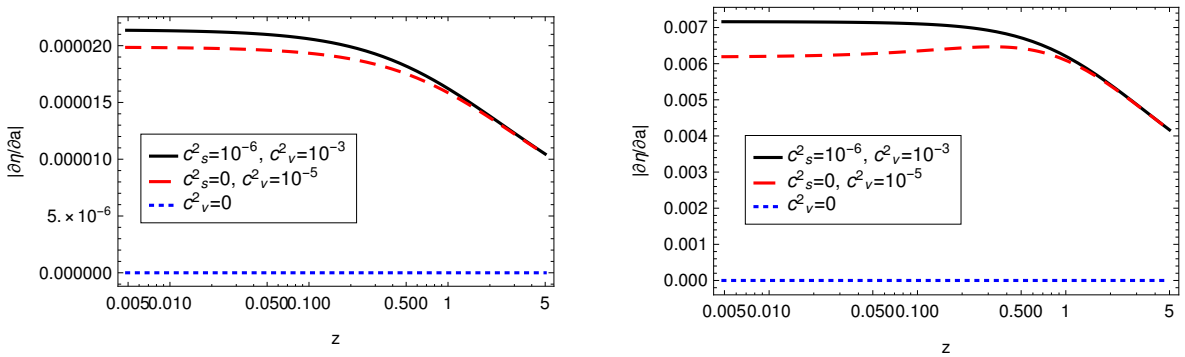

Figure 8.20: Rate of change of the anisotropic stress due to the presence of viscosity. Left: perturbation mode $k = 200H_0$. Right: perturbation mode $k = 10H_0$.

Figure 8.20 shows the rate of change in the anisotropic stress $\partial\eta/\partial a$ for two different perturbation modes. We note that this is roughly two orders of magnitude larger (in absolute value) for the perturbation mode $k = 10H_0 \sim 10^{-3}\text{Mpc}^{-1}$ than for $k = 200H_0 \sim 10^{-2}\text{Mpc}^{-1}$, which is consistent with the fact that anisotropic stress effects at very large scales are able imprint its features in the ISW power spectrum at low multipoles ($\ell \leq 5$) for $z = 2$.

Conclusion

In this work we have studied the observed angular power spectrum of a quintessence-like effective dark energy fluid model which is characterized by two degrees of freedom; an equation of state parameter $w \neq 1$ and a sound speed $0 \leq c_s^2 \leq 1$. We explored five different sound speed cases between $c_s^2 = 0$ and $c_s^2 = 1$, and we have compared the predictions against a fiducial ΛCDM cosmology up to multipoles $\ell \sim 100$ and redshift $z = 2$.

We have found that, overall, deviations from ΛCDM are stronger at low redshift, since the dark energy fluid starts to cluster more effectively during the late time universe. We find that matter density fluctuations deviates up to $\sim 15\%$ at $z = 0.1$, while redshift-space distortion and Doppler effect are enhanced up to $\sim 115\%$ with respect to ΛCDM for $c_s^2 = 0$, where the dark energy fluid can cluster at all scales. At higher redshifts, deviations in these terms decrease and remain bounded, except for gravitational lensing which shows deviations of up to 20% at $z = 2$ as it is an integrated effect from source to observer. For the relativistic effects we have shown that the Shapiro time-delay and the local potential terms behave in a qualitatively similar way, deviating up to $\sim 20\%$ at low redshift. The latter can also deviate at very large scales at higher redshifts. Finally, the integrated Sachs-Wolfe effect shows the most impact from the dark energy fluid, as its deviations may reach up to $\sim 80\%$ of relative difference with respect to ΛCDM around $z = 2$ due to its capacity to probe cumulatively not only the rate of growth of G itself but also its evolution, which is consistent with previous studies [33, 66]. In addition, this effect might be sensible to the presence of viscosity in the dark energy fluid at high redshift, converting it in a particularly valuable tool for testing and constraining dark energy models using galaxy surveys. However, the amplitude of this effect is the weakest of the full power spectrum, and then it needs to be extracted or isolated from the full signal very carefully.

It is important to remind that in order to make the effect of dark energy perturbations stronger in the studied model we have used a value of the equation of state parameter $w = -0.8$. For values close enough to $w = -1$ the effects on the observables due to the dark energy perturbations are drastically reduced, as all the phenomenological functions used (e.g. Q and η) have a contribution which is modulated by the combination $(1 + w)$. Likewise, in such case the amplitude of the power spectrum (or transfer functions) would become closer to ΛCDM. At the background level this also implies a smaller difference in the comoving distances and expansion histories. We also emphasize that the angular power spectrum calculated adopting the (Q, η) parametrization in Chapter 7 is not restricted to the dark energy fluid description studied in this thesis but it allows to test a broad class of dark energy and modified gravity models that might be taken into account in such a framework,

as $f(R)$ gravity and DGP model, among others.

Even if the observational evidence keeps reducing the range of viable dark energy models [50], and thus providing additional support to ΛCDM, the study of this kind of theories and their observational consequences remain transcendent not only as an attempt to unveil the physical origin of the accelerated cosmic expansion, but also to keep pushing the boundaries of our current cosmological picture and testing the concordance model in all regimes.

Bibliography

[1] Ya. B. Zeldovich, "Gravitational instability: An Approximate theory for large density perturbations," *Astron. Astrophys.*, vol. 5, pp. 84–89, 1970.

[2] D. G. York *et al.*, "The Sloan Digital Sky Survey: Technical Summary," *Astron. J.*, vol. 120, pp. 1579–1587, 2000.

[3] V. Springel *et al.*, "Simulating the joint evolution of quasars, galaxies and their large-scale distribution," *Nature*, vol. 435, pp. 629–636, 2005.

[4] M. Colless *et al.*, "The 2dF Galaxy Redshift Survey: Spectra and redshifts," *Mon. Not. Roy. Astron. Soc.*, vol. 328, p. 1039, 2001.

[5] R. Laureijs, J. Amiaux, S. Arduini, J. . Augueres, J. Brinchmann, R. Cole, M. Cropper, C. Dabin, L. Duvet, A. Ealet, and et al., "Euclid Definition Study Report," *ArXiv e-prints*, Oct. 2011.

[6] D. H. Weinberg, M. J. Mortonson, D. J. Eisenstein, C. Hirata, A. G. Riess, and E. Rozo, "Observational Probes of Cosmic Acceleration," *Phys. Rept.*, vol. 530, pp. 87–255, 2013.

[7] E. Hubble, "A Relation between Distance and Radial Velocity among Extra-Galactic Nebulae," *Proceedings of the National Academy of Science*, vol. 15, pp. 168–173, Mar. 1929.

[8] A. G. Riess *et al.*, "Observational evidence from supernovae for an accelerating universe and a cosmological constant," *Astron. J.*, vol. 116, pp. 1009–1038, 1998.

[9] D. N. Spergel *et al.*, "First year Wilkinson Microwave Anisotropy Probe (WMAP) observations: Determination of cosmological parameters," *Astrophys. J. Suppl.*, vol. 148, pp. 175–194, 2003.

[10] M. Tegmark *et al.*, "Cosmological parameters from SDSS and WMAP," *Phys. Rev.*, vol. D69, p. 103501, 2004.

[11] S. Weinberg, "The Cosmological Constant Problem," *Rev. Mod. Phys.*, vol. 61, pp. 1–23, 1989.

[12] S. Capozziello and M. De Laurentis, "Extended Theories of Gravity," *Phys. Rept.*, vol. 509, pp. 167–321, 2011.

[13] S. Nojiri and S. D. Odintsov, "Introduction to modified gravity and gravitational alternative for dark energy," *eConf*, vol. C0602061, p. 06, 2006. [Int. J. Geom. Meth. Mod. Phys.4,115(2007)].

[14] Y. Dirian, S. Foffa, N. Khosravi, M. Kunz, and M. Maggiore, "Cosmological perturbations and structure formation in nonlocal infrared modifications of general relativity," *JCAP*, vol. 1406, p. 033, 2014.

[15] G. R. Dvali, G. Gabadadze, and M. Porrati, "4-D gravity on a brane in 5-D Minkowski space," *Phys. Lett.*, vol. B485, pp. 208–214, 2000.

[16] G. W. Horndeski, "Second-order scalar-tensor field equations in a four-dimensional space," *Int. J. Theor. Phys.*, vol. 10, pp. 363–384, 1974.

[17] I. Zlatev, L.-M. Wang, and P. J. Steinhardt, "Quintessence, cosmic coincidence, and the cosmological constant," *Phys. Rev. Lett.*, vol. 82, pp. 896–899, 1999.

[18] C. Armendariz-Picon, V. F. Mukhanov, and P. J. Steinhardt, "A Dynamical solution to the problem of a small cosmological constant and late time cosmic acceleration," *Phys. Rev. Lett.*, vol. 85, pp. 4438–4441, 2000.

[19] N. Kaiser, "Clustering in real space and in redshift space," *Mon. Not. Roy. Astron. Soc.*, vol. 227, pp. 1–27, 1987.

[20] A. J. S. Hamilton, "Measuring Omega and the real correlation function from the redshift correlation function," *Astrophys. J.*, vol. 385, pp. L5–L8, 1992.

[21] T. J. Broadhurst, A. N. Taylor, and J. A. Peacock, "Mapping cluster mass distributions via gravitational lensing of background galaxies," *Astrophys. J.*, vol. 438, p. 49, 1995.

[22] R. Moessner, B. Jain, and J. V. Villumsen, "The effect of weak lensing on the angular correlation function of faint galaxies," *Mon. Not. Roy. Astron. Soc.*, vol. 294, p. 291, 1998.

[23] C. Bonvin, "Effect of Peculiar Motion in Weak Lensing," *Phys. Rev.*, vol. D78, p. 123530, 2008.

[24] J. Yoo, A. L. Fitzpatrick, and M. Zaldarriaga, "A New Perspective on Galaxy Clustering as a Cosmological Probe: General Relativistic Effects," *Phys. Rev.*, vol. D80, p. 083514, 2009.

[25] J. Yoo, "General Relativistic Description of the Observed Galaxy Power Spectrum: Do We Understand What We Measure?," *Phys. Rev.*, vol. D82, p. 083508, 2010.

[26] C. Bonvin and R. Durrer, "What galaxy surveys really measure," *Phys. Rev.*, vol. D84, p. 063505, 2011.

[27] C. Bonvin, C. Caprini, R. Sturani, and N. Tamanini, "Effect of matter structure on the gravitational waveform," *Phys. Rev.*, vol. D95, no. 4, p. 044029, 2017.

[28] C. Bonvin, "Isolating relativistic effects in large-scale structure," *Class. Quant. Grav.*, vol. 31, no. 23, p. 234002, 2014.

[29] C. Bonvin, L. Hui, and E. Gaztanaga, "Optimising the measurement of relativistic distortions in large-scale structure," *JCAP*, vol. 1608, no. 08, p. 021, 2016.

[30] J. Yoo, N. Hamaus, U. Seljak, and M. Zaldarriaga, "Going beyond the Kaiser redshift-space distortion formula: a full general relativistic account of the effects and their detectability in galaxy clustering," *Phys. Rev.*, vol. D86, p. 063514, 2012.

[31] L. Lombriser, J. Yoo, and K. Koyama, "Relativistic effects in galaxy clustering in a parametrized post-Friedmann universe," *Phys. Rev.*, vol. D87, p. 104019, 2013.

[32] L. Amendola, M. Kunz, and D. Sapone, "Measuring the dark side (with weak lensing)," *JCAP*, vol. 0804, p. 013, 2008.

[33] D. Sapone, M. Kunz, and M. Kunz, "Fingerprinting Dark Energy," *Phys. Rev.*, vol. D80, p. 083519, 2009.

[34] S. Nesseris and D. Sapone, "Accuracy of the growth index in the presence of dark energy perturbations," *Phys. Rev.*, vol. D92, no. 2, p. 023013, 2015.

[35] S. Tsujikawa, "Matter density perturbations and effective gravitational constant in modified gravity models of dark energy," *Phys. Rev.*, vol. D76, p. 023514, 2007.

[36] J. J. M. Carrasco, M. P. Hertzberg, and L. Senatore, "The Effective Field Theory of Cosmological Large Scale Structures," *JHEP*, vol. 09, p. 082, 2012.

[37] E. Lifshitz, "Republication of: On the gravitational stability of the expanding universe," *J. Phys.(USSR)*, vol. 10, p. 116, 1946. [Gen. Rel. Grav.49,no.2,18(2017)].

[38] J. M. Bardeen, "Gauge Invariant Cosmological Perturbations," *Phys. Rev.*, vol. D22, pp. 1882–1905, 1980.

[39] R. Durrer, *The Cosmic Microwave Background*. Cambridge, UK: Cambridge University Press, 2008.

[40] S. Dodelson, *Modern cosmology*. San Diego, CA: Academic Press, 2003.

[41] D. Huterer *et al.*, "Growth of cosmic structure: Probing dark energy beyond expansion," *Astroparticle Physics*, vol. 63, pp. 23 – 41, 2015. Dark Energy and CMB.

[42] A. Lewis and A. Challinor, "Weak gravitational lensing of the cmb," *Phys. Rept.*, vol. 429, pp. 1–65, 2006.

[43] J. Renk, M. Zumalacarregui, and F. Montanari, "Gravity at the horizon: on relativistic effects, CMB-LSS correlations and ultra-large scales in Horndeski's theory," *JCAP*, vol. 1607, no. 07, p. 040, 2016.

[44] J. Khoury and A. Weltman, "Chameleon fields: Awaiting surprises for tests of gravity

in space," *Phys. Rev. Lett.*, vol. 93, p. 171104, 2004.

[45] P. A. R. Ade *et al.*, "Planck 2015 results. XIII. Cosmological parameters," *Astron. Astrophys.*, vol. 594, p. A13, 2016.

[46] C. L. Bennett, D. Larson, J. L. Weiland, N. Jarosik, G. Hinshaw, N. Odegard, K. M. Smith, R. S. Hill, B. Gold, M. Halpern, E. Komatsu, M. R. Nolta, L. Page, D. N. Spergel, E. Wollack, J. Dunkley, A. Kogut, M. Limon, S. S. Meyer, G. S. Tucker, and E. L. Wright, "Nine-year Wilkinson Microwave Anisotropy Probe (WMAP) Observations: Final Maps and Results," *apjs*, vol. 208, p. 20, Oct. 2013.

[47] A. G. c. Riess, "A 2.4% Determination of the Local Value of the Hubble Constant," *Astrophys. J.*, vol. 826, no. 1, p. 56, 2016.

[48] M. P. Hobson, G. P. Efstathiou, and A. N. Lasenby, *General Relativity: An Introduction for Physicists*. Cambridge, UK: Cambridge University Press, 2006.

[49] B. P. Abbott *et al.*, "Multi-messenger Observations of a Binary Neutron Star Merger," *Astrophys. J.*, vol. 848, no. 2, p. L12, 2017.

[50] J. M. Ezquiaga and M. Zumalacárregui, "Dark Energy After GW170817: Dead Ends and the Road Ahead," *Phys. Rev. Lett.*, vol. 119, no. 25, p. 251304, 2017.

[51] W. Hu and I. Sawicki, "Models of f(R) Cosmic Acceleration that Evade Solar-System Tests," *Phys. Rev.*, vol. D76, p. 064004, 2007.

[52] S. M. Carroll, "Quintessence and the rest of the world," *Phys. Rev. Lett.*, vol. 81, pp. 3067–3070, 1998.

[53] M. Chevallier and D. Polarski, "Accelerating universes with scaling dark matter," *Int. J. Mod. Phys.*, vol. D10, pp. 213–224, 2001.

[54] E. V. Linder, "Exploring the expansion history of the universe," *Phys. Rev. Lett.*, vol. 90, p. 091301, 2003.

[55] G. Gubitosi, F. Piazza, and F. Vernizzi, "The Effective Field Theory of Dark Energy," *JCAP*, vol. 1302, p. 032, 2013. [JCAP1302,032(2013)].

[56] E. C. G. Stueckelberg, "Interaction energy in electrodynamics and in the field theory of nuclear forces," *Helv. Phys. Acta*, vol. 11, pp. 225–244, 1938.

[57] M. Kunz and D. Sapone, "Dark Energy versus Modified Gravity," *Phys. Rev. Lett.*, vol. 98, p. 121301, 2007.

[58] D. Sapone and E. Majerotto, "Fingerprinting Dark Energy III: distinctive marks of viscosity," *Phys. Rev.*, vol. D85, p. 123529, 2012.

[59] H. Kodama and M. Sasaki, "Cosmological perturbation theory," *Progress of Theoretical Physics Supplement*, vol. 78, pp. 1–166, 1984.

[60] W. Hu, "Structure formation with generalized dark matter," *Astrophys. J.*, vol. 506, pp. 485–494, 1998.

[61] E. V. Linder and R. N. Cahn, "Parameterized Beyond-Einstein Growth," *Astropart. Phys.*, vol. 28, pp. 481–488, 2007.

[62] A. Hojjati, L. Pogosian, and G.-B. Zhao, "Testing gravity with CAMB and CosmoMC," *JCAP*, vol. 1108, p. 005, 2011.

[63] M. LoVerde and N. Afshordi, "Extended Limber Approximation," *Phys. Rev.*, vol. D78, p. 123506, 2008.

[64] A. Lewis, A. Challinor, and A. Lasenby, "Efficient computation of CMB anisotropies in closed FRW models," *Astrophys. J.*, vol. 538, pp. 473–476, 2000.

[65] D. J. Eisenstein *et al.*, "Detection of the baryon acoustic peak in the large-scale correlation function of sdss luminous red galaxies," *The Astrophysical Journal*, vol. 633, no. 2, p. 560, 2005.

[66] A. Cooray, D. Huterer, and D. Baumann, "Growth rate of large scale structure as a powerful probe of dark energy," *Phys. Rev.*, vol. D69, p. 027301, 2004.

Appendix A

Conventions

In Chapter 4 we work with the general representation of the metric, i.e. without choosing any particular gauge. This is useful for determining whether a given expression is gauge invariant and hence physically observable. The perturbed FLRW metric is

$$ds^2 = a^2\big(-(1+2A)d\tau^2 - 2B_i d\tau dx^i + [(1+2H_L)\delta_{ij} + 2H_{Tij} + 2H_{ij}]\, dx^i dx^j\big)\,, \tag{A.1}$$

where A, H_L, B_i and H_{Tij} are scalar degrees of freedom, two of which can be removed by gauge transformations, and H_{ij} is the transverse traceless gravitational wave term, which is set to zero throughout the present analysis. The metric perturbations B_i and H_{Tij} in terms of their Fourier transforms are

$$B_i(\mathbf{k},t) = -\frac{1}{k}\partial_i B\,, \tag{A.2}$$

$$H_{Tij}(\mathbf{k},t) = \frac{1}{k^2}\partial_i\partial_j H_T + \frac{1}{3}\delta_{ij}H_T\,. \tag{A.3}$$

The variables Φ and Ψ represent the gauge invariant Bardeen potentials [38], which are given by

$$\Phi \equiv -H_L - \frac{1}{3}H_T + \frac{\mathcal{H}}{k^2}\dot{H}_L - \frac{\mathcal{H}}{k}B\,, \tag{A.4}$$

$$\Psi \equiv A + \frac{\mathcal{H}}{k}B + \frac{1}{k}\dot{B} - \frac{\mathcal{H}}{k^2}\dot{H}_L - \frac{1}{k^2}\ddot{H}_T\,. \tag{A.5}$$

In the Newtonian (or longitudinal) gauge we have that $B = H_T = 0$ and these potentials reduce to $\Psi = A$, $\Phi = -H_L$, so that the metric in such case takes the well-known form

$$ds^2 = a^2[-(1+2\Psi)d\tau^2 + (1-2\Phi)\delta_{ij}dx^i dx^j]\,. \tag{A.6}$$

The Christoffel symbols (connection coefficients) are given by

$$\Gamma^{\mu}_{\alpha\beta} = \frac{1}{2}g^{\mu\lambda}(\partial_\alpha g_{\lambda\beta} + \partial_\beta g_{\lambda\alpha} - \partial_\lambda g_{\alpha\beta})\,. \tag{A.7}$$

With this, the Ricci tensor is computed as

$$R_{\mu\nu} = \partial_\alpha\Gamma^{\alpha}_{\mu\nu} - \partial_\nu\Gamma^{\alpha}_{\mu\alpha} + \Gamma^{\beta}_{\beta\alpha}\Gamma^{\alpha}_{\mu\nu} - \Gamma^{\alpha}_{\mu\beta}\Gamma^{\beta}_{\nu\alpha} \tag{A.8}$$

and the Ricci scalar is given by the contraction

$$R = g^{\mu\nu}R_{\mu\nu}\,. \tag{A.9}$$

Appendix B

Relativistic effects calculations

In this appendix we include some calculations complementing the discussion in Chapter 4.

B.1 Calculation of redshift fluctuations

As we discussed in Sec. 4.2.1, if a photon is emitted at the time t_s and it is received at t_o, the temperature at emission T_s and the observed temperature T_o are related to each other via

$$\frac{T_o}{T_s} = \frac{\omega_o}{\omega_s} = \frac{(n^\mu u_\mu)_o}{(n^\mu u_\mu)_s} = \frac{a(t_s)}{a(t_o)} = \frac{1}{1+z}\,, \tag{B.1}$$

where $a(t_s)$ and $a(t_o)$ are the scale factors of the universe at the time of emission and observation, respectively. Taking variations on both sides we find

$$\delta\left(\frac{T_o}{T_s}\right) = \delta\left(\frac{(n^\mu u_\mu)_o}{(n^\mu u_\mu)_s}\right) = \delta\left(\frac{1}{1+z}\right) = -\frac{1}{(1+z)^2}\delta z\,. \tag{B.2}$$

The left hand side of the previous expression can be simplified further since up to first order this can be written as

$$\delta\left(\frac{(n^\mu u_\mu)_o}{(n^\mu u_\mu)_s}\right) = \frac{1}{1+z}\left(\frac{\delta(n^\mu u_\mu)_o}{(n^\mu u_\mu)_o} - \frac{\delta(n^\mu u_\mu)_s}{(n^\mu u_\mu)_s}\right) \equiv \frac{1}{1+z}\left[\frac{\delta(n^\mu u_\mu)}{(n^\mu u_\mu)}\right]_s^o\,. \tag{B.3}$$

Then, using the right hand side of (B.2) we obtain that the redshift fluctuation is given in terms of the four-velocity of the fluid and photon momenta as

$$\delta z = -(1+z)\left[\frac{\delta(n^\mu u_\mu)}{(n^\mu u_\mu)}\right]_s^o\,. \tag{B.4}$$

Since $u^\mu = a^{-1}[(1-A), v^i]$, where v^i is the peculiar velocity of the matter, once the photon four-momentum n^μ is known we can then compute the redshift fluctuation in terms of observable quantities using (B.4). Notice that at zeroth order we have $\bar{n}^\mu \bar{u}_\mu = \bar{n}^0 \bar{u}_0 = \bar{u}_0$ since v^i is perturbative quantity and $\bar{n}^0 = 1$. Then, the last factor in the above equation can be expanded up to first order as

$$\frac{\delta(n^\mu u_\mu)}{n^\mu u_\mu} = \frac{\delta n^\mu u_\mu + n^\mu \delta u_\mu}{n^\mu u_\mu} \approx \frac{\delta n^\mu \bar{u}_\mu + \bar{n}^\mu \delta u_\mu}{\bar{n}^0 \bar{u}_0} = \delta n^0 + \frac{\delta u_0 + \bar{n}^i \delta u_i}{\bar{u}_0} \,. \tag{B.5}$$

Finally, lowering indexes so that $u_0 = g_{0\nu}u^\nu = -(1+A)$ and $u_i = g_{i\nu}u^\nu = -B_i + v_i$, we find that the redshift fluctuation is given by

$$\delta z = -(1+z)\left[\delta n^0 + A + \bar{n}^i B_i - \bar{n}^i v_i\right]_s^o \,, \tag{B.6}$$

which correspond to the result presented in Sec. 4.2.1. Notice that δz depends on the fluctuation in the time component of the photon four-momenta, δn^0. Then, we next study the $\mu = 0$ component of the geodesic equation at first order for computing such contribution. As discussed in Chapter 2, in term of conformal coordinates the background Christoffel symbols vanish, then the $\mu = 0$ component of the geodesic equation at first order is simply

$$\frac{d\delta n^0}{d\lambda} = -\delta\Gamma^0_{\alpha\beta}\bar{n}^\alpha \bar{n}^\beta \,. \tag{B.7}$$

The perturbed quantities $\delta\Gamma^0_{\alpha\beta}$ written in terms of the metric perturbations are given by

$$\delta\Gamma^0_{\alpha\beta} = -\frac{1}{2}\left[h_{0\alpha,\beta} + h_{0\beta,\alpha} - \dot{h}_{\alpha\beta}\right] \,, \tag{B.8}$$

and then, integrating (B.7) from the source to the observer position, we have

$$\delta n^0 = \left[h_{00} + h_{0j}n^j\right]_0^{r_s} - \frac{1}{2}\int_0^{r_s} d\lambda \dot{h}_{\alpha\beta}n^\alpha n^\beta \,. \tag{B.9}$$

Working out the term inside the last integral we find that

$$\dot{h}_{\alpha\beta}n^\alpha n^\beta = 2\left[-(\Psi+\Phi) + \frac{1}{k}\frac{d\dot{B}}{d\lambda} + \frac{1}{k^2}\left(\frac{d^2\dot{H}_T}{d\lambda^2} - 2\frac{d\ddot{H}_T}{d\lambda}\right)\right] \,. \tag{B.10}$$

Finally, substituting back into (B.6) and using the explicit form for A given by (A.5) we arrive at our final expression for the redshift fluctuation

$$\delta z = -(1+z)\left[-\Psi|_s^o + \mathbf{V}\cdot\mathbf{n}|_s^o - \int_s^o d\lambda(\dot{\Phi} + \dot{\Psi})\right] \,, \tag{B.11}$$

where $V \equiv v - k^{-1}\dot{H}_T$ is the gauge invariant velocity potential. This is the result presented at the end of Sec. 4.2.1.

B.2 Calculation of volume fluctuations

In this section we present the details of the calculations presented in Sec. 4.2.2. We start by writing the volume element in terms of the observational coordinate system

$$\begin{aligned} dV &= \sqrt{-g}\varepsilon_{\mu\nu\alpha\beta}u^\mu \frac{\partial x^\nu}{\partial z}\frac{\partial x^\alpha}{\partial \theta_s}\frac{\partial x^\beta}{\partial \phi_s}|J| dz d\theta_o d\phi_o \\ &\equiv v(z,\theta_o,\phi_o) dz d\theta_o d\phi_o \,, \end{aligned} \tag{B.12}$$

where $|J|$ is the determinant of the Jacobian of the coordinate transformation going from the angles at the source (θ_s, ϕ_s) to the angles at the observer (θ_o, ϕ_o), and $\varepsilon_{\mu\nu\alpha\beta} = \varepsilon_{[\mu\nu\alpha\beta]}$ is the Levi-Civita symbol. In the second line of (B.12) we have introduced the density v which determines the actual volume perturbation appearing in (4.7), i.e.

$$\frac{\delta V}{\bar{V}} = \frac{v(z) - \bar{v}(z)}{\bar{v}(z)} = \frac{\delta v}{\bar{v}}\,. \tag{B.13}$$

As previously discussed, in a homogeneous and isotropic FLRW universe, photons propagates on straight lines, so that $\theta_o = \theta_s$ and $\phi_o = \phi_s$. However, in the perturbed universe the observation and emission angles do not coincide. We can write the fluctuation in the observation angle up to first order as

$$\theta_s = \theta_o + \delta\theta\,, \tag{B.14}$$

$$\phi_s = \phi_o + \delta\phi\,. \tag{B.15}$$

implying that $|J| = 1 + \partial\delta\theta/\partial\theta + \partial\delta\phi/\partial\phi$. Also, for the metric determinant we find $\sqrt{-g} = a^4(1 + A + 3H_L) = a^4(1 + \Psi - 3\Phi)$. The background physical volume element $d\bar{V} = d^3\bar{x}$ in spherical coordinates is then

$$d\bar{V}(\bar{z}) = \frac{\bar{r}^2}{(1+\bar{z})^4\mathcal{H}} d\bar{z} \sin\theta_o d\theta_o d\phi_o\,. \tag{B.16}$$

Here, the relation between the original differential element dr and the actual dz appearing in this volume element is understood by recalling that at the background level $a(t) = 1/(1+z)$ and along a photon geodesic we have that $d\bar{r} = -dt$ (using $c = 1$). Then

$$\frac{d\bar{r}}{d\bar{z}} = -\frac{dt}{d\bar{z}} = \frac{\dot{a}}{a^2} = \frac{\mathcal{H}}{a}\,. \tag{B.17}$$

Using the previous expressions we find that the volume element v defined in the second line of (B.12) is

$$v(z) = a^3(1 + A + 3H_L)\left[\frac{dr}{dz} r^2 \sin\theta_s \left(1 + \frac{\partial\delta\theta}{\partial\theta} + \frac{\partial\delta\phi}{\partial\phi}\right) - \left(A\frac{d\bar{r}}{d\bar{z}} + v_r \frac{dt}{dz}\right)\bar{r}^2 \sin\theta_o\right]\,, \tag{B.18}$$

where we already know the redshift perturbation δz from (B.11). At linear order we can write the change in comoving distance $r = \bar{r} + \delta r$ with redshift along the perturbed photon geodesic as

$$\frac{dr}{dz} = \frac{d\bar{r}}{dz} + \frac{d\delta r}{d\bar{z}} - \frac{d\delta z}{d\bar{z}}\frac{d\bar{r}}{d\bar{z}} = \left(\frac{d\bar{r}}{dt} + \frac{d\delta r}{d\lambda} - \frac{d\delta z}{d\lambda}\frac{d\bar{r}}{d\bar{z}}\right)\frac{dt}{d\bar{z}}\,, \tag{B.19}$$

where we have used that at background level $dt = d\lambda$. The last term of the previous equation contains the redshift-space distortion effect, which represents the largest correction to the matter power spectrum. Now, using that $d\bar{r} = -dt$, then $d\bar{r}/d\bar{z} = -dt/d\bar{z} = \mathcal{H}/a$, and with this the volume element becomes,

$$v(z) = \frac{a^4}{\mathcal{H}}\left[-\left(\frac{d\bar{r}}{dt} + \frac{d\delta r}{d\lambda} - \frac{d\delta z}{d\lambda}\frac{d\bar{r}}{d\bar{z}}\right) r^2 \sin\theta_s + \bar{r}^2 \sin\theta_o \left(\frac{\partial\delta\theta}{\partial\theta} + \frac{\partial\delta\phi}{\partial\phi} - A - v_r\right)\right]\,. \tag{B.20}$$

The first term can be reduced using that up to first order $r^2 = \bar{r}^2 + 2\bar{r}\delta r$ and $\sin\theta_s = \sin(\theta_o + \delta\theta) = \sin\theta_o + \cos\theta_o\delta\theta$. Then, rearranging terms we obtain (herein after we drop the superscript in θ and ϕ)

$$v(z) = \frac{a^4\bar{r}^2\sin\theta}{\mathcal{H}}\times \left[1 + 3H_L + \left(\cot\theta + \frac{\partial}{\partial\theta}\right)\delta\theta + \frac{\partial\delta\phi}{\partial\phi} - \mathbf{v}\cdot\mathbf{n} + 2\frac{\delta r}{r} - \frac{d\delta r}{d\lambda} + \frac{1}{\mathcal{H}(1+\bar{z})}\frac{d\delta z}{d\lambda}\right], \tag{B.21}$$

where we have used that $v_r = \mathbf{v}\cdot\mathbf{n}$. Notice that the expression (B.21) is evaluated at the observed redshift, and to obtain the fluctuation appearing in (B.13) we need to subtract the unperturbed part $\bar{v}(z)$. Then, writing the observed redshift as a perturbation with respect to a background quantity as $z = \bar{z} + \delta z$, the second term in the numerator can be expanded in Taylor series as

$$\bar{v}(z) \approx \bar{v}(\bar{z}) + \left.\frac{\partial\bar{v}}{\partial z}\right|_{\bar{z}}\delta z\,, \tag{B.22}$$

and comparing with (B.21) we have that the background term is

$$\bar{v}(\bar{z}) = \frac{\bar{r}^2\sin\theta}{(1+\bar{z})^4\mathcal{H}}\,, \tag{B.23}$$

then, taking the derivative with respect to $\bar{z}$ and using the Leibniz rule for the three factors we find that

$$\frac{\partial\bar{v}}{\partial\bar{z}} = \frac{\bar{v}(\bar{z})}{1+\bar{z}}\left(-4 + \frac{2}{r}\frac{d\bar{r}}{d\bar{z}} + (1+\bar{z})\frac{1}{\mathcal{H}}\frac{d\mathcal{H}}{d\bar{z}}\right). \tag{B.24}$$

Now, using that for background quantities $dr = -dt$ so that $d\mathcal{H}/d\bar{z} = (dt/d\bar{z})(d\mathcal{H}/d\bar{t}) = -a\dot{\mathcal{H}}/\mathcal{H} = -(1+\bar{z})^{-1}\dot{\mathcal{H}}/\mathcal{H}$, the previous expressions reduces to

$$\frac{\partial\bar{v}}{\partial\bar{z}} = \frac{\bar{v}(\bar{z})}{1+\bar{z}}\left(-4 + \frac{2}{r\mathcal{H}} + \frac{\dot{\mathcal{H}}}{\mathcal{H}^2}\right). \tag{B.25}$$

Then, combining (B.18), (B.22) and (B.25) into (B.13) we find that the volume element perturbation up to first order is given by

$$\begin{aligned}\frac{\delta v}{\bar{v}}(z) \approx \frac{v(z) - \bar{v}(\bar{z}) - \bar{v}'(\bar{z})\delta z}{\bar{v}(\bar{z})} &= 3H_L + \left(\frac{\delta v}{v}\right)_\Omega - \mathbf{v}\cdot\mathbf{n} + 2\frac{\delta r}{r} - \frac{d\delta r}{d\lambda} + \frac{1}{\mathcal{H}(1+\bar{z})}\frac{d\delta z}{d\lambda} \\ &\quad - \frac{1}{1+\bar{z}}\left(-4 + \frac{2}{r\mathcal{H}} + \frac{\dot{\mathcal{H}}}{\mathcal{H}^2}\right)\delta z\,,\end{aligned} \tag{B.26}$$

where we have defined the angular part of the volume perturbation as

$$\left(\frac{\delta v}{v}\right)_\Omega \equiv \left(\cot\theta + \frac{\partial}{\partial\theta}\right)\delta\theta + \frac{\partial\delta\phi}{\partial\phi}\,. \tag{B.27}$$

Then, in order to obtain the volume fluctuation we need to compute every perturbation appearing in the right hand side of the previous equation. We have already computed the redshift fluctuation δz appearing in the second line of the above expression in (B.11), and the contribution from the rightmost term in the first line can be computed by differentiating

the former. Omitting the 'unmeasurable quantities' evaluated at the observer position and using the Leibniz rule for differentiating both round and square parentheses, we find

$$\frac{1}{\mathcal{H}(1+\bar{z})}\frac{d\delta z}{d\lambda} = \left[-\Psi + \mathbf{V}\cdot\mathbf{n} - \int_s^o \left(\frac{\partial\Phi}{\partial t} - \frac{\partial\Psi}{\partial t}\right) dt\right] \tag{B.28}$$

$$- \frac{1}{\mathcal{H}}\frac{d}{d\lambda}\left[-\Psi + \mathbf{V}\cdot\mathbf{n} - \int_s^o \left(\frac{\partial\Phi}{\partial t} - \frac{\partial\Psi}{\partial t}\right) dt\right] . \tag{B.29}$$

Next, using that at background level $\bar{n}^i\partial_i + \partial_t = d/d\lambda = d/dt$ we can differentiate the integral term for obtaining

$$\frac{1}{\mathcal{H}(1+\bar{z})}\frac{d\delta z}{d\lambda} = -\Psi + \mathbf{V}\cdot\mathbf{n} - \int_0^{r_s} d\lambda(\dot{\Phi} - \dot{\Psi}) - \frac{1}{\mathcal{H}}\left[-\frac{d\Psi}{d\lambda} + \frac{d(\mathbf{V}\cdot\mathbf{n})}{d\lambda} - \frac{d}{d\lambda}\int_s^o \left(\frac{\partial\Phi}{\partial t} - \frac{\partial\Psi}{\partial t}\right) dt\right] . \tag{B.30}$$

This expression is then substituted back into (B.26).

Next, we need to calculate the spatial fluctuations δr, $\delta\theta$ and $\delta\phi$ in order to construct the final expression for the volume perturbation (B.26) in terms of observables.

As we discussed in Sec. 4.2.2 the fluctuation in the photon momenta at an arbitrary position r, giving

$$\delta n^i(r) = \int_0^r dr' \delta\Gamma^i_{\alpha\beta}\bar{n}^\alpha\bar{n}^\beta . \tag{B.31}$$

As previously stated, here and in the following analysis we are neglecting perturbations evaluated at the observer position $r = 0$ ($\lambda = r_s$) since, as already mentioned, they contribute with an unmeasurable monopole term or a dipole term [26]. The Christoffel symbols with upper time and spatial indexes in this metric are given by

$$\delta\Gamma^0_{\alpha\beta} = -\frac{1}{2}\left[h_{0\alpha,\beta} + h_{0\beta,\alpha} - \dot{h}_{\alpha\beta}\right] , \tag{B.32}$$

$$\delta\Gamma^i_{\alpha\beta} = +\frac{1}{2}\left[h_{i\alpha,\beta} + h_{i\beta,\alpha} - h_{\alpha\beta,i}\right] , \tag{B.33}$$

and when contracted with $\bar{n}^\alpha\bar{n}^\beta$ they yield, respectively

$$\delta\Gamma^0_{\alpha\beta}\bar{n}^\alpha\bar{n}^\beta = +\frac{d}{dr}\left(h_{0\alpha}\bar{n}^\alpha\right) + \frac{1}{2}\dot{h}_{\alpha\beta}\bar{n}^\alpha\bar{n}^\beta , \tag{B.34}$$

$$\delta\Gamma^i_{\alpha\beta}\bar{n}^\alpha\bar{n}^\beta = -\frac{d}{dr}\left(h_{i\alpha}\bar{n}^\alpha\right) - \frac{1}{2}h_{\alpha\beta,i}\bar{n}^\alpha\bar{n}^\beta , \tag{B.35}$$

Now, substituting (B.31) back into $\delta x^i = -\int_0^{r_s} d\lambda(\delta n^i - \bar{n}^i\delta n^0) = -\int_0^{r_s} dr(\delta n^i - \bar{n}^i\delta n^0)$ and using the above expressions, we find

$$\delta x^i = -\int_0^{r_s} dr\left[\int_0^r dr'\left(-\frac{d}{dr'}\left(h_{i\alpha}\bar{n}^\alpha\right) - \frac{1}{2}h_{\alpha\beta,i}\bar{n}^\alpha\bar{n}^\beta\right) - \bar{n}^i\int_0^r dr'\left(\frac{d}{dr'}\left(h_{0\alpha}\bar{n}^\alpha\right) + \frac{1}{2}\dot{h}_{\alpha\beta}\bar{n}^\alpha\bar{n}^\beta\right)\right] , \tag{B.36}$$

rearranging terms we find

$$\delta x^i = \int_0^{r_s} dr\int_0^r dr'\frac{d}{dr'}\left(h_{i\alpha}\bar{n}^\alpha + h_{0\alpha}\bar{n}^i\bar{n}^\alpha\right) + \frac{1}{2}\int_0^{r_s} dr\int_0^r dr'\left(h_{\alpha\beta,i} + \dot{h}_{\alpha\beta}\bar{n}^i\right)\bar{n}^\alpha\bar{n}^\beta . \tag{B.37}$$

The total derivative in the first term allows to get rid of one of the integrals, while the integrals of the second term can be permuted identifying correctly the integration limits as

$$\int_0^{r_s} dr \int_0^{r} dr' = \int_0^{r_s} dr' \int_{r'}^{r_s} dr \,, \tag{B.38}$$

which allows to reduce the second term to

$$\int_0^{r_s} dr \int_0^{r} dr' \Big(h_{\alpha\beta,i} + \dot{h}_{\alpha\beta}\bar{n}^i \Big) \bar{n}^\alpha \bar{n}^\beta = \int_0^{r_s} dr' (r_s - r') \Big(h_{\alpha\beta,i} + \dot{h}_{\alpha\beta}\bar{n}^i \Big) \bar{n}^\alpha \bar{n}^\beta \,. \tag{B.39}$$

Then, after dropping the primes in the latter term, the spatial fluctuation δx^i is given by

$$\delta x^i = \int_0^{r_s} dr \Big(h_{i\alpha}\bar{n}^\alpha + h_{0\alpha}\bar{n}^i\bar{n}^\alpha \Big) + \frac{1}{2}\int_0^{r_s} dr (r_s - r) \Big(h_{\alpha\beta,i} + \dot{h}_{\alpha\beta}\bar{n}^i \Big) \bar{n}^\alpha \bar{n}^\beta \,. \tag{B.40}$$

We can now compute $\delta r \equiv \delta x^i e_{ri} = -\delta x^i \bar{n}_i$. Using that $\bar{n}^i\bar{n}_i = 1$, $\bar{n}^i = \bar{n}_i$ and $\bar{n}^i\partial_i + \partial_0 = d/d\lambda = -d/dr$ we find that

$$\delta r = -\int_0^{r_s} dr \Big(h_{i\alpha}\bar{n}^i\bar{n}^\alpha + h_{0\alpha}\bar{n}^\alpha \Big) + \frac{1}{2}\int_0^{r_s} dr (r_s - r) \frac{d}{dr}\Big(h_{\alpha\beta}\bar{n}^\alpha\bar{n}^\beta \Big) \tag{B.41}$$

$$= -\int_0^{r_s} dr \Big(h_{\alpha\beta}\bar{n}^\alpha\bar{n}^\beta \Big) + \frac{1}{2}\int_0^{r_s} dr (r_s - r) \frac{d}{dr}\Big(h_{\alpha\beta}\bar{n}^\alpha\bar{n}^\beta \Big) \,. \tag{B.42}$$

The second integral can be reduced by using integration by parts, i.e. passing the total derivative to the first factor. Since $d(r_s - r)/dr = -1$ this term is carried out as

$$\int_0^{r_s} dr (r_s - r) \frac{d}{dr}\Big(h_{\alpha\beta}\bar{n}^\alpha\bar{n}^\beta \Big) = (r_s - r)\Big(h_{\alpha\beta}\bar{n}^\alpha\bar{n}^\beta \Big)\Big|_0^{r_s} - \int_0^{r_s} dr \Big(h_{\alpha\beta}\bar{n}^\alpha\bar{n}^\beta \Big)(-1) \tag{B.43}$$

$$= 0 + \int_0^{r_s} dr \Big(h_{\alpha\beta}\bar{n}^\alpha\bar{n}^\beta \Big) \,. \tag{B.44}$$

Thus, substituting in the previous expression we can add both integrals and obtain

$$\delta r = -\frac{1}{2}\int_0^{r_s} dr \Big(h_{\alpha\beta}\bar{n}^\alpha\bar{n}^\beta \Big) \,, \tag{B.45}$$

which in term of the components of the metric perturbation is explicitly given by

$$\delta r = \int_0^{r_s} dr (\Psi + \Phi) + \frac{B}{k} + \frac{1}{k^2}\left(\frac{dH_T}{d\lambda} - 2\dot{H}_T \right) . \tag{B.46}$$

Similarly, for computing the angular perturbations $\delta\theta \equiv \delta x^i e_{\theta i}/r_s$ and $\delta\phi \equiv \delta x^i e_{\phi i}/r_s \sin\theta$ we take into account that $\bar{n}^i e_{\theta i} = \bar{n}^i e_{\varphi i} = 0$ as the background geodesics are radial. Hence, projecting (B.40) we find that

$$\delta\theta = \frac{1}{r_s}\int_0^{r_s} d\lambda (h_{\alpha i} e_{\theta i})\bar{n}^\alpha + \frac{1}{2r_s}\int_0^{r_s} d\lambda (r_s - r) \left(h_{\alpha\beta,i} e_{\theta i} \right) \bar{n}^\alpha \bar{n}^\beta \,, \tag{B.47}$$

the second term in the integral can be rearranged using that

$$e_\theta^i \partial_i (h_{\alpha\beta})\bar{n}^\alpha\bar{n}^\beta = \frac{1}{r}\partial_\theta (h_{\alpha\beta})\bar{n}^\alpha\bar{n}^\beta = \frac{1}{r}\partial_\theta (h_{\alpha\beta}\bar{n}^\alpha\bar{n}^\beta) - \frac{1}{r} h_{\alpha\beta}\partial_\theta (\bar{n}^\alpha\bar{n}^\beta) \,, \tag{B.48}$$

which allows to write (B.47) as

$$\delta\theta = \frac{1}{r_s}\int_0^{r_s} dr \frac{(r_s - r)}{r}\partial_\theta(h_{\alpha\beta}\bar{n}^\alpha\bar{n}^\beta) + \frac{1}{r_s}\int_0^{r_s} dr\left[h_{\alpha i}n^\alpha e^i_\theta - \frac{(r_s - s)}{r}h_{\alpha\beta}\partial_\theta(n^\alpha n^\beta)\right]. \quad \text{(B.49)}$$

Using that $\partial_\theta\bar{n}^\alpha = -e^i_\theta\delta_{i\alpha}$ the last term inside the integral becomes $h_{\alpha\beta}\partial_\theta(n^\alpha n^\beta) = -2h_{i\alpha}e^i_\theta n^\alpha$, so that we find

$$\delta\theta = \frac{1}{r_s}\int_0^{r_s} dr \frac{(r_s - r)}{r}\partial_\theta(h_{\alpha\beta}\bar{n}^\alpha\bar{n}^\beta) + \frac{1}{r_s}\int_0^{r_s} dr\frac{1}{r}h_{i\alpha}e^i_\theta n^\alpha\,. \quad \text{(B.50)}$$

Analogously, for the azimuthal projection we have

$$\delta\varphi = \frac{1}{r_s\sin\theta}\left[\int_0^{r_s} d\lambda(h_{\alpha i}e_{\varphi i})\bar{n}^\alpha + \int_0^{r_s} d\lambda(r_s - r)\left(h_{\alpha\beta,i}e_{\varphi i}\right)\bar{n}^\alpha\bar{n}^\beta\right], \quad \text{(B.51)}$$

the second term in the integral can be rearranged using that

$$e^i_\varphi\partial_i(h_{\alpha\beta})\bar{n}^\alpha\bar{n}^\beta = \frac{1}{r\sin\theta}\partial_\varphi(h_{\alpha\beta})\bar{n}^\alpha\bar{n}^\beta = \frac{1}{r\sin\theta}\partial_\varphi(h_{\alpha\beta}\bar{n}^\alpha\bar{n}^\beta) - \frac{h_{\alpha\beta}}{r\sin\theta}\partial_\varphi(\bar{n}^\alpha\bar{n}^\beta)\,, \quad \text{(B.52)}$$

so that the fluctuation in the azimuthal coordinates is given by

$$\delta\varphi = \frac{1}{r_s\sin^2\theta}\int_0^{r_s} dr \frac{(r_s - r)}{r}\partial_\varphi(h_{\alpha\beta}\bar{n}^\alpha\bar{n}^\beta) + \frac{1}{\sin\theta}\int_0^{r_s} dr\frac{1}{r}h_{i\alpha}e^i_\theta n^\alpha\,. \quad \text{(B.53)}$$

Note that the displacements δr, $\delta\theta$ and $\delta\varphi$ are all gauge dependent and hence not measurable by themselves. Finally, substituting the expressions for the angular fluctuations (B.47) and (B.53) the angular contribution for the volume is then

$$\begin{aligned}\left(\frac{\delta v}{v}\right)_\Omega &= \int_0^{r_s} d\lambda\frac{(r_s - r)}{2r_s r}\Delta_\Omega h_{\alpha\beta}\bar{n}^\alpha\bar{n}^\beta \\ &\quad + \int_0^{r_s} d\lambda\frac{1}{r}\left[(\cot\theta + \partial_\theta)h_{i\alpha}e^i_\theta\bar{n}^\alpha + \frac{1}{\sin\theta}\partial_\varphi h_{i\alpha}e^i_\varphi\bar{n}^\alpha\right], \end{aligned} \quad \text{(B.54)}$$

where $\Delta_\Omega = \cot\theta\partial_\theta + \partial^2_\theta + \partial^2_\varphi/\sin^2\theta$ denotes the angular part of the Laplacian operator. The first term in the previous equation can be simplified as follows. First, the contracted term is explicitly given by

$$h_{\alpha\beta}\bar{n}^\alpha\bar{n}^\beta = 2\left[-(\Psi + \Phi) + \frac{1}{k}\frac{dB}{d\lambda} + \frac{1}{k^2}\left(\frac{d^2H_T}{d\lambda^2} - 2\frac{d\dot{H}_T}{d\lambda}\right)\right]. \quad \text{(B.55)}$$

Apart from the Bardeen potentials, the rest of terms can be written as a total derivative, $df/d\lambda$. Then, substituting back into the integral and using that $dr = -d\lambda$ they can be integrated by parts as

$$\frac{1}{r_s}\Delta_\Omega\int_0^{r_s} dr\frac{(r_s - r)}{r}\frac{df}{dr} = -\Delta_\Omega\int_0^{r_s} d\lambda\frac{1}{r^2}\left[\frac{B}{k} + \frac{1}{k^2}\left(\frac{dH_T}{d\lambda} - 2\dot{H}_T\right)\right], \quad \text{(B.56)}$$

by other hand, using that

$$h_{i\alpha}e^i_\theta\bar{n}^\alpha = \frac{1}{kr}\partial_\theta B + 2\left[\frac{\partial_\theta}{k^2 r}\left(\frac{dH_T}{d\lambda} - \dot{H}_T\right) + \frac{\partial_\theta}{(kr)^2}H_T\right], \quad \text{(B.57)}$$

$$h_{i\alpha}e^i_\varphi\bar{n}^\alpha = \frac{1}{kr\sin\theta}\partial_\varphi B + 2\left[\frac{\partial_\varphi}{k^2 r\sin\theta}\left(\frac{dH_T}{d\lambda} - \dot{H}_T\right) + \frac{\partial_\varphi}{k^2 r^2\sin\theta}H_T\right], \quad \text{(B.58)}$$

the last integral in (B.54) can be reduced to

$$\int_0^{r_s} d\lambda \frac{1}{r}\left[(\cot\theta+\partial_\theta)h_{i\alpha}e^i_\theta\bar{n}^\alpha+\frac{1}{\sin\theta}\partial_\varphi h_{i\alpha}e^i_\varphi\bar{n}^\alpha\right]=\Delta_\Omega\int_0^{r_s}d\lambda \times\frac{1}{r^2}\left[\frac{B}{k}+\frac{2}{k^2}\left(\frac{dH_T}{d\lambda}-\dot{H}_T+\frac{H_T}{r}\right)\right]. \tag{B.59}$$

Collecting the previous expressions, after some direct cancellations we find that

$$\left(\frac{\delta v}{v}\right)_\Omega=-\frac{1}{r_s}\int_0^{r_s}d\lambda\frac{(r_s-r)}{r}\Delta_\Omega(\Phi+\Psi)+\Delta_\Omega\int_0^{r_s}d\lambda\frac{2}{k^2r^3}H_T+\Delta_\Omega\int_0^{r_s}d\lambda\frac{2}{k^2r^2}\frac{dH_T}{d\lambda}\,. \tag{B.60}$$

Finally, after integrating by parts the last term it cancels the second integral, while the boundary term evaluated at the source position survives. Then, we find that the angular volume fluctuation is given by

$$\left(\frac{\delta v}{v}\right)_\Omega=-\frac{1}{r_s}\int_0^{r_s}d\lambda\frac{(r_s-r)}{r}\Delta_\Omega(\Phi+\Psi)-\frac{\Delta_\Omega H_T(t_s)}{k^2r_s^2}\,. \tag{B.61}$$

Notice that the first term appearing in the previous equation is the standard expression for weak gravitational lensing in a perturbed FRW universe [42]. Since this effect depends only on the derivatives of the metric perturbations along the line-of-sight, it is clear that a constant gravitational field results in no observable effect.

We can now add up all the terms for obtaining the total volume perturbation.

$$\begin{aligned}\frac{\delta v}{v}=&-2(\Psi+\Phi)-4\mathbf{V}\cdot\mathbf{n}+\frac{1}{\mathcal{H}}\left[\dot{\Phi}+\partial_r\Psi-\frac{d(\mathbf{V}\cdot\mathbf{n})}{d\lambda}\right]\\&+\left(\frac{\dot{\mathcal{H}}}{\mathcal{H}^2}+\frac{2}{r\mathcal{H}}\right)\left(\Psi+\mathbf{V}\cdot\mathbf{n}+\int_0^{r_s}d\lambda(\dot{\Phi}+\dot{\Psi})\right)\\&-3\int_0^{r_s}d\lambda(\dot{\Phi}+\dot{\Psi})+\frac{2}{r_s}\int_0^{r_s}d\lambda(\Phi+\Psi)-\frac{1}{r_s}\int_0^{r_s}d\lambda\frac{r_s-r}{r}\Delta_\Omega(\Phi+\Psi)\,.\end{aligned} \tag{B.62}$$

Combining this result with the previous one we obtain our final expression for the observed overdensity of matter as

$$\begin{aligned}\Delta(z,\hat{\mathbf{n}})=&D_s+\frac{1}{\mathcal{H}}\partial_r(\mathbf{V}\cdot\mathbf{n})+\frac{1}{\mathcal{H}}\dot{\mathbf{V}}\cdot\mathbf{n}+\left(\frac{\dot{\mathcal{H}}}{\mathcal{H}^2}+\frac{2}{r\mathcal{H}}-1\right)\mathbf{V}\cdot\mathbf{n}+\frac{1}{\mathcal{H}}\partial_r\Psi\\&-\frac{1}{r_s}\int_0^{r_s}d\lambda\frac{r_s-r}{r}\Delta_\Omega(\Phi+\Psi)\\&+\left(\frac{\dot{\mathcal{H}}}{\mathcal{H}^2}+\frac{2}{r\mathcal{H}}\right)\left(\Psi+\int_0^{r_s}d\lambda(\dot{\Phi}+\dot{\Psi})\right)+\frac{2}{r_s}\int_0^{r_s}dr(\Phi+\Psi)+\Psi-2\Phi+\frac{1}{\mathcal{H}}\dot{\Phi}.\end{aligned} \tag{B.63}$$

This is the final result presented in Chapter 4.

Appendix C

Power spectrum calculations

Here we present the complementary calculations to those shown in Chapter 7 for deriving the angular power spectrum. We want to calculate the coefficients

$$a_{\ell m}(z) = \int d\Omega_{\hat{\mathbf{n}}} Y^*_{\ell m}(\hat{\mathbf{n}}) \Delta(z, \hat{\mathbf{n}}) \,, \tag{C.1}$$

from which the angular power spectrum is obtained as

$$\delta_{\ell\ell'}\delta_{mm'} C_\ell = \langle a_{\ell m} a^*_{\ell' m'} \rangle \,. \tag{C.2}$$

For calculating these coefficients, notice that according to (4.41)-(4.48) the observed density fluctuation consists of a linear combination of various terms Δ_i, whose k-dependence are given by either a perturbation variable evaluated at the source position $r_s = |\mathbf{x}|$ or an integral of a perturbation variable over the unperturbed photon trajectory (due to Born approximation).

Let us first consider a contribution coming from a generic term belonging to the first class, for instance Ψ, which appears in (4.46). We calculate in detail the coefficient $a^{\Psi}_{\ell m}$ coming from such term using the definition (C.1) as

$$a^{\Psi}_{\ell m}(z) = \int d\Omega_{\hat{\mathbf{n}}} Y^*_{\ell m}(\hat{\mathbf{n}}) \Psi(\tau, \mathbf{k}) \,. \tag{C.3}$$

Next, the field $\Psi(\mathbf{x}, t)$ is expanded in terms of its Fourier transform using the following convention

$$\Psi(\tau, \mathbf{x}) = \frac{1}{(2\pi)^3} \int d^3\mathbf{k} \Psi(\tau, \mathbf{k}) e^{-i\mathbf{k}\cdot\mathbf{x}} \,. \tag{C.4}$$

Substituting back this Fourier expansion into (C.3) we find that

$$a^{\Psi}_{\ell m}(z) = \frac{1}{(2\pi)^3} \int d^3\mathbf{k} \int d\Omega_{\hat{\mathbf{n}}} Y^*_{\ell m}(\hat{\mathbf{n}}) \Psi(\tau, \mathbf{k}) e^{-i\mathbf{k}\cdot\mathbf{x}} \,. \tag{C.5}$$

We now use the so-called Rayleigh formula which allows to decompose a plane wave in terms of spherical harmonics and spherical Bessel functions as

$$e^{-i\mathbf{k}\cdot\mathbf{x}} = 4\pi \sum_{\ell m} i^\ell j_\ell(kx) Y_{\ell m}(\hat{\mathbf{n}}) Y^*_{\ell m}(\hat{\mathbf{k}}) \,, \tag{C.6}$$

where $k = |\mathbf{k}|$ and $x = |\mathbf{x}|$. Substituting back into the previous expression we obtain

$$a^{\Psi}_{\ell m}(z) = \frac{4\pi}{(2\pi)^3}\int d^3\mathbf{k}\int d\Omega_{\hat{\mathbf{n}}} Y^*_{\ell m}(\hat{\mathbf{n}})\Psi(\tau,\mathbf{k})\sum_{\ell' m'} i^{\ell} j_{\ell'}(kx) Y_{\ell' m'}(\hat{\mathbf{n}}) Y^*_{\ell' m'}(\hat{\mathbf{k}})\,. \tag{C.7}$$

Finally, we can make use of the orthonormality condition $\int d\Omega_{\hat{\mathbf{n}}} Y^*_{\ell m}(\hat{\mathbf{n}}) Y_{\ell' m'}(\hat{\mathbf{n}}) = \delta_{\ell\ell'}\delta_{mm'}$ to get rid of the integral over the solid angle and the sum. Thus, we arrive at the final expression for this coefficient

$$a^{\Psi}_{\ell m}(z) = \frac{i^{\ell}}{2\pi^2}\int d^3\mathbf{k}\Psi(\tau,\mathbf{k}) j_{\ell}(kx) Y^*_{\ell m}(\hat{\mathbf{k}})\,. \tag{C.8}$$

Likewise, we can compute the contribution coming from an integral term $\int_0^{r_s} d\lambda f(\mathbf{x}(\lambda),\tau(\lambda))$ which belongs to the second class mentioned above. Using the Fourier transform of the term inside the integral

$$f(\mathbf{x},t) = \frac{1}{(2\pi)^3}\int d^3\mathbf{k} f(\tau,\mathbf{k}) e^{-i\mathbf{k}\cdot\mathbf{x}}\,. \tag{C.9}$$

a similar calculation leads to

$$a^{\int f}_{\ell m}(z) = \frac{i^{\ell}}{2\pi^2}\int_0^{r_s} d\lambda \int d^3\mathbf{k} f(\tau,\mathbf{k}) j_{\ell}(k\lambda) Y^*_{\ell m}(\hat{\mathbf{k}})\,, \tag{C.10}$$

where we have chosen the parametrization $x = |\mathbf{x}| = \lambda$. Next, we calculate the coefficient due to the term $\mathbf{V}\cdot\mathbf{n}$, i.e.

$$a^{\mathbf{V}\cdot\mathbf{n}}(z) = \int d\Omega_{\hat{\mathbf{n}}} Y^*_{\ell m}(\hat{\mathbf{n}})(\mathbf{V}\cdot\mathbf{n})\,. \tag{C.11}$$

We use the Fourier transform for the velocity

$$V(\tau,\mathbf{x}) = \frac{1}{(2\pi)^3}\int d^3\mathbf{k} V(\tau,\mathbf{k}) e^{-i\mathbf{k}\cdot\mathbf{x}}\,. \tag{C.12}$$

Notice that in Fourier space $\mathbf{V}(\tau,\mathbf{k}) = i\hat{\mathbf{k}}V(\tau,\mathbf{k})$, so we can write the identity

$$\mathbf{V}\cdot\mathbf{n} e^{i(\mathbf{k}\cdot\mathbf{n})r} = V i(\hat{\mathbf{k}}\cdot\mathbf{n}) e^{i(\hat{\mathbf{k}}\cdot\mathbf{n})kr} = V\partial_{kr} e^{i(\mathbf{k}\cdot\mathbf{n})r}\,, \tag{C.13}$$

where the position vector is written as $\mathbf{x} = |\mathbf{x}|\hat{\mathbf{n}} = r\hat{\mathbf{n}}$. Substituting this back into (C.11) and using the Rayleigh decomposition, the derivative ∂_{kr} will act on the Bessel function, so we define $j'_{\ell}(kr) \equiv \partial_{kr} j_{\ell}(kx)$. Then, following the same steps as before we find that the related coefficient is

$$a^{\mathbf{V}\cdot\mathbf{n}}(z) = \frac{i^{\ell}}{2\pi^2}\int d^3\mathbf{k} V(\tau,\mathbf{k}) j'_{\ell}(kx) Y^*_{\ell m}(\hat{\mathbf{k}})\,. \tag{C.14}$$

Finally, for the redshift-space distortion we have that $\partial_r(\mathbf{V}\cdot\mathbf{n}) = -n^i\partial_i(\mathbf{V}\cdot\mathbf{n}) = -\mathbf{n}\cdot\nabla(\mathbf{V}\cdot\mathbf{n})$, so we can use the identity (C.13) twice and we arrive at

$$a^{\partial_r(\mathbf{V}\cdot\mathbf{n})}(z) = \frac{i^{\ell}}{2\pi^2}\int d^3\mathbf{k}\frac{V(\tau,\mathbf{k})}{k} j''_{\ell}(kx) Y^*_{\ell m}(\hat{\mathbf{k}})\,. \tag{C.15}$$

Now, according to the discussion at the end of Chapter 3, we decompose each variable in terms of a set of transfer functions which evolve the primordial field $\Psi_{\rm in}(\mathbf{k})$ as

$$D(\tau,\mathbf{k}) = T_D(\tau,k)\Psi_{\rm in}(\mathbf{k})\,, \tag{C.16}$$
$$V(\tau,\mathbf{k}) = T_V(\tau,k)\Psi_{\rm in}(\mathbf{k})\,, \tag{C.17}$$
$$\Psi(\tau,\mathbf{k}) = T_\Psi(\tau,k)\Psi_{\rm in}(\mathbf{k})\,, \tag{C.18}$$
$$\Phi(\tau,\mathbf{k}) = T_\Phi(\tau,k)\Psi_{\rm in}(\mathbf{k})\,. \tag{C.19}$$

Next, we use the simplest form for the power spectrum for the primordial perturbation $\Psi_{\rm in}$, which is characterized in terms of a spectral index n_s and an amplitude A as

$$k^3\langle\Psi_{\rm in}(\mathbf{k})\Psi^*_{\rm in}(\mathbf{k}')\rangle = (2\pi)^3 A_s(k\tau_o)^{n_s-1}\delta(\mathbf{k}-\mathbf{k}')\,. \tag{C.20}$$

Here, we have multiplied by the constant $\tau_o^{n_s-1}$, the actual comoving size of the horizon, in order to keep A_s dimensionless for all values of n_s. Then, A_s represents the amplitude of the metric perturbations at horizon scale today, $k = 1/\tau_o$.

We can now compute the various $C_\ell's$ that contribute to (C.2). For instance, if we consider the potential term we have

$$\begin{aligned}
C_\ell^{\Psi\Psi} &= \langle a^\Psi_{\ell m} a^{\Psi *}_{\ell' m'}\rangle = \frac{1}{4\pi^4}\int d^3\mathbf{k}\int d^3\mathbf{k}'\langle\Psi(\tau,\mathbf{k})\Psi(\mathbf{k}',\tau)\rangle j_\ell(kx)j_{\ell'}(k'x)Y^*_{\ell m}(\hat{\mathbf{k}})Y_{\ell' m'}(\hat{\mathbf{k}}') \\
&= \frac{1}{4\pi^4}\int d^3\mathbf{k}\int d^3\mathbf{k}' T_\Psi(\tau,k)T_\Psi(\tau,k')\langle\Psi_{\rm in}(\mathbf{k})\Psi_{\rm in}(\mathbf{k}')\rangle j_\ell(kx)j_{\ell'}(k'x)Y^*_{\ell m}(\hat{\mathbf{k}})Y_{\ell' m'}(\hat{\mathbf{k}}') \\
&= \frac{2A_s}{\pi}\int d^3\mathbf{k}\int d^3\mathbf{k}' T_\Psi(\tau,k)T_\Psi(\tau,k')\frac{(k\tau_0)^{n_s-1}}{k^3}\delta(\mathbf{k}-\mathbf{k}')j_\ell(kx)j_{\ell'}(k'x)Y^*_{\ell m}(\hat{\mathbf{k}})Y_{\ell' m'}(\hat{\mathbf{k}}') \\
&= \frac{2A_s}{\pi}\int d^3\mathbf{k} T^2_\Psi(\tau,k)\frac{(k\tau_0)^{n_s-1}}{k^3}j_\ell(kx)j_{\ell'}(kx)Y^*_{\ell m}(\hat{\mathbf{k}})Y_{\ell' m'}(\hat{\mathbf{k}})\,,
\end{aligned} \tag{C.21}$$

where in the second and third steps, respectively, we have used the primordial power spectrum (C.20) and the Dirac delta that it contributes to get rid of the integral over $d^3\mathbf{k}'$. In terms of spherical coordinates $d^3\mathbf{k} = \int_0^\infty dk k^2\int d\Omega_{\hat{\mathbf{k}}}$. Then we have

$$C_\ell^{\Psi\Psi} = \frac{2A_s}{\pi}\int_0^\infty\frac{dk}{k}T^2_\Psi(\tau,k)(k\tau_0)^{n_s-1}j_\ell(kx)j_{\ell'}(kx)\int d\Omega_{\hat{\mathbf{k}}}Y^*_{\ell m}(\hat{\mathbf{k}})Y_{\ell' m'}(\hat{\mathbf{k}})\,. \tag{C.22}$$

Finally, using the orthogonality condition for the spherical harmonics $\int d\Omega_{\hat{\mathbf{k}}}Y^*_{\ell m}(\hat{\mathbf{k}})Y_{\ell' m'}(\hat{\mathbf{k}}) = \delta_{\ell\ell'}\delta_{mm'}$ we find

$$C_\ell^{\Psi\Psi} = \frac{2A_s}{\pi}\int_0^\infty\frac{dk}{k}(k\tau_0)^{n_s-1}T^2_\Psi(t,k)j^2_\ell(kx)\,. \tag{C.23}$$

Using this methodology we can repeat the calculations for the other terms and include the contributions coming from all the $a_{\ell m}$'s. In this way, the full calculation gives

$$C_\ell(z_s) = \frac{2A_s}{\pi}\int_0^\infty\frac{dk}{k}(k\tau_0)^{n_s-1}|\Delta_\ell(z_s,k)|^2\,, \tag{C.24}$$

where

$$\Delta_\ell(z_s,k) = j_\ell(kr_s)\left[T_D + \left(1+\frac{\dot{\mathcal{H}}}{\mathcal{H}^2}+\frac{2}{r_s\mathcal{H}}\right)T_\Psi + T_\Phi + \frac{1}{\mathcal{H}}\dot{T}_\Phi\right] + j'_\ell(kr_s)\left(\frac{\dot{\mathcal{H}}}{\mathcal{H}^2}+\frac{2}{r_s\mathcal{H}}\right)T_V$$
$$+ \frac{k}{\mathcal{H}}j''_\ell(kr_s)T_V + \frac{1}{r_s}\int_0^{r_s} d\lambda j_\ell(k\lambda)\left(2+\frac{r_s-\lambda}{\lambda}\ell(\ell+1)\right)(T_\Psi+T_\Phi)$$
$$+ \left(\frac{\dot{\mathcal{H}}}{\mathcal{H}^2}+\frac{2}{r_s\mathcal{H}}\right)\int_0^{r_s} d\lambda j_\ell(k\lambda)(\dot{T}_\Psi+\dot{T}_\Phi)\,, \tag{C.25}$$

which is the general expression presented in Chapter 7.

Appendix D

The Limber approximation

In Chapter 7 we use the Limber approximation [63] for computing the C_ℓ's involving integrals over k and r, i.e. for gravitational lensing, Shapiro time-delay and ISW effect, as well as their cross-correlations with density. Let us consider a generic integral with the form of (7.14), which involves two of these terms labelled as i and j

$$C_\ell^{ij} = \frac{2}{\pi} \int dk k^2 P_{ij}(k) \int dr_1 F_i(r_1) j_\ell(kr_1) \int dr_2 F_j(r_2) j_\ell(kr_2) \,. \tag{D.1}$$

The spherical Bessel functions are related to the Bessel functions of the first kind by

$$j_\ell(x) = \sqrt{\frac{\pi}{2x}} J_{\ell+1/2}(x) \,. \tag{D.2}$$

Substituting this last expression, we can rewrite the correlation between the two effects as

$$C_\ell^{ij} = \int dk k P_{ij}(k) \int dr_1 f_i(r_1) J_{\ell+1/2}(kr_1) \int dr_2 f_j(r_2) J_{\ell+1/2}(kr_2) \,, \tag{D.3}$$

where we have defined

$$f_i(r) \equiv \frac{F_i(r)}{\sqrt{r}}, \qquad f_j(r) \equiv \frac{F_j(r)}{\sqrt{r}} \,. \tag{D.4}$$

The integrals of the generic functions $f(r)$'s multiplied by Bessel functions have a series representation in terms of $(\ell + 1/2)^{-1} \equiv \nu^{-1}$ that allows to rewrite the correlation as [63]

$$C_\ell^{ij} = \int dk k P_{ij}(k) \left(\frac{1}{k} f_i(r) + ... \right) \left(\frac{1}{k} f_j(r) + ... \right) \,, \tag{D.5}$$

where $kr = \nu = \ell + 1/2$. Then, eliminating k in favour of r, up to first order we are left with the result

$$C_\ell^{ij} = \int \frac{dr}{r} P_{ij} \left(\frac{\ell + 1/2}{r} \right) f_i(r) f_j(r) \,. \tag{D.6}$$

Then, comparing with (D.1) we see that using this approximation we can reduce the number of integrals in the C_ℓ's from three to one, which allows to reduce the numerical calculations significantly.